Satellite Swarm Sensor NETwork

D1.1 - S3NET System Requirements

Project	S3NET-H2020-687351		
Deliverable N°	D1.1		
Deliverable leader	Jamin Naghmouchi (iTUBS)		
Contributor(s)	Riccardo Freddi (CGS), Rolf Scheiber (DLR), Eviatar Edlerman (TECHNION)		
Internal Reviewers	Paolo Colandrea (CGS), Riccardo Freddi (CGS), Jamin Naghmouchi (iTUBS)		
Due Date (DoA)	31/10/2016	**Submission date**	08/12/2017
Dissemination level	CO (CONFIDENTIAL, restricted under conditions set out in MGA)		
	PU (PUBLIC, fully open, e.g. web)		X
Type	R (Document, report excluding the periodic and final reports)		x
	DEM (Demonstrator, pilot, prototype, plan designs)		
	DEC (Websites, patents filing, press & media actions, videos, etc.)		
	OTHER (Software, technical diagram, etc.)		

Table of Contents

Table of figures

Table of Tables

List of acronyms/ abbreviations used in this document

Acronym/ abbreviation	Definition
AASR	Azimuth Ambiguity-to-Signal Ratio
AIS	Automatic Identification System
AoA	Angle of Arrival
ASI	Italian Space Agency
BLU	Best Linear Unbiased
CONAE	Argentina's Space Agency
CYGNSS	Cyclone Global Navigation Satellite System, NASA mission
DBF	Digital BeamForming
DDM	Delay Doppler Map
DEM	Digital Elevation Model
DPC	Displaced Phase Centre
EDRS	European Data Relay Satellite
ERS	European Remote sensing Satellite (ESA's first SAR satellite)
FFT	Fast Fourier Transform
LCT	Laser Communication Terminal
GNSS	Global Navigation Satellite System
GNSS-R	GNNS Reflectometry
MAPS	Multiple Azimuth displaced Phase centre Signal
MIMO	Multiple-Input Multiple-Output
PRF	Pulse Repetition Frequency
PRI	Pulse Repetition Interval
S-1(A,B)	Sentinel-1; the radar sensors of the EU's Copernicus program
SAAB	Space Applications Advisory Board
SAR	Synthetic aperture radar
SAOCOM	Argentine Microwaves Observation Satellite
SAOCOM-CS	SAOCOM Companion Satellite
SCORE	Scan-On-Receive: antenna beam-steering using multiple digitized channels
SESAME	Sentinel-1 SAR Companion Multi-static Explorer
SIMO	Single-Input Multiple-Output
SMAP	Soil Moisture Active Passive, NASA mission
SNR	Signal-to-Noise Ratio
Rx	Receive
ToA	Time of Arrival
TDX	TanDEM-X, the twin satellite of TerraSAR-X; their joint formation
TSX	TerraSAR-X, the German radar satellite
Tx	Transmit
VERITAS	Venus Emissivity, Radio Science, InSAR, Topography, and Spectroscopy
VISAR	Venus Interferometric Synthetic Aperture Radar

1 EXECUTIVE SUMMARY

This document represents deliverable D1.1 prepared in the frame of Task 1.1 of Work Package 1 of S3Net project H2020 Grant agreement number 687351.

These requirements have been derived from an analysis performed on possible future S3Net applications, and also are based on the experience in developing equipment and on board computers for space application and specifically for use on spacecraft developed in Europe.

The requirements address S3Net benchmark application candidates.

2 SCOPE AND OVERVIEW

This document covers identification and definition of the candidate Earth Observation (EO) applications that can contribute to resolving the European Societal Challenges and the collection/benchmarking of the user requirements on the applications areas. The EO application user requirements are analysed and collapsed in a well-structured set of application scenarios.

3 APPLICATION AREAS AND SOCIETAL CHALLENGES

S3NET has identified the relevant application areas in the overview table shown below. These areas and scenarios differ regarding needs for resolution, revisit time, and type of monitoring. Although we have identified relevance for all of the described areas, we find that some of these application areas are more relevant to space-borne earth observation missions. In particular those with short revisit time and urgent or routine monitoring will be in our focus due to higher expected cost-effectiveness.

Application	Scenario	Resolution	Revisit Time	Type
Agriculture	Precision Farming	1-5 m	2/3 days	Support to operations
	Crop Health mapping	5-10 m	Weekly	Routine/Monitoring
	Crop pests	5-10 m	5 days	Routine/Monitoring
	Illicit crop monitoring	1-5 m	5/7 days	Support to operations
Forestry	Forest stock mapping	10-100 m	Monthly+	Routine/Monitoring
	Burn scar mapping	1-50 m	Daily	Support to operations
	Illegal deforestation	50-100 m	5/7 days	Support to operations
Land monitoring	Urban growth	1-10 m	Monthly+	Routine/Monitoring
	Soil sealing	10-50 m	Weekly+	Routine/Monitoring
	Land cover classification	10-100 m	Monthly+	Routine/Monitoring
Maritime monitoring	Oil spill monitoring	10-50 m	Daily	Urgent task
	Hydrology	1-10 m	5/7 days	Routine/Monitoring
	Ship detection	1-10 m	Daily	Urgent task
Disaster monitoring	Flooding	1-10 m	Daily	Urgent task
Security	Homeland security	1-10 m	Daily	Urgent task
Natural	Water resource	5-100 m	2/3 days	Routine/Monitoring

Application	Scenario	Resolution	Revisit Time	Type
resource management	management			
	Oil and gas	50-100 m	Weekly+	Support to operations

In the following sub-chapters we describe societal challenges that can be fulfilled by every single application.

3.1 Homeland Security

With the general term “Homeland Security” we indicate one of the most complex “system of systems”, which is in charge of protecting human life and activities either from natural events, or from anthropic threats like terrorism.

Security is one of the strategic aspects for the European Union, as established by the European Earth observation programme termed Copernicus (Copernicus Service), previously known as GMES (Global Monitoring for Environment and Security).

The challenge in this arena is thus to realize algorithms integrated in systems that must fulfil many requirements and in particular, least yet instrumental, have to be as little invasive as possible in such a way to protect people, for example from the very real threat of terrorist attacks while imposing the least changes into their everyday life (Finotto et al., 2008). In this context, then, and in the framework of this project, **EO is a key factor in achieving such result**.

The Integration between satellite and terrestrial systems, today available “near real-time” also thanks to cloud computing (Fazio et al., 2011) and the increasing performances of the sensors, in particular for **resolution increase and revisit time reduction**, enable observation from satellite to become a key tool in providing proper and “rapid” non-intrusive monitoring for homeland security purposes.

Homeland security is part of a wider scenario that is composed of, and can be split into, several “security sub-applications”, each one with a distinctive history and state of art, its own issues and resources. Since dealing with the entire range of possible declinations of homeland security would have led to a giant review, reaching far out of the scope of the S3NET project, we decided to focus on fewer topics. These latter are reputed, either for historical reasons or because of recent technological achievements, to be the most important among those based on on-satellite imagery. The topics can be grouped into three main items:

- **Applications in-port monitoring and, more generally, ship detection**
- **Applications in vehicle detection/identification ;**
- **Applications that can be generally “tagged” as search-and-rescue support.**

Under the hat of Port security applications a number of different activities aiming at controlling who and what enters and leaves the port area are included. A lot of application have been developed in the recent years, thanks to the availability of very-high-resolution satellite images, focusing on ensuring a proper level of security from the water side (Garnier et al., 2010). Ship routing along coastlines becomes more time consuming and an important responsibility for coastal authorities and the trend is focused on investing on tools for automatic coastal monitoring. Since this field is in general carried out by SAR sensors (Greidanus, H. et al, 2003) different algorithms have been developed using optical sensors. In addition to the problem of ship detection also the issues of vessel

detection (including offshore areas) are nowadays examined by using RS data, mainly in order to tackle the migrants emergency. The optical approach has some advantages with respect to the SAR one; for instance: wooden and fiberglass boats can be detected; manual interpretation, in Hi-Res images, is feasible and can lead to a high level of detail (refinement of ships' activities - fishing non fishing).

Nevertheless, for instance, a part of vessels in the European Union (those larger than 15 m) are equipped with a vessel monitoring system (VMS) which allows the monitoring of vessels' location, "activity" and movements in real time; yet many ships are not equipped with these systems, and civilian systems rely on the active cooperation with the authorities for their identification. In general, thus, the trend is in pushing the development of space-borne (but also airborne) systems as a technology to support active systems for monitoring non-cooperative ships.

3.2 Ship detection

With the increasing volume of satellite image data, which are collected from air- and space-borne sensors, automatic ship detection from remote sensing images is a crucial application for civilian fields (Crisp, 2004). Examples of possible uses are illegal oil spill detection, monitoring of fishing activities, maritime security, commercial transportation in civil sectors, naval terrorism, vessel salvage, shipping and export of oil and natural gas. The importance of this field has also been remarked by numerous projects and initiatives supported by European Space Agency (ESA), European Commission (EC) or other significant organizations. Relevant examples include the 'Sea Search Project', the 'MAPP' (MAritime Prevention Project) Demonstrator, the EO CROWD Project - Feasibility Study on Joint EO and Crowdsource Bathymetry, the METSAR Project (**Figure 1**) the PROTECT Project (Piracy Prevention and Commercial Navigation in Insecure Waters), the DESIRE II Project (Demonstration of the Use of Satellites Complementing Remotely Piloted Aircraft Systems Integrated in Non-Segregated Airspace - Second Element), SpaceNav (Space-Based Maritime Navigation), EONav (Earth Observation for Maritime Navigation), 'NEREIDS' (New Service Capabilities for Integrated and Advanced Maritime Surveillance), MARISS (Maritime Security Services), 'DOLPHIN' ('Development of Pre-operational Services for Highly Innovative Maritime Surveillance Capabilities'), and 'SIMTISYS' (Simulator for Moving Target Indicator System) (https://artes-apps.esa.int/projects/theme/maritime-offshore; http://www.copernicus.eu/search/node/maritime).

In literature there are several papers which propose methods for exploiting SAR data in ship detection (Greidanus et al, 2004; Vespe and Greidanus, 2012; Stasolla et al, 2015; Song et al, 2016). The main reasons are full capability to acquire images at day and night, and the capacity to penetrate the clouds, resulting in reliable data at any time and (almost) any weather conditions. Notwithstanding this, SAR data are difficult to interpret in general, they have a long latency due to heavy pre-processing, and they can have some problems in detecting (non-metallic) small ships/vessel (Zhang et al, 2006). Limitations of SAR, together with the increasing number of private industries launching optical satellites (e.g. Planet, Terra Bella), which will produce day-by-day images (Belward and Skøien, 2015), **make the studies on optical data useful and necessary**. Moreover, SAR data and optical data can be put to work in a complementary way (radar+optical data fusion) to produce better results.

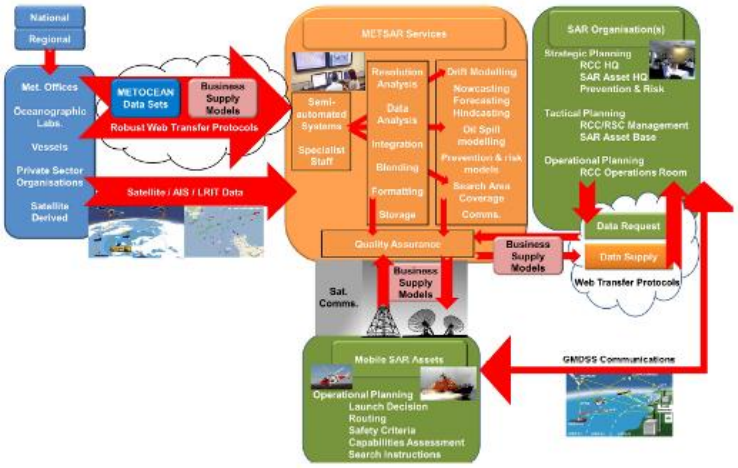

Figure 1: METSTAR Project

3.3 Oil spill monitoring

Environmental pollution, including oil spill, is one of the major ecological problems. Remote sensing is a key instrument for successful response to the onshore and offshore oil spills impacts. There is an extreme need for timely recognition of oil-spilled areas with their exact location, extent of oil contamination and verification of predictions of the movement and fate of oil slicks.

Generally, oil spill monitoring in the offshore and onshore areas is carried out by means of specially equipped aircraft, ships and satellites. Obviously, daylight and weather conditions limit marine and aerial surveillance of oil spills.
Remote sensing offers the advantage of being able to observe events in remote and often inaccessible areas. For ocean spills, remote sensing data can provide information on the rate and direction of oil movement through multi-temporal imaging, and input to drift prediction modelling; this in turn generally facilitates stakeholders in targeting clean-up and control efforts.

The key operational data requirements are fast turnaround time and frequent imaging of the site to monitor the dynamics of the spill. For spill identification, high resolution sensors are generally required, although wide area coverage is very important for initial monitoring and detection. Airborne sensors have the advantage of frequent site specific coverage on demand, but they can be very costly. Spills often occur in inclement weather, which can hinder airborne surveillance. Airborne and satellite remote sensing can aid oil spill response, yet face significant challenges. Passive approaches detect naturally occurring reflected and/or emitted electromagnetic radiation. Active approaches include light detection and ranging (Lidar) and radar. Satellites can play a role in oil spill response by providing preliminary spill assessment for remote locations and synoptic scale data. This role was increased significantly through the International Charter on Space and Major Disasters Agreement, which requires that all signatory countries' space assets be provided during events such as major oil spills (www.disasterscharter.org , 2000).

3.4 Agriculture

3.4.1 Precision farming

Precision farming is a technique combining GPS technology with satellite imagery to enable farmers to use resources and interventions more efficiently (Figure 2). Potential benefits may include increasing crop yields and animal performance, cost and labour reduction and optimization of

process inputs, all of which would increase profitability. At the same time, Precision Farming could increase work safety and reduce the environmental impacts of agriculture and farming practices, thus contributing to the sustainability of agricultural production. Farmers can target resources to where they are needed and reduce excess resources being expended on healthy field areas. The reduction in resources, as well as in chemical products such as fertilizers and pesticides, results in both economic and environmental benefits. The concept has been made possible by the rapid development of observation technologies and procedures along with dedicated software that, in the case of arable farming, provides the link between spatially-distributed variables and appropriate farming practices such as tillage, seeding, fertilization, herbicide and pesticide application, and harvesting. Rapid revisit imagery acquired over agricultural areas during variable crop growth cycles is analyzed and can be delivered to farmers online, providing field level services such as leaf area index (LAI) and nitrogen application maps.

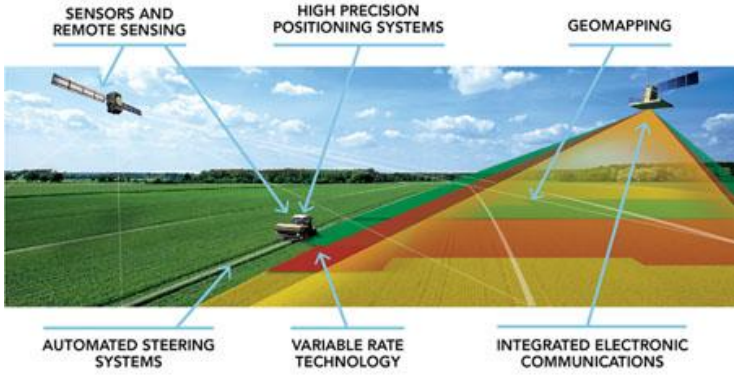

Figure 2: Precision farming

3.4.2 Crop health mapping

With increasing population pressure throughout the world and the need for increased agricultural production, there is a definite need for improved management of the world's agricultural resources. To make this happen, it is first necessary to obtain reliable data on not only the types, but also the quality, quantity and location of these resources. Satellite imagery and GIS (Geographic Information Systems) will always continue to be a very important factor in the improvement of the present systems for acquiring and generating agricultural maps and resource data.

Nearly all crops can be assessed for their health using satellite data. The Normalized Differential Vegetation Index (NDVI) classification can be used to monitor the growth stages. NDVI has been shown to be proportional to the amount of chlorophyll that is found in vegetation. The volume of chlorophyll changes as the crop grows and as the crop health changes. By using a simple NDVI to monitor the chlorophyll content through the growth cycle, the producer can pinpoint areas of concern and apply fertilizer and water appropriately. The biggest cost savings are found when fertilizer application is targeted to areas that show a need. The first analysis is to take a normalized ratio of the Red and Near Infrared bands to give the NDVI values. The healthy areas are then mapped according to their relative NDVI values, which gives a crop health map. Many other uses of this data exist, including building water consumption models and mapping and monitoring pest hazards and crop blight.

Images can show variations in organic matter and drainage patterns. Soils higher in organic matter can be differentiated from lighter sandier soil that has a lower organic matter content. This

information is valuable when used in conjunction with ancillary data to define management zones for a field. Once data has been collected it can be implemented into a mapping environment such as GIS for management and control of agricultural resources.

3.4.3 Crop pests detection and mapping

Plant diseases and pests can affect a wide range of commercial crops, and result in a significant yield loss. It is reported that at least 10% of global food production is lost due to plant diseases (Christou and Twyman, 2004; Strange and Scott, 2005). To rid crops of a disease, pest or weed, farmers typically treat an entire field with a crop protection chemical even if the problem is only found in a specific area. This not only increases the cost of production, but also raises the danger of toxic residue in agricultural products. Disease and pest control could be more efficient if disease and pest patches within fields can be identified timely and treated locally. This requires obtaining the information of disease infected boundaries in the field as early and accurately as possible. The most common and conventional method is manual field survey. The traditional ground-based survey method requires high labor cost and achieves low efficiency. Thus, it is unfeasible for large area. Fortunately, remote sensing technology can provide spatial distribution information of diseases and pests over a large area with relatively low cost. The presence of diseases or insect feedings on plants or canopy surface causes changes in pigment, chemical concentrations, cell structure, nutrient, water uptake, and gas exchange. These changes result in differences in color and temperature of the canopy, and affect canopy reflectance characteristics, which can be detectable by remote sensing (Raikes and Burpee, 1998). Therefore, remote sensing provides a harmless, rapid, and cost-effective means of identifying and quantifying crop stress from differences in the spectral characteristics of canopy surfaces affected by biotic and abiotic stress agents (Mahlein et al, 2012).

3.4.4 Illicit crop monitoring

High-resolution satellite imagery is used for the survey and identification of illegal crops such as opium poppy cultivation. Opium production is an increasing problem for law enforcement agencies due to expanding crops and increasing yields. Imagery acquisition is programmed to coincide with forecast harvest and crop cycle events to reveal areas of cultivation. Satellite imagery enables accurate information to be determined concerning crop yield and annual change. This information is used to support enforcement, social measures and policy changes to help understand and control the production and distribution of illicit crops.

Early investigation of remote sensing methods for detection of opium and other narcotics were driven by the difficulty of collecting ground data in areas of illicit crop production. Sader (1990) reported on unpublished studies conducted in Thailand and India on the detection of opium poppy. This early work encouraged the formation of an Expert Group on remote sensing of illicit narcotics by the United Nations and further investigations into the utility of remote sensing of opium poppy and coca (Sader, 1990).

Chuinsiri et al. (1997) investigated poppy detection in Chang Mai Province of northern Thailand with opium cultivation in remote large fields, small fields on steep slopes and fields close to settlements (0.25 ha). They achieved classification accuracies of 67% and 70% for two dates of Landsat TM using Maximum Likelihood at test sites compared with image interpretation of poppy from aerial photography.

Land cover maps derived from image classification cannot be used to directly calculate area unless classification accuracies are >90% (Gallego, 2004). The systematic error in the classifier can be corrected by regression with an unbiased sample of higher accuracy (Cochran, 1977). Tian et al. (2011) used this approach to measure poppy cultivation in North Myanmar using unsupervised classification and manual editing of multiple image sources (SPOT-5, ALOS and ASTER), bias corrected with visual interpretation of very high resolution (VHR) QuickBird and IKONOS imagery. Although ground data was collected for verification, no accuracy figures were presented to support the claim that their information was more reliable than the UNODC's figures, which differed by up to 146.5%.

Bennington (2008) investigated the temporal and spatial variation in spectral properties of opium poppy in VHR IKONOS imagery affecting classification accuracies. She found that at the flowering growth stage, the spectral signature of opium is separable from the surrounding crop types (mainly wheat and alfalfa) and classification accuracies over 75% are possible. The research also showed use of multi-temporal images did not improve classification if single dated images were collected around the time of poppy flowering.

Jia et al. (2011) investigated spectral separability at field sites in north western China using field spectrometry to demonstrate the feasibility of poppy detection using optical remote sensing. They compared spectral profiles of opium poppy, wheat and alfalfa before, during and after poppy flowering and found a distinct spectral signature for opium poppy at all three growth stages.

More recently, hyperspectral methods were investigated by Wang et al. (2014) using satellite data from EO-1 Hyperion. Although the study was limited in scope, they reported classification accuracies of about 75% using unsupervised endmember-selection.

3.5 Forestry

3.5.1 Forest stock mapping

Many government, state, and private forestry organizations and agencies today utilize geospatial technology such as satellite imagery for various applications supporting analysis, assessment, and management of our forests.

Many applications of forestry and natural resources require accurate land cover and change analysis. Changing conditions due to urban sprawl, as well as increasing forest fragmentation, make land cover and change detection analysis an extremely important consideration for management, planning and inventory mapping. This includes ecosystem and species diversity, forest productivity, reforestation, forest health, conservation of soil, water resources, and nutrient cycling

Deforestation has been attributed to socio-demographic factors, such as population growth and the political economy of class structure, and specific exploitation activities like commercial logging, forest farming, fuel wood gathering, agriculture and pasture clearance for cattle production. Satellite image processing in conjunction with GIS data are effective means for quantifying deforestation and for assessment and monitoring of our forests.

Detailed, reliable and up-to-date information is anyway essential for optimized management of forests. Usually, the required information is obtained from ground surveying and sample-based forest inventories. Several studies have however proved that the combination of terrestrial inventories with remote sensing (Immitzer et al., 2016) increases the value of terrestrial approaches

such as supporting national forest inventories (e.g. McRoberts et al., 2014a and McRoberts and Tomppo, 2007). Remote sensing techniques can provide useful information over large areas, at reasonable costs, with short repetition intervals and with a higher level of detail (Masek et al., 2015, McRoberts-Liknes-Domke, 2014, Stoffels et al., 2015 and Wulder and Franklin, 2003). This is of great interest for forest management applications (Næsset, 2014) and for ecological purposes (Wulder et al., 2004 and Zlinszky et al., 2015). Remote sensing data can be used In combination with inventory data for stratification purposes (McRoberts et al., 2002 and Tomppo et al., 2008), small area estimations (e.g. Breidenbach and Astrup, 2012 and Steinmann et al., 2013) and to describe direct relationships between the two data sets (e.g. Stepper et al., 2015a).

For mapping of structural forest variables such as spatial distribution of growing stock, a variety of different passive and active remote sensing sensors have been tested along the years. Some studies used spectral information from passive optical satellite sensors such as Landsat or MODIS to model growing stock over large areas (e.g. Chirici et al., 2008, Falkowski et al., 2009, Gallaun et al., 2010, Koukal et al., 2007 and Reese et al., 2002). In some North European countries, the combination of satellite imagery and NFI data is already used to produce nationwide forest cover maps (Tomppo et al., 2008).

3.5.2 Burn scar mapping

A “burn scar” or “fire scar” is the visibly blackened land surface left after bushfires burn vegetation and leaf litter. When viewed from space using satellite imagery, fire scars are usually visible as blackened or charred areas. Sometimes, if the satellite passes over the fire at the right time, the active fire front can be seen. Remote sensing scientists use satellite imagery, which is captured on a regular basis, to identify and map fire scars by looking for changes in the landscape over time.

The development of innovative change detection and image classification methods using the time-series of satellite imagery and the high performance computing has allowed scientists to produce detailed fire scar maps for different areas. This can be done measuring the reflectance of land cover features in a number of different wavelengths. The remote sensing scientists use reflectance information as well as changes in reflectance over time to map landscape features, including fire scars.

This presents a significant challenge for fire planning and management and impacts the ecology of our landscapes. The economic, social and environmental cost of fires can be great but conversely, too few fire episodes can also be detrimental to pasture and woodland management in some landscapes. An appropriate fire regime can be a valuable management tool for renovating pastures, controlling introduced weeds and woody vegetation. Fire scar mapping and historical fire information is important for improving our understanding and management of fire, and its interactions with climate variability, vegetation and land use. The fire scar mapping can be used for: managing natural resources assessing fire hazard and risk understanding the impacts of fire on grazing production monitoring and reporting ecological impacts of fire assessing variability in fire regimes over time strategic and operational fire planning and management.

Over the last decades, monitoring and mapping of areas affected by biomass burning has been performed using a wide variety of different sensors. These latter ranged indeed from very high-spatial resolution, such as Ikonos, for fine scales (Kachmar & Sanchez-Azofeifa, 2006); to medium resolution sensors such as Landsat-TM/ETM + or SPOT-HRV for regional coverages (Bastarrika et al.,

2011; Pu and Gong, 2004); and to coarse-spatial-resolution sensors for continental to global studies (Alonso-Canas and Chuvieco, 2015; Chang and Song, 2009; Chuvieco et al., 2008; Giglio et al., 2010; Roy et al., 2008; Tansey et al., 2008). These latter results are the most relevant in the context of climate modelling and they are commonly offered in coarser resolution grids (0.25 to 0.5 degree cell).

3.5.3 Illegal deforestation

A cutting-edge satellite-based alert system could help policymakers and conservationists put a dent in illegal logging by notifying users in real time of new bald patches in the world's forests. The goal is to provide high-resolution tree loss data across the most vulnerable swaths of forests, potentially helping researchers and officials catch illegal logging before too much damage is done. Healthy trees absorb vast amounts of carbon dioxide. So while illegal logging devastates biodiversity and robs local communities of their economic benefits, deforestation also accelerates climate change, since forest degradation is the second-largest contributor of global carbon emissions.

Illegal logging has been difficult to prevent or even catch because most of it occurs deep in rainforest, hidden from forest law enforcement officials. Nowadays, systems such as the GLAD (Global Land Analysis and Discovery alert system, developed by the Department of Geographical Sciences at the University of Maryland and Google: http://www.glad.umd.edu/) downloads satellite images from satellites to a program running an algorithm that compares each pixel in the new image to the previous four years of images. If it senses a significant difference in the pixel's patterns, an alert is triggered. Those alerts can be compiled every week and then made available online at high resolution. The images are now clear enough to detect new roads and pathways beginning to snake through uncut primary forests, usually a sign that logging or illegal gold mining is starting, but the alerts also highlight what are likely new patches of cleared forest in bright pink. Previously, images were not detailed enough to catch loss from logging or mining.

A satellite-based alert system could prove a potent weapon in the fight against deforestation. As few as eight hours after it detects that trees are being cut down, the system will send out e-mails warning that an area is endangered. That rapid response could enable environmental managers to catch illegal loggers before they damage large swathes of forest.

Satellites are already valuable tools for monitoring deforestation; in recent decades, they have delivered consistent data on forest change over large and often remote areas. One such effort, the Real Time System for Detection of Deforestation, or DETER, has helped Brazil’s government to reduce its deforestation rate by almost 80% since 2004, by alerting the country’s environmental police to large-scale forest clearing.

But DETER and other existing alert systems can be relatively slow to yield useful information. They use data from the Moderate Resolution Imaging Spectroradiometer (MODIS) on NASA’s Terra satellite, which at its top resolution produces images with pixels covering an area 250 metres on each side, roughly equivalent to 10 football pitches. This is too big to spot small changes in land cover, so it can take computer programs that process MODIS data weeks or even months to detect that a forest is being cleared. Therefore, pixels with smaller ground dimension can provide great advantage for the overcoming of such a challenge.

In general, two main approaches have been used frequently for deforestation monitoring (Karimi et al. 2016), i.e., vegetation indices and image classification. Vegetation indices (e.g., NDVI,1 LAI2) have been used frequently to analyse forest and rangeland condition with satellite images (Dawelbait and

Morari 2012; Hashemi and Fallah Chai 2013; Hashemi et al. 2013; Tucker 1979). Image classification methods are usually based on statistical analyses including minimum distance, maximum likelihood, etc. (Kelarestaghi and Jafarian Jeloudar 2011); however, for deforestation monitoring and to obtain precise measurements, the spatial resolution of the considered data must be finer than the variability scale of at least one of the principle landscape features. In order to tackle the problem of mixed pixels, (Anderson et al. 2005) developed a method for using MODIS data through the mixing algorithm as a basis for deforestation alert system. In their mixing model, three endmembers, namely vegetation, soil, and shade, were used. They used Landsat-ETM+ data for validation. Results showed the robustness of the technique applied to the MODIS data for deforestation detection. Dawelbait and Morari (2012) applied SMA method along with change vector analysis (CVA) to Landsat images to monitor vegetated land-cover degradation. The results showed the consistency of their method in obtaining information on vegetation cover, soil surface type, and identifying risk areas.

3.6 Land monitoring

3.6.1 Urban growth

As cities play a central role in human-environment interactions, the concepts of sustainable development and good governance have become important topics in urban policy. One of the main challenges is to safeguard and improve the quality of life in cities, while mitigating the negative effects of urban growth on the functioning of natural ecosystems. Spatially explicit data and models for mapping, analysing and forecasting changes in urban form and function are indispensable decision-support tools to develop and evaluate strategies aimed at ensuring sustainable urban development. Earth observation satellites are useful in this respect as they provide regular information on changing urban landscapes.

The most relevant technological development in urban remote sensing is without a doubt the increased spatial resolution of sensor systems, which allows a more detailed and accurate mapping of complex urban landscapes from space. The launch in 1999 of Ikonos, the first commercial satellite capable of acquiring images with high spatial detail, was an important milestone. Subsequent missions such as Quickbird, GeoEye-1, WorldView1-2 and Pleiades have further increased the spatial resolution to 50 centimeters per pixel. Besides the trend toward higher spatial detail, Earth observation satellites providing images of moderate spatial resolution (100 meters or less) have been collecting valuable data since the early 1970s and therefore provide a historic perspective on urban growth. Archives from sensors such as Landsat and SPOT offer images with a vast potential for monitoring, modelling and understanding urban dynamics and associated environmental impacts. Such “medium-resolution” sensors provide less spatial detail, but can observe extensive areas in a relatively limited timeframe. This is valuable for synoptic monitoring of urban growth at a regional or (inter)national scale (Van de Voorde et al. , 2013)

3.6.2 Soil sealing

Soil sealing is the covering of the soil surface with impermeable layers of materials such as stone and concrete used for increasing housing and infrastructure. This causes irreversible loss of the soils natural functions which can lead to floods as water can no longer drain away and cities are increasingly affected by heat waves due to lack of evaporation in the summer.

Soil sealing can also affect human health as well as medium- and long-term economic development and food security. Soil is a non-renewable resource: its health is important for Europe's sustainable development and therefore needs to be preserved and managed carefully. Satellite data form an excellent information base to monitor changes on Earth's surface as result of human activity and natural changes. Multispectral optical sensors are particularly useful, but complementary radar-based techniques are being investigated to exploit their all-weather, day-and-night characteristics. Soil that has been sealed off can be mapped and monitored with satellite images, providing valuable and comprehensive information to support improved soil management and spatial planning. This information can also be used to evaluate processes influenced by the state of the soil, such as floods.

High-resolution remote sensing data may be a useful data source for accurate and spatially detailed mapping of sealed surface cover (De Roeck et al., 2009, Hu and Weng, 2011; Lu and Weng, 2009; Van de Voorde et al., 2004; Zhou and Wang, 2008), which is in turn useful for soil consumption forecasting (Vanderhagen et al., 2015). Large-scale applications of this approach, however, may be hampered by financial constraints or by the amount of effort that is required. Multi-sensor approaches, combining medium resolution remote sensing data like Landsat or SPOT imagery with detailed high-resolution maps of sealed surface cover for a small, but representative part of the targeted area, offers the possibility to build models for full coverage estimation of the proportion of soil sealing at sub-pixel level with relatively high accuracy (Van de Voorde et al., 2009, Yang et al., 2003 and Yang and Liu, 2005).

3.6.3 Land cover classification

Land cover can be defined as the observed (bio)physical cover on the earth's surface. It is an essential information for change detection applications or derivation of relevant planning or modelling parameters. Other fields of applications are the analysis and visualization of complex topics like climate change, biodiversity, resource management, living quality assessment, land use derivation or disaster management. Manual digitization of land cover or land surveying methods results in huge efforts in terms of time consumption, as well as in terms of financial and personal resources. Therefore, methods for automated land cover extraction on the basis of area-wide available remote sensing data are utilized and continually improved (Ban et al., 2015).

Remote sensing has indeed been widely recognized as the cheapest and most feasible approach to map land cover over large areas (Cihlar, 2000; Gong, 2012). Despite the huge research efforts spent on land cover mapping at various spatial scales (Lu and Weng, 2007; Yu et al., 2014), there are still few land cover maps produced at global scale. In order to support global climate change studies, several global land cover (GLC) map products have been developed at spatial resolutions ranging from 100 km to 300 m (DeFries and Townshend, 1994; Loveland et al., 2000; Hansen et al., 2000; Bartholomé and Belward, 2005; Friedl et al., 2010; Arino et al., 2008; Tateishi et al., 2011). Pretty soon, however, it appeared clear how difficult those product are to harmonize in terms of classification system, in addition to the extensive errors found in areas with rapidly changing ecotones (Giri et al., 2005, Herold et al., 2008 and Verburg et al., 2011). Furthermore, previous global land cover products derived using time series optical satellite data at coarse spatial resolution (300 m–1 km) did not provide sufficient thematic detail or change information for global change studies and for resource management (Giri et al., 2013). Following a survey on the land cover data requirements of climate system modellers, Bontemps et al. (2012) found that higher spatial resolution and more temporal frequent data products were needed. In the meantime, requirement for finer resolution land cover mapping at the global scale has emerged in the field of biodiversity,

food security and forest carbon studies (Dobson, 2005, Buchanan et al., 2009, Fritz et al., 2013, Giri et al., 2013 and Pereira et al., 2013). Higher resolution (~30 m) land cover characterization and monitoring permits detection of land change at the scale of most human activity and offers the increased flexibility of environmental model parameterization needed for global change studies. However, there are a number of challenges to overcome before producing such data sets including unavailability of consistent global coverage of satellite data, sheer volume of data, unavailability of timely and accurate training and validation data, difficulties in preparing image mosaics, and high performance computing requirements (Giri et al., 2013).

High spatial resolution satellite images, such as QuickBird, Ikonos, or WorldView, enable to map the heterogeneous range of urban land cover. By the availability of such high resolution images, OBIA-methods (Object-Based Image Analysis) were developed, which are preferred to pixel-based methods in urban context. Pixel-based methods consider only spectral and, possibly, textural properties. Object-based classification processes observe, apart from spectral properties, characteristics like shape, texture or adjacency criteria (Froelich et al, 2013).

3.7 Hydrology

Hydrological survey is critical to the understanding of a territory's coastal zones and inland waterways. The use, consumption and distribution of water resources can be monitored through the use of imagery. Manual surveys are labour intensive and rarely offer a complete overview of the resource in question. Automated sensors are important to monitor single points in waterways, levels at gauges and points of critical concern. However, they do not provide data elsewhere and can suffer in remote areas from a lack of connectivity and power. There is therefore a role for Earth observation from space.

Satellites offer a method to routinely and regularly survey water resources for operational or research projects. Cross-border issues are often of key concern to policy makers. The use of satellite imagery provides an impartial and comprehensive surveying method. Some satellites measure the precise height of the water level, others measure the soil moisture level directly. By looking at the water use of farms and the amount of crops grown, it can be seen how much water is wasted. The fertilizer that runs off these farms can be monitored as it causes algal blooms in inland waterways, starving fish and other inhabitants of oxygen. Coastal and tidal zones subject to regular changes due to meteorological influences can be of concern. Utilizing the technical capabilities of satellites, information may be derived such as shallow water depths, topology of mudflats or presence or absence of outflow or sediments. In coastal zones, satellite imagery provides information on the changing bathymetry, which can be particularly useful around ports and busy shipping areas. The surveys that can be undertaken from space give a regular accurate overview.

Spatially distributed physically based hydrological models, with their ability to estimate energy and water fluxes at the agricultural district scale, are invaluable tools for water resources management for agricultural water use (Corbari et al., 2015). Satellite data, thanks to their intrinsic raster structure, can be effectively used for the internal calibration/validation of distributed hydrological models in each pixel of the domain. This can be achieved with those models based on energy and water balance algorithms in combination with remotely sensed data, in particular of land surface temperature (Corbari and Mancini, 2014).

The information content of satellite images may be useful not only in providing a temporal dataset to calibrate and validate hydrological models, but even for assessment of biophysical attributes, such as leaf area index (LAI) (Colombo et al., 2003), and surface albedo (Corbari et al., 2014), and their temporal variation (Mattar et al., 2014). Thus, the combined use of physically raster based hydrological models and satellite data, may be an answer to the question about extending prediction to larger ungauged area.

3.8 Disaster monitoring: flooding

Floods are one of the most devastating and costly natural disasters. They can wash away or destroy homes, pollute drinking water, and wipe out croplands. Diseases like water-borne cholera can follow in their wake.

In developing countries with limited infrastructure, locating flood waters in order to assess the risk it poses to people – and help decision-makers prioritize aid efforts – is one of the most important jobs of weather forecasters. But it's not always easy, since flood and rainfall information varies widely by country. In this frame, satellite-based tools can help evaluate ground conditions. Being able to monitor soil moisture, water levels and changes to these over time gives a good indication of how likely flood and drought risks are. This can be done utilizing medium/high resolution optical imagery and ground truth measurements to identify changes in levels.

Being able to combine this with detailed weather predictions to understand the likelihood and expected level of rain allows identification of potential threats from flooding and also drought. The ability to provide rapid mapping of areas affected by disasters is also critical for safety of life and rescue operations. It allows relief efforts on the ground to be targeted, routes through affected areas to be identified and help to be directed to areas which most need it.

More recently, fusion of various types of EO data and models has been exploited for EO-based flood detection and monitoring (Schumann and Domeneghetti, 2016).

3.9 Natural resources management

3.9.1 Water

Parameters relevant for hydro(geo)logy are spatially distributed and may show significant temporal variability. Earth Observation (EO) data can provide an essential contribution for the creation of inventories of surface water resources, the extraction of thematic maps relevant for hydrogeological studies and models (landcover, surface geology, lineaments, geomorphology...) or for the retrieval of (bio)geophysical parameters (water quality and temperature, soil moisture. The large area coverage of each observation, on the one hand, helps moving beyond the point-based readings provided by gauge networks to –for instance- basin-wide measurements of discharge and storage, and on the other hand derives common databases of inter-country comparable information. Repeatability of observations allows the generation of a time-series of observed parameters and may result in an improved capability to analyse, monitor and forecast the evolution of phenomena, facilitating water resources management. The importance of having reliable observations of hydrological states and fluxes becomes evident when considering the broad impact of droughts, floods, agriculture, and climate effects on water resources.

Water resources management can benefit from the application of remote sensing and hydrologic models. Satellite remote sensing observations can provide valuable information and can be used to support the operational water resources community for management practices and decisions. However, several challenges to effectively applying these data remain, including identifying and categorizing near-term priority observations and finding opportunities to address near-term information gaps or limitations for improving access to data, information, and decision making. Efficient resource management of water is essential to ensure that an adequate supply of freshwater is available for all users in the future. Earth observation satellites provide the benefit of improving the knowledge of freshwater supply and assist in the management of the distribution of water to users. One particular common use is to determine the rate of evapotranspiration in irrigated agriculture. This increases the efficiency and productivity in agricultural usage of water, which frees up availability of water for other sectors such as municipal and industrial uses. Satellite imagery can effectively be utilized to detect groundwater regions. It is very apparent that both satellite derived data and geographic information systems are ideal tools for aiding authorities with the resource management of water. Satellite imagery should range from high to medium resolution within the visible and near infrared bands with regular revisits to be of use for water resource management.

3.9.2 Oil & gas

Accurate satellite imagery is the most cost-effective method of oil exploration available to petroleum experts today. Acquiring and processing images can lower exploration risk and decrease project cost.

Satellite images can be used to:

- Detect seismic lines and well locations
- Document persistent offshore oil seepage
- Map rock formations, elevation, and major structures
- Update coordinates of old well locations
- Differentiate major rock types Identify barren and productive basin areas
- Perform non-invasive mapping to preserved areas

Some of the most popular applications for oil and gas include iceberg monitoring, which improves shipping safety. There is also a need to spot leaks and spills of oil in the maritime domain. The oil flattens out the surface of the ocean, which can be seen in satellite imagery. The requirements of oil and gas operations also share some similarities with security requirements. When working in remote, unforgiving areas, services from satellites can help improve safety.

One of the main benefits of satellite surveys is indeed that they can be carried out across a range of countries and potential sites, and provide an efficient tool for the identification of potential new prospects. Satellite earth observation data is currently being used to support planning and resource management challenges in the oil and gas industry, for example in relation to moving and placing equipment and monitoring instruments and analysing the extent of slopes, terrain and ground cover. The range of possible uses and applications to assist the oil and gas industry represents an opportunity to expand commercial business.

Unintentional pipeline breaches, equipment failure or illegal tapping can present a hazard to personnel and the release of oil into the local area. Other consequences of such spills may include a loss of revenue, clean-up costs and impact the local environment, together with reputational damage.

While illegal tapping onshore is largely caused by deliberate intervention, pipeline integrity is also at risk from accidental damage through human activity and pipeline corridors may undergo encroachment due to agriculture or unlicensed construction. In this instance, satellite imagery has a role in identifying oil impacted ground post-event, or pre-event to assess changes which may indicate preparations for pipeline tapping or damage, such as unplanned access roads or other activity in the vicinity, complementing traditional methods of pipeline monitoring. Due to the data volumes involved with modern high resolution satellite imagery, change detection methods are being developed to automatically identify change associated with human activity.

In the specific, environmental monitoring of oil production regions applying satellite imagery generally includes the following tasks:

- Providing satellite imagery coverage with specified characteristics (revisit time, spatial resolution, spectral channels, etc.)
- Creation of a basemap (reference mosaic) in order to ensure the geolocation accuracy of raster and vector data.
- Pre-processing of satellite images for each monitoring cycle (atmospheric, geometric correction, etc.).
- Thematic processing of satellite images – the process of identification the infrastructure changes and ecological condition of the territory.

The selection of satellite imagery plays the major role in space monitoring. It should be noted that there is no universal sensor which provides a solution to all monitoring problems. Generally we consider the following key parameters:

- Type of remote sensing data (optical is ineffective in cloudy conditions, but it is suitable for interpretation;
- Spatial resolution (the size of the smallest observed object in the image depends on the pixel size of the image)
- Revisit time (satellite constellations carry an advantage)
- Spatial coverage (determines the possibility to cover the area of interest from one satellite pass)
- Multispectral payload (an important parameter for identifying materials)

4 OPTICAL APPLICATION SCENARIOS

4.1 Optical Earth Observation Application Areas

This chapter covers the activities of collecting, validating, translating and organizing downstream needs in the optical EO application scenarios.

Current State of the Art:

Optical instruments provide images of the Earth measuring the radiation naturally reflected or emitted from ground, atmosphere and clouds, in specific spectral bands. This enables satellites to research and monitor our earth in several ways. Passive remote sensing based on optical instruments offers a wide range of spectral, spatial and temporal observation parameters. Depending on the application domains, end-users can have a demand for very frequent updates of information

retained by earth observation, very high spatial resolution imagery, very precise imaging spectroscopy, rapid image delivery/service and other needs.

In optical Earth Observations (EO), the increase of ground resolution, spectral resolution, coverage and revisit time are key factors for future missions. Low Earth Orbit (LEO), Medium Earth Orbit and Global Earth Observation (GEO) missions offer different observation time and target visibility. EO from geostationary orbit provides great advantages in terms of coverage and frequent update of the information, but the great distance from the Earth reduces the spatial and spectral resolution. Increasing such resolution implies the use of large aperture optics. Concentrating on LEO missions, the primary aspects that have to be approached for the development of future missions is the enhancement of resolution, coverage and revisit time, as well as potentially the reduction of the overall satellite size.

Currently High Resolution Earth images have stirred the interest of a wide user community. Since the successful launch and operations of the IKONOS satellite by Space Imaging in 1999, sub-meter resolution is now available on a commercial basis. High resolution images are very interesting for several applications, since they provide a strong spatial relationship among features on ground, similar to cartographic maps. One can understand why an ever-increasing precision (spatial ground resolution) is required: a better resolution allows better observation and discrimination of smaller objects, which is of great interest in many applications especially for security and emergency related use.

Present commercial mission GEO-EYE 2 (WorldView-4) with its 2615 kg, can acquire panchromatic images with a ground resolution of around 34 cm and multispectral at 1.36-meter. The acquisition of multispectral or hyperspectral sensors, are characterized by a lower spatial resolution due to the use of less sensitive instruments (sensors). Usually these images are characterized by a resolution 4 times larger than panchromatic.

The telescope size, sensors and the satellite altitude are the factors that most influence the ground resolution, spectral resolution, coverage and revisit time. The optical instrument cannot be analysed without taking into account the orbit altitude, that is a critical key point for the design of an imaging satellite. All high-resolution imaging satellites are in low earth orbit , flying above about 350 km (to avoid premature orbit decay due to atmospheric drag) and below 1500 km (to avoid the most severe portions of the lower Van Allen belt and to avoid too large telescope dimensions).

The satellite altitude impacts also on the orbit periodicity that influences the temporal coverage. One of the most important requirements, directly connected to the application domain, is the frequent update of information. Regular revisits of the same area are important for agriculture, disaster management, but also for atmosphere and oceans monitoring.

Starting from November 2013, the SkySat constellation has been in orbit. It is a commercial EO proposed constellation of 24 satellites. Currently two satellites have been launched, SkySat-1 and SkySat-2. SkySat satellites represent the most advanced commercial space solution to achieve a good compromise among satellite size and ground resolution. It acquires high resolution panchromatic (resolution: 0.9m) and multispectral images (4 bands, resolution: 4m), on an orbit at approximately 450 km above earth. Its weight is roughly 120 kilograms and approximate dimensions are 60 x 60 x 95 cm.

Not just ground resolution and revisit time are important for space applications. Multispectral and hyperspectral sensors can provide a diversity of information in different bands. In this case we can analyse the data dimension itself, not just the spatial relationship among ground features. At the European level, Sentinel-2 is the optical mission in visible, near infrared and shortwave infrared. It comprising 13 spectral bands: 4 bands at 10 m, 6 bands at 20 m and 3 bands at 60 m spatial resolution, with a swath width of 290 km. The mission altitude is approximately 800 km and, with the pair of satellites in operation, has a revisit time of 2–3 days at mid-latitudes. The Sentinel-2 spectral information, together with the increased coverage and revisit time allows the monitoring of several phenomena.

4.2 Multispectral and Hyperspectral optical observation

The main difference between multispectral and hyperspectral missions is the number of bands and how narrow the bands are. Multispectral imagery generally refers to 2 to approximately 10-20 bands and generally each band is obtained using a remote sensing radiometer.

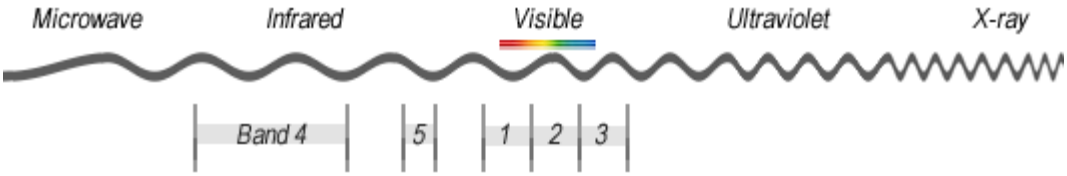

Figure 3: Multispectral Example: 5 wide bands (Image not drawn to scale).

Hyperspectral imagery consists of much narrower bands (10-20 nm). A hyperspectral image could have **hundreds or thousands of bands**. In general, it comes from an imaging spectrometer.

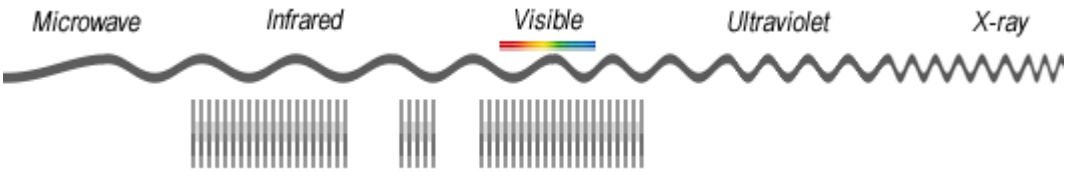

Figure 4: Hyperspectral Example: Imagine hundreds of narrow bands (Image not drawn to scale).

Considering a fixed acquisition time, multispectral imagers allow to achieve greater spatial resolution and lower spectral resolution with respect hyperspectral imagers, whereas hyperspectral imagers add complexity to the mission. Depending on the desired output, multispectral or hyperspectral imagers may be more suited. Wider spectral bands allow the collection of more intense signals in a wide range of different wavelengths, leading to the availability of “discrete” information in different spectral areas. Instead, narrower and more numerous bands close together allow sampling and defining a more precise spectral behaviour within a certain range of wavelengths. This is usually required for application regarding the precise identification of specific spectral signatures.

The following table summarizes some examples of multispectral and hyperspectral missions, depending on how they are usually considered or classified by the international community.

ID	Multispectral payload	Hyperspectral payload	Number of Bands	Application
EO-1		X	220	Earth surface characterization
Sentinel 2	X		13	Land and vegetation
Sentinel 3		X	21	Reflected solar radiation and clouds
Landsat 8	X		11	Visible, near-infrared, short wave infrared, and thermal infrared spectrums acquisition
EuMap		X	244	Ascertainment of global ecological system parameters as well as biophysical, biochemical and geochemical variables
Proba-1/CHRIS		X	19	Collection of BRDF
MTI mission	X		15	Ground temperature measurements
PRISMA		X	239	Natural resources and processes observation
ENVISAT	X		7	Trace gases monitoring and land and ocean monitoring

Table 1: Summary of some relevant multispectral and hyperspectral missions. Here hyperspectral payload are considered with more than 15 bands.

4.3 Potential User Requirements and Prospective Plans for Future Optical EO Missions

In S3NET the optical instruments to be carried by small and inexpensive sensor mission in LEO orbit will be investigated. Ground resolution, spectral resolution, coverage and revisit time will be the driven factors in this study, according to application domain requirements.

Depending on application areas, the use of a single sensor cannot be the best solution to acquire the all desired measurements of our Earth. In this case we have to rely on data coming from several sensors to achieve this result. One of the way to realize this concept is to bring sensors on board of different satellites, travelling in the same orbit separated by short time intervals (constellation) or work together in a group (clusters). In S3NET this approach is called fractional acquisition. The notion of fractionation can be elegantly applied in cluster missions. The elements – or nodes – of a fractionated sensor network are connected to create a "virtual sensor". In cluster missions one approach, which will be examined in S3NET, is the application of fractionated sensing mode using a series of approximately identical images displaced by a short, controlled line-of-sight (LOS) offsets. The original concept was studied for using directed and controlled LOS offsets of a single Telescope, the Hubble Space Telescope, and restore the loss of image resolution caused by the under-sampling. This method could be applied to images collected from a cluster of small independent satellites observing the same area with random LOS offsets in the 3 axes, provided that the off-sets are reasonable fractions of the image size and the LOS offsets can be estimated with good accuracy. The application of this technology requires identical spatial sampling of each sensor and coherency between measurements. The lower-resolution images acquired by each small single-sensor mission are recombined into a higher-resolution image through the image post-processing applying data fusion techniques.

Small single-sensor missions can be realized also in constellation. In this configuration satellites are spaced in time from each other on the same orbit, and their collective acquisitions may be used to build high-definition images in terms of ground or spectral resolution. When optical sensors are used in constellations the close timing of data collection is needed to minimize temporal changes, especially in the atmosphere. S3NET will investigate the different approaches to bring on board of constellation different sensors or the same sensor depending on user requirements. In both cases (cluster and constellation) we will investigate on board identical instruments or different instruments.

In the frame of the proposed work the following aspects will be dealt in order to define specific methods to process satellite data. Co-registration methods, applied to multi-scale and multi sensor data will be analysed and defined. As a matter of fact, a pixel based data fusion approach requires images to be well co-registered. Sensors data intercalibration is also a key issue to be analysed. This implies the possibility to cross calibrate instrument measurements in order to process coherent data. Particular care will be given to the dimensionality reduction issue. As a matter of fact, especially for multi/hyperspectral images, data may be overabundant for representing the contained information. This is due to several factors including sensor noise, low signal in atmospheric absorption wavebands and to the earth spectral response itself. Reducing images dimensionality helps data processing and transmission (acting as a sort of lossy compressor, but with small information loss), information extraction and processing speed (acting on processing convergence).

A trade-off of the different methods will be accomplished according to the specific application case study and considering also the on board processing, communication and storage characteristics.

S3NET will research and evaluate algorithms for selected, representative use cases and benchmark them in terms of compute performance and communication needs, in order to determine to what extend such applications can and should be realized in the future and what increase of service quality therefore will be feasible.

4.4 Qualitative Description of Optical EO Application Demands

In S3NET possible optical instruments to be carried by small and inexpensive sensor mission in LEO orbit will be investigated and analyzed. Ground spatial resolution, spectral resolution, coverage and revisit time will be the driven factors in this study, according to application domain requirements.

Depending on application areas, the use of a single sensor cannot be the best solution to acquire the all desired measurements of our Earth. In this case we have to rely on data coming from several sensors to achieve this result. One of the possible ways to realize this concept is to bring sensors on board different satellites, travelling on the same or a close by orbit but separated by short time intervals (constellation) or working together in a group (cluster). In S3NET this approach is called fractional acquisition. The notion of fractionation can be elegantly applied in cluster missions. The elements – or nodes – of a fractionated sensor network are inter-connected to create a “virtual sensor”. In cluster missions one approach, which will be examined in S3NET, is the application of fractionated sensing mode using a series of approximately identical images displaced by a short, controlled line-of-sight (LOS) offsets. The original concept was studied for using directed and controlled LOS offsets of a single telescope, i.e. the Hubble Space Telescope, and restore the loss of image resolution caused by the under-sampling. This method could be applied to images collected from a cluster of small independent satellites observing the same area with random LOS offsets in the 3 axes, provided that the offsets are reasonable fractions of the image size and the LOS offsets can be estimated with good accuracy. The application of this technology requires identical spatial sampling of each sensor and coherency between measurements. The lower-resolution images acquired by each small single-sensor mission are recombined into a higher-resolution image through the image post-processing by applying data fusion techniques.

Small single-sensor missions can be realized also in constellation. In this configuration, satellites are spaced in time from each other on the same orbit, and their collective acquisitions may be used to build high-definition images in terms of ground or spectral resolution. When optical sensors are used in constellations, the close timing of data collection is needed to minimize temporal changes, especially in the atmosphere. S3NET will investigate the different approaches to bring on board of constellation different sensors or the same sensor depending on user requirements. In both cases (cluster and constellation) we will investigate on-board identical instruments or different instruments.

In the frame of the proposed work the following aspects will be dealt with in order to define specific methods to process satellite data. Co-registration methods, applied to multi-scale and multi sensor data will be analysed and defined. As a matter of fact, a pixel based data fusion approach requires images to be well co-registered. Sensors data inter-calibration is also a key issue to be analysed. This implies the possibility to cross calibrate instrument measurements in order to process coherent data. Particular care will be given to the dimensionality reduction issue. As a matter of fact, especially for

multi-/hyperspectral images, data may be overabundant for representing the contained information. This is due to several factors including sensor noise, low signal in atmospheric absorption wavebands and to the earth spectral response itself. Reducing images dimensionality helps data processing and transmission (acting as a sort of lossy compressor, but with small information loss), information extraction and processing speed (acting on processing convergence).

A trade-off of the different methods will be accomplished according to the specific application case study and considering also the on board processing, communication and storage characteristics.

S3NET will research and evaluate algorithms for selected, representative use cases and benchmark them in terms of computing performance and communication needs, in order to determine to what extent such applications can and should be realized in the future and what increase of service quality therefore will be feasible. In the following, the requirements posed by the specific applications that have been chosen as the most relevant (ship detection, oil spill detection, homeland security) are discussed in terms of their impact on the system to be designed.

Ship detection

Since the first Earth Observation satellites started their operation, the ship detection application has always been of interest for commercial bodies and public authorities. The reasons are many and include enhanced capabilities to monitor legal activities such as fishing as well as illegal ones such as uncontrolled oil spill; monitoring of commercial transportation and maritime security may also greatly benefit from satellite operation.

In literature, many papers have been retrieved, which tackle the cited problem. Most of them take advantage of SAR sensors and their capability to acquire images at day and night, and their capacity to penetrate clouds, resulting in reliable data at any time and (almost) any weather conditions. Nowadays, though, optical sensors are starting to produce data with such a high temporal frequency (multiple images at the same day) and especially, with such a high spatial resolution, that they are starting to compete with SAR data and its distinctive and well-known advantages. High spatial resolution in particular is fundamental to recognize not only the presence of a ship, but also its operational use and role.

The following table resumes the main characteristics of the space borne optical sensors found to be most often used in literature as a satellite data source for ship detection.

	SPOT-2	**SPOT-4**	**SPOT-5**	**QuickBird**	**Google Earth pictures**	**CBERS CCD**	**Gaofen-1**
Spatial resolution Panchromatic image	10 m	10 m	5 m	0.73 m (off-nadir)	0.6 m	20 m	2 m
Revisit frequency (indicatively	1-3 days	2/3 days	2/3 days	1-3.5 days	Unknown	3 days	≤4 days

	SPOT-2	SPOT-4	SPOT-5	QuickBird	Google Earth pictures	CBERS CCD	Gaofen-1
- dependent upon the latitude)							
Dynamic Range	8 bits	8 bits	8 bits	11 bits	Unknown	8 bits	10 bits

Table 2: Main sensors founded in literature and their characteristics. The most widely used sensors are highlighted in green.

Homeland security

All over the world, Homeland Security (HS) is one of the most instrumental and sensitive tasks, especially nowadays with the higher-than-ever level of terroristic threats. This theme is thus of interest **for all Countries**, but in particular **US and Europe** are the main characters in this arena. As mentioned in the proper section, homeland security includes, in fact, a multifaceted panorama of applications that span from the support of humanitarian missions in high-risk areas of the world to the monitoring and control, inside each nation, of sensitive areas, from vehicle or vessel (port monitoring/harbour monitoring etc.).

The approaches analysed from the literature for all the sub-tasks enclosed here, are mainly based on the extraction of significant features (FE) for the classification of the object of interest (vehicle, vessel/ship, rapid mapping for situation awareness). These features translate into geometric or statistical elements extraction, mainly from Hi-Res. panchromatic images.

The following table resumes the three main characteristics of the three main data source sensor founded to be often used in literature.

	IKONOS (launched in 1999)	QuickBird (launched in 2001)	WorldView-2 (launched in 2009)
Spatial resolution (Off-Nadir) - Panchromatic image	1 m	0.73 m	0.52 m
Revisit frequency (indicatively - dependent upon the latitude)	≈3 days	1-3.5 days	1-3.7 days
Dynamic Range	11 bits	11 bits	11 bits

Table 3: Main sensors founded in literature and their characteristics - ordered per descending resolution (ascending launch date) from left to right.

As one can imagine and see from the table, since these approaches are mainly based on extraction of physical features, the main satellite parameter is the **spatial resolution of the acquired** image. This is the main reasons why traditional techniques in this field are based on airborne imagery, and just in the recent years became applicable also to satellite imagery, due to continuous improvement in the spatial resolution of spaceborne optical sensors. The constraint on the spatial resolution depends on the physical dimension of the object to be detected/classified; for instance, vehicles are the most demanding in this terms (Zhao et al., 2001) requiring sub-meter resolution (better if less than 50 cm) in order to rely just on pure FE and classification.

Also for this case, anyway, context-based approaches (using for example non-EO information on the road network) allow the classification of this vehicle even at 1 m resolution - as tested also in recent papers.

Also for ship and rapid mapping of an area, sub-meter resolution in welcomed (for example approaches based on WorldView-2 panchromatic image have been found for rapid mapping - see (Voigt S. et al., 2014) but not strictly needed.

Considering instead the **revisit frequency** of the satellites, all the reviewed papers do not consider this parameter in detail, since they are mainly focused on demonstrate the feasibility of a certain classification approach on available datasets. Certainly this parameter could become instrumental in some applications, as rapid mapping for humanitarian situation, thus making daily revisit frequency desirable.

The **swath width**, indeed, is a secondary parameter not considered by reviewed papers, because it is not crucial for such applications.

In this chapter, an overview of the most interesting applications, based on optical satellite imagery, are being presented and discussed in detail. Practically all of the described applications, and in general all applications based on satellite imagery, require different pre-processing steps in order to prepare the data for further processing.

Thanks to the increasing availability of on-board computational power on satellite platforms and efficient energy management, designers can now consider integrating some algorithms into the space segment, which can be useful for different applications. This does not mean that very complex or heavy algorithms can be considered for on-board implementation; yet, once the different constraints have been taken into account, some pre-processing can take place on-board the satellite platforms, thus possibly saving time and power by enhancing the “informative content density” of downstreamed data.

A notable advance in on-board processing was done for the Earth Observing One (EO-1) spacecraft (Middleton et al, 2013). It carries three instruments: the Advanced Land Imager (ALI), the LEISA Atmospheric Corrector (LAC) and the Hyperion imaging spectrometer. Moreover, it has a flight software named ‘Autonomous Sciencecraft Experiment’ (ASE) (Chien et al., 2005; Chien et al., 2009). ASE has science processing, mission planning, and on-board execution components. The first one enables on-board analysis of Hyperion imagery to develop smaller products for rapid downlink, downlink of alerts, and to drive on-board decision making. From 2005 to 2009, three event types have been analysed directly on-board: thermal detection and summarization (Davies et al., 2006), flood classification (Ip et al, 2006), and cryosphere classification (Dogget et al., 2006; Castano et al., 2006). Mandrake et al. (2009) has also studied on-board detection of active sulfur springs using EO-1 data and its ‘Support Vector Machine’ (SVM) classifier.

In 2007, Yuhaniz et al. (2007) analysed the trend in on-board image processing algorithms (i.e. image compression, change detection, and recognition and classification) on small satellites (e.g. PROBA, X-SAT, FEDSAT, Uo-Sat-5), and they also proposed a change detection approach for flood monitoring. In the same year, Durden et al. (2007) presented a FPGA-based prototype for Doppler spectral processing for a specific application, i.e. spaceborne precipitation radar.

Nowadays, 'Reconfigurable Field Programmable Gate Arrays' (FPGAs) can implement many interesting algorithms. Pingree (2010) discussed the use of FPGAs for three different on-board processing algorithms, which are: SVM Classifiers similar to those in operation on the EO-1 Hyperion instrument, a Fourier transform infrared (FTIR) spectrometer, and a Multiangle Spectropolarimetric Imager (MSPI). Schwenk et al. (2011) have evaluated both per-pixel (i.e. ground cover classification) and per-object (i.e. segmentation) analysis on FPGA for real-time on-board satellite applications.

The 'NASA Goddard Space Flight Center' proposed an FPGA-based, on-board data processing system named 'SpaceCube' (Flatley, 2010). The SpaceCube can perform complex on-board functions such as data reduction, calibration, classification, event/feature detection and real-time autonomous operations. An interesting feature is the possibility to fully reconfigure the system in flight, through either ground commanding or autonomously in response to detected events/features in the instrument data stream.

In a different context (i.e. mobile application), Brousseau and Rose (2012) proposed a FPGA architecture for an application (i.e. object-detection) of the very popular OpenCV image processing library (Culjak et al., 2012). Recently, Krajník et al.(2014) proposed a FPGA-based module for the SURF extraction algorithm, which can be used for band-to band co-registration and image-to-image co-registration. These two papers highlight a clear interest in increasing the use of FPGA for image processing problems.

In the following subchapters, as a result of previous discussions on envisaged applications, concrete examples of useful processing steps that may be taken on-board are given. Specific algorithms are suggested to implement them in a resource-effective way given the constraints, especially in terms of storage and computational resources.

4.4.1 Application Definition of Cloud Detection

One of the most important pre-processing applications, when considering optical data, is cloud detection. Clouds prevent Earth surface reflectivity from being estimated as Mie diffusion blocks direct propagation of light. Cloud detection can thus be useful to rapidly suppress non-informative pixels, and thus increase the compression factor of the data to be downlinked. The state-of-the-art of clouds detection proposed for on-board analysis is described in the following.

In conclusion, **the common outcome of the state-of-the-art remarks the advisability of on-board cloud detection procedures** for multiple purposes and, especially, to reduce the data volume to be downlinked. The majority of FPGA-based **algorithms look mainly at spectral features**, and their combinations, to identify and mask out large fraction of cloudy pixels. **Textural features can also be implemented to improve results, but at a high computational cost**, and this is suggested only where highly accurate results are required. Moreover, the presented papers did not suggest any preferred spatial resolution for this application. The authors, as expected, have also remarked a trade-off between cloud detection accuracy and loss of scientific data. Finally, the selection of the desired algorithm is mostly related to the communication constraints.

For HR and VHR optical data, the algorithm proposed by Camarero et al., (2010) is suggested for on-board cloud detection. The authors also described the computational complexity which will be relevant, and extremely useful, in case of a new on-board implementation. The approach is based on an SVM classifier, which can be also re-used for different applications (e.g. automatic on-board maritime detection).

A second on-board suggested algorithm is the work proposed by Thompson et al. (2014). This last one is more suited for optical data at low-spatial-resolution. The proposed algorithm has been deployed (details are provided), and tested, on-board the AVIRIS-NG airborne imaging spectrometer. New and different approaches can be also considered but it will require an adaption of ground-segment algorithms on FPGA architectures. A good starting point is a recent work by Harb et al. (2016), which proposes a novel simple approach to identify the shape of the clouds, and their shadows. In this paper, a deep state-of-the-art is presented for cloud detection applications using Landsat data, and can be a good basis for a new algorithm to be implemented/adapted for real-time analysis, in case more on-board computing power turns out to be usable for this purpose

4.4.1.1 Automatic Cloud Cover Assessment

The 'Automatic Cloud Cover Assessment' (ACCA) algorithm (Irish, 2000) has been developed to identify clouds on the very popular Landsat data. The algorithm is a two-pass processing chain, and it is based on the observation that clouds are highly reflective and cold. Their high reflectivity can be detected in the visible, near- and mid- IR bands. The thermal properties of clouds can be detected in thermal IR band. In the first pass, a set of fixed thresholds is applied to all the pixel over eight indexes (composed of single bands, band composition, and band ratio). The output identifies potential cloudy pixels. Finally, an adaptive threshold is computed from statistical analysis (i.e. mean, standard deviation, distribution skewness, kurtosis) of the result of the first pass. The output after threshold application is a cloud map. Williams et al. (2002) were the first to propose an FPGA version of the ACCA algorithm for on-board applications. El-Araby et al. (2006) proposed also their FPGA architecture of ACCA applied for both Landsat and MODIS datasets. The final assessment confirmed high performances and high detection accuracies.

4.4.1.2 Hartzell-Cheng – Cloud Detection

A further FPGA-based cloud detection algorithm has been proposed by Hartzell and Cheng (2009). The authors, as in the previous case, proposed a threshold-based algorithm to curb the computational cost. The method was thought to work for VSWIR instrument (within the HyspIRI mission), and the experimental analysis were carried out on AVIRIS dataset. Cloud detection is simply accomplished using three thresholds over mean spectral values on a range of bands. The final results are pretty good. It must be remarked that the authors suggested to loosen the thresholds in order to avoid possible loss of data lost due to false positives.

4.4.1.3 Shan - Cloud Assessment

Shan et al. (2009) analysed a new cloud assessment method based on both spectral and texture features. The classification is done on an hierarchical scheme. The first level uses spectral band values to identify the clear presence of clouds (i.e. high probability of clouds). The remaining pixels pass to the following levels of classification, which imply texture analysis. The second and third levels classify the pixel using, respectively, fractal dimension (Takayasu, 1990; Ding et al., 1999) and angle second moments (Haralick, 1979). This method suffered from the computationally expensive implementation of texture analysis on FPGAs. A new, computationally-cheaper, FPGA-based implementation was proposed by Shan et al. (2010) in 2010.

4.4.1.4 SVM Classifier Method

The French Space Agency (Centre National d'Etudes Spatiales – CNES) also tackled the cloud detection problem on on-board sensors (Camarero et al., 2010). The implemented method is based on a previous SVM classifier already available at ground segments (Latry et al., 2007). The classifier

receives -as discriminative features - both radiometric and geometric parameters. The radiometric parameters involve the whole set of spectral reflectances, as well as several types of reflectance combinations (e.g. ratios). The geometrical criteria are associated to parallax measurement between panchromatic and multispectral images, due to cloud altitude and displacement velocity. The FPGA-based algorithm considers, instead, just the spectral reflectances to limit on board computation. Nevertheless, cloud detection accuracies are very high and thus, this method is considered suitable for the envisaged application.

4.4.1.5 Thompson – Cloud Detection

More recently, Thompson et al. (2014) proposed a new cloud detection method to be implemented on-board. It mostly takes advantage of spectral values. In contrast with the above described algorithms, the thresholds are not fixed but they are dynamically adapted to account for predicted brightness of clouds and terrain. They are recomputed before each observation using foreknowledge of scene parameters, i.e., solar irradiance from orbital ephemeris, instrument calibration data, terrain properties from historical data. The authors proposed a Bayesian probabilistic method for selecting thresholds, which is similar to Merchant et al. (2005). In the end, a spatial aggregation step is done to fix misclassified, isolated bright terrain pixels, e.g. anthropogenic features, sun glint, etc. The authors also describe a deployment on-board the AVIRIS-NG airborne imaging spectrometer (Hamlin et al., 2011). Real-time results were satisfactory and the proposed method can reduce instrument data volumes by a factor of two with insignificant loss of science data.

4.4.2 Application Definition of "Band-to-Band Registration"

Onboard band-to-band registration (BBR) in another important application for on-board sensors. **Very few hints can be found in literature about standard systems for on-board band-to-band registration**. A reason for such scarce presence in the current scientific literature may be due to a limited access on the architecture platform and its tailored definition, and thus few actors are involved in this field of research. Nevertheless, **BBR is a critical pre-processing requirement** for different applications such as image compression, spectral-signature-based classification, change detection, etc.

Image registration techniques for Earth-Observation satellites were described in Eastman et al. (2007). These regard different sensors, such the ones for ASTER (Iwasaki and Fujisada, 2005), GOES I-M (Madani et al., 2004), MISR (Jovanovic et al., 2002), MODIS (Wolfe et al., 2002; Xiong et al., 2005), HRS (Baillarin et al., 2005), ETM+ (Lee et al., 2004), HRS (Baillarin et al., 2005), and VEGETATION (Sylvander et al., 2000).

Regarding BBR in general, as of today, several techniques can be found in scientific literature. The main issue in our case is related to **their transferability on on-board sensors**, where significant additional constraints are imposed with respect to ground-segment processing. A state-of-the-art of BBR on board application is described in the following.

4.4.2.1 Algorithms

In 1970, Anuta (1970) was the first to propose a BBR technique which can still be applied today. The method was based on producing a gradient representation of the image, threshold it, and then apply a registration based on a Fast Fourier Transform (FFT). Nandy et al. (2004) proposed an algorithm over a 15-band multi-spectral image. It was based on producing an edge image, then applying a

phase-based correlation, and finally using spatial-filters to the result to calculate the relative shifts between bands. A similar one was proposed by Foroosh et al. (2002).

Yu et al. (2007) proposed a specific four-stage BBR algorithm: gradient image generation, phase correlation, sub-pixel extension, and valid registration determination. The first two stages are required to identify the locations of the 'peaks' to be used in the last stage. The third stage is instead added in order to reduce peaks in homogeneous areas, mainly generated by the noise component. Once done, sub-pixel displacements are computed (Foroosh et al.,2002) and the bands are consequently co-registered. The method was compared with 'complex gradient image based phase correlation' (Argyriou and Vlachos, 2004) resulting in better performances in term of robustness, and less implementation complexity. The main source of error is related to additive noise in homogeneous zones.

Albinet et al. (2013) proposed a BBR for high-spatial-resolution multispectral optical data. The work derived from the recognized need to tackle the high amount of data for new generation of 'Centre National d'Etudes Spatiales' (CNES) sensors, and thus to apply efficient on-board data compression. In fact, CNES studies have developed a data compression algorithm which can work efficiently only on perfectly registered bands. The proposed algorithm is composed of three steps: generation of registration grids, spatial transformation, and radiometric transformation. The first step consists of generating two grids giving the local subpixel estimated misregistration along the two axes. This is assumed to be done by another satellite subsystem, named 'Attitude and Orbital Control System', which estimates the misregistration caused by several factors (e.g. dynamic low-frequency satellite vibration). The spatial transformation step consists of using the registration grids to determine the coordinates of each pixel of the reference band into the considered unregistered band. Once done, the pixel radiometric value is computed using interpolation with its neighbours. Bi-cubic interpolation was used to achieve high levels of image quality. Results were pretty good when compared to an efficient DFT subpixel registration algorithm (Guizar-Sicairos et al., 2008).

More recently, in 2015, Wang et al. (2015) proposed a BBR relying on the Moon as a reference. This is done based on the fact that the lunar surface reflectance is spectrally and spatially stable in the long term. The method was proposed for the VIIRS sensor, which is a follow-on instrument to MODIS. The image registration is described in Weiss (2010). In this case, the BBR is useful to evaluate the registration accuracy. The BBR is quantized by the offset between the matching pixels of two bands. The offset can be calculated from the 2-D profiles of the same target with the assumption that the spatial profiles of the target are spectrally and temporally stable. A few approaches have been developed to calculate the offsets for MODIS and, in this case, the centroid method was applied (Xiong et al.,2005; Xie and Xiong, 2011; Xiong et al., 2011). The results of BBR satisfy the requirement both along-scan and along-track directions.

As already remarked, the BBR is a fundamental operation to be carried out prior to many, diverse applications (e.g. data compression, change detection). Computational and time constraints on on-board sensors drive the selection of the algorithm. For real-time analysis, BBR must be considered directly on-board the sensors. In these cases, **for low-spatial-resolution data, mature algorithms such as the one proposed by Yu et al. (2007) are suggested for BBR**. **The algorithm proposed by Albinet et al. (2013), instead, is suggested for HR and VHR optical data.** For other situations, where no strict time constraints apply, it can done on ground segments efficiently with ever improving image processing techniques.

4.4.3 Application Definition of Data Compression

The ever-increasing rate at which new EO data is acquired clashes with the limited downlink resources available to each satellite. Unfortunately, this latter capacity did not increase sufficiently to make it trouble-free the downloading of the huge volume of data acquired by recent sensors. In order to tackle this bottleneck, **many data compression techniques have been proposed during the last few years**.

Image compression techniques can be grouped in two types: lossless and lossy. The main difference lies in the presence (lossy compression), or absence (lossless compression) of information loss (i.e. basically mismatch in pixel values) in the reconstructed image with respect to the original one.. Generally, some information loss can be traded for higher compression rates; near-lossless compression is defined as lossy compression where the amount of information loss can be limited to an a-priori fixed ceiling. The higher the ceiling, the higher the achievable compression rates.

Lossy compression may be acceptable where the small amount of additional error/noise corresponding to information lost in the process is negligible with respect to the specific application requirements. On the other hand, it pays back through much better exploitation of the downlink channel. The intended application(s) will determine the level(s) of acceptable loss, and the lossy compression method may be tuned to comply with the strictest of such levels to generate actionable data while making data transmission more efficient in terms of information flow vs. channel capacity. Though, if one does not know a priori the application requirements, utmost care must be exercised in applying lossy compression, in order to avoid ending up with unusable data due to excess compression noise.

In literature there are different state-of-the-art reviews of the image compression problem for satellite data (Huang, 2011; Qian, 2013). **In this document, the attention is oriented on application developed in the framework of the 'Consultative Committee for Space Data Systems' (CCSDS)** (Available: http://www.ccsds.org). The CCSDS has defined several techniques for data compression to be implemented on on-board satellites. These are related to multi- and hyper-spectral images, and many on-board constraints have been tackled, such as computational capability, and memory. Specifically, the CCSDS have defined standard for lossless compression for multi- and hyper- spectral data (CCSDS-123), lossless and lossy compression for single band data (CCSDS-122).

The CCSDS-123 standard can be summarized in two main stages, prediction and encoding, which are implemented through two dedicated blocks: a predictor and an encoder. Prediction consists of making a prediction of a current pixel based on some sort of correlation with previously visited pixels. This stage can be set up as reduced prediction or as full prediction. The reduced version casts its prediction by just looking at the spectral values. The full one, instead, considers both spectrally and spatially neighbouring pixels. The quality of the prediction is measured, as expected, using an error term (i.e. prediction error). The resulting error is then mapped to a non-negative integer named 'mapped prediction residual'. The second stage encodes the mapped prediction residual without any loss. It can be done on block-adaptive or sample-adaptive basis. The first one is less efficient, but it is still in use for single-band lossless compression. The sample-adaptive scheme uses variable-length binary codewords to encode the mapped prediction residual. The compression performances are mostly related to the choice of the prediction parameter and less to the encoding ones (Auge et al., 2011).

Lossy compression is instead defined in the CCSDS-122 standard and, in 2005, a 'Blue-Book' (CCSDS, 2005) was approved as an international standard for Image Data Compression. As for the previous standard, there are two stages: spatial wavelet transform and bit-plane encoder. The first stage is defined as DWT, and it is applied using a fixed number of levels (i.e. three). For a lossy compression, the 9/7 biorthogonal filter is employed (i.e. 9/7 Float DWT). It must be noted that the lossless compression can also be achieved using a non-linear approximation. After the DWT, the wavelet coefficient are rearranged into 8x8 pixel blocks, following a pre-defined scheme, for better encoding through a bit-plane encoder. For lossy multiband compression, the key decision is the choice of transform to be applied along the spectral dimension (i.e. most correlated data). A possible choice presented by many authors is the Karhunen-Loeve transform (KLT) and its approximations.

A third, hybrid group of data reduction technique is called, as cited above, near-lossless compression. This category of techniques somehow blend advantages of both lossless and lossy compression. Typically, in lossy compression, it is generally possible to achieve the desired mean-square-error level between the decoded and the original image. It can be done via a spatial transform technique. Unfortunately, in the inverse transform, it is pretty hard to maintain the desired 'error level', and thus the desired compression. Instead, in near-lossless compression, a bounded maximum reconstruction error can be defined. The technique is similar to the lossless compression cited before, but the prediction is done in a differential predictive coded modulation (DPCM) scheme (Jayant and Noll, 1984). In lossless techniques, the predictor calculates the current pixel based on previous pixels. In near-lossless reconstruction, this is not possible because the original values of the data will not be available at the decoder. Because of this, the predicted current pixel is not obtained starting from previous pixels, but looking at previous sample of the decoded image. To achieve this processing, a local decoder must obviously be implemented at the encoder. In doing so, it is possible to adapt any lossless compression algorithms to its near-lossless version. The reason to implement a near-lossless compression can be many. An example can be to maximize the compression only outside a region of interest.

4.4.3.1 Algorithms

Yu et al. (2007) developed a compression techniques for LEO Earth Observation satellites. It involves a spectral decorrelation using the Karhunen-Loeve Transform (KLT) (Saghri et al., 1995; Lambert-Nebout et al., 2002), followed an image compression based on the CCSDS recommendation. JPEG-LS and JPEG2000 have been selected for, respectively, lossless and lossy compression (Vladimirova and Steffens, 2005).
Yu et al. (2008) developed a new compression techniques (different from the one proposed in 2007). The authors propose to scan the data using a different scheme and modify the 'Gradient-Adjusted Predictor' (Wu and Memon, 1997) rotating it by 90 degrees, and adapting it from 2D (single band) -operation to a 3D (multiple bands) -operation. They also add the 'Brightness Difference Compensation' (BDC) to fix the brightness for even and odd row acquisitions, and thus improving the data compression rate. In the end, a Rice entropy encoder (CCSDS, 1997; CCSDS,2005) is used to compress the data. It works by running various variable-length codes in parallel. The coding option achieving the highest compression is then selected.

Wang et al. (2010) proposed an algorithm based on the adaptive JPEG-LS, and its LOw COmplexity LOssless COmpression (LOCO-I) scheme (Weinberger et al., 2000). The authors proposed a method to improve performances while reducing the processing time. The proposed solution is mainly based on parallelizing the processing of the adaptive predictor. The authors also performed experiments

deploying an FPGA architecture. The final results, compared to different techniques, show an higher throughput, together with an higher processing speed.

Nelson et al. (2012) describe the space-to-ground architecture for the 'Landsat Data Continuity Mission'. In this paper, the author confirms the lossless 'Rice' algorithm to manage the data compression (CCSDS, 1997; CCSDS,2005). The basic Rice adaptive coding algorithm chooses the best of several code options to use on a block of data. These options are targeted to be efficient over different ranges of data activity.

Klimesh (2005) propose a fast lossless algorithm that relies on a low-complexity adaptive filtering technique. Specifically, the sign algorithm (Gersho, 1984) is used in the prediction step, and it is a relative of the 'least mean square' algorithm. In the prediction process, a local mean subtraction is also done to increase the performances. The residual prediction is then encoded using Golomb codes (Gallager and Van Voorhis, 1975) with parameters that are powers of two (i.e. Golomb-Rice codes). One of the main advantages of this proposed lossless compression techniques is the possibility to parallelize it easily. Furthermore, it is characterized by a low complexity together with a high compression rate. In 2012, Keymeulen et al. (2012) proposed a GPU version of this technique, suitable for space application, applied to hyperspectral data. In 2006, a FPGA version was presented by Aranki et al. (2006). More recently, in 2016, Santos et al. (2016) proposed a new FPGA implementation which follows the CCSDS-123 scheme.

Nian et al. (2016) proposed a lossy multi-spectral compression technique. It can be summarized in three stages: spatial discrete wavelet transform (DWT), spectral Karhunen–Loève transform (KLT), and coding. The first consists of applying a spatial DWT (9/7 biorthogonal filters) over the entire image, per each band, to reduce the spatial correlation. Then, a KLT is applied over non-overlapping image blocks (all bands included) to reduce the spectral correlation. Finally, an 'Embedded Block Coding with Optimized Truncation' (EBCOT) is used to generate the final bit-stream (Taubman, 2000). The experimental results show good performances when compared to techniques which use either only DWT, or only KLT.

In the end, **the great volume of papers regarding data compression highlights its importance for on-board applications**. The selection of a specific algorithm must consider many factors, such as encoder-complexity, error resilience, raw-data handling, etc... The CCSDS supports scientific and technical efforts in this important field; it has released standards to avoid dispersion of resources and to facilitate the optimization of space systems. Because of this, in the following, two techniques based on CCSDS scheme are suggested. **The first is a lossless data compression scheme, specifically the one proposed by Klimesh (2005)**. **Recently, Santos et al. (2016) also proposed an efficient FPGA architecture which can be deployed on on-board satellites**. In the same paper, the authors evaluate the complexity of the proposed method. Five different options have been proposed, and one of them has been chosen looking at the hardware utilization and internal memory access. In doing so, eleven target images (e.g. SPOT-5, Pleiades, Landsat, AVIRIS, HYPERION) have been used to evaluate the hardware complexity. More detailed hardware information can be found in Santos et al. (2016). **The second approach** is, instead, a lossy one. It **is proposed by Nian et al. (2016)**, but very similar approaches have been also presented during the last years. The complexity of the method has been compared to other methods (i.e. JPEG2000, Global KLT-DWT, Global DWT-KLT) using the encoding time, and applied over 1024x1024 SPOT-Vegetation multi-spectral images. The JPEG2000 (Part 1) show better performances (around 114 ms) because it does not perform the spectral decorrelation.

The Global-based compression (JPEG2000 Part-3) have an encoding time around 139 ms. The suggested approach varies its encoding time from 140 ms (512x512 block size) to 160 ms (32x32 block size). An intermediate value of 128x128 block size achieve an encoding time of 143 ms, which is pretty similar to the other methods. In the end, the complexity of the algorithm is slightly higher than the Global-based ones, resulting in an interesting choice for on-board application.

4.5 Summary of optical use cases and selection of applications for S3NET

4.5.1 Summary of optical use cases and selection of applications for S3NET

The following table summarizes the investigated optical use cases and identifies high-level requirements for on-board processing, communication and formation control.

Use case	Optical Use Case	Requirements			Dependency
		Computational/ Algorithmic	Communication	Formation Flying	
1	*Lossless Data Compression*	Prediction step (on board)	-	-	-
2	*Lossless Data Decompression*	Rice decoding (on ground)	Transfer of data to GS	-	1
3	*Lossy Data Compression*	JPEG2000 coding (it includes DWT)	Transfer of data to GS	-	-
4	*Band-to-band co-registration*	Gradient filtering followed by a FFT and CPS (on board or on ground, depending on the application)	Transfer of data to common compute node	If used in cluster: precise pointing knowledge, orbit position	-
5	*Cloud training*	Training the SVM (on ground)	-	-	-
6	*Cloud detection*	Classification and refinement, i.e. morphological filtering binary (on board)	-	-	5
7	*SVM - Ship training*	Training the SVM (on ground)	-	-	-
8	*SVM - Ship detection*	Classification and refinement	-	-	7
9	*Automatic Ship detection*	Wavelet and Radon transform, morphological filters and binary logistic regression	-	-	-
10	*Homeland security*	Morphological operators and road vector extraction	-	-	-
11	*Port security*	Deep Neutral Network	-	-	-
12	*Crop health mapping (agriculture)*	Calculate the NDVI	-	-	-

Table 4: Summary of identified optical use cases

4.5.2 Selection of optical use cases for further investigation within S3NET

From the table above the following three primary optical use cases are selected for further evaluation:

- *Lossless Data Compression (1):* This use case has been oriented in the 'Consultative Committee for Space Data Systems' (CCSDS) framework. The CCSDS has defined several techniques for data compression to be implemented on on-board satellites. The proposed algorithm (Klimesh, 2005) implements a 'lossless' technique, which has the advantage to retain all the information at the cost of a lower data compression.
- *Band-to-Band Co-registration (4):* This use case refers to an algorithm developed by (Yu, Vladimirova, & Sweeting, 2007), and it is selected because it offers a clear definition of the processing steps, and it has been proved to be robust and computationally performant.
- *Cloud Detection (6):* This use case was selected because it can help in reducing the total amount of data to be downlinked and in reducing the amount of errors done downstream by e.g. land cover classification algorithms. The algorithm by (Camarero, Thiebaut, Dejean, & Speciel, 2010) and has been selected because it offers very low computational requirements, and is thus extremely well suited for operation on-board satellites.

5 RADAR APPLICATION SCENARIOS

This chapter covers the activities of collecting, validating, translating and organizing downstream needs in the radar based EO application scenarios.

Synthetic Aperture Radar (SAR) based Earth observation of the past decade was characterized by the transition from science oriented single platform missions (e.g. ERS & ENVISAT) to, at least in part, multiple platform missions providing mature operational products for a variety of applications. The following two sections describe the present status and the ongoing developments to be expected on European level. For all cases the focus is on the requirements imposed on on-board processing and - where applicable - also the ones on formation flying and intra-satellite communication.

5.1 Radar Based Earth Observation Application Areas

The SAR sensors presently in space are single platform sensors, although some of them are operated in a constellation (e.g., Sentinel-1, Cosmo-Sky-Med) or in a formation (e.g., TerraSAR-X and TanDEM-X). Each sensor is operated on its own, having independent command up-link and data downlink functionality. Also the satellites scheduled for launch within the next 2 to 5 years do not include relevant on-board data processing capabilities. The only processing performed so far on-board is for adaptive quantization to reduce the data amount for downlink. Also the cluster flight satellites or those forming a constellation do not exchange data or communicate with each other. Instead their operation is independently controlled from ground. In the following, details on some of these sensors are provided.

5.1.1 Sentinel-1

In the frame of the EU's Copernicus program, the European Space Agency (ESA) undertook the development of a European Radar Observatory (Sentinel-1), a polar orbiting two-satellite constellation for the continuation and improvement of SAR operational services and applications (Torres, et al., 2012). While a first satellite, S1-A, was launched in April 2014, its companion S1-B was placed in orbit just recently on April 25, 2016. Together they will ensure a 6 day interferometric repeat-cycle. Besides its radar payload, S1-A carries on board a Laser Communication Terminal (LCT), intended to aid the fast transmission of data with optical laser link to the European Data Relay Satellite (EDRS) and further to the ground facility. Although this service is not yet operational, its performance has successfully been tested in November 2014 using AlphaSat as geostationary counterpart. In June 2016 Sentinel-1A transmitted the first images to the EDRS-A node in geostationary orbit via a laser beam at 600 Mbit/s. Exploiting fast data downlink via EDRS is intended to support the Near-Real-Time Services offered by the Copernicus program.

5.1.2 TerraSAR-X and TanDEM-X

TerraSAR-X is the first German radar satellite being able to acquire SAR images in high resolution mode (< 1m). It was built in a public-private-partnership between Airbus DS (formerly EADS-Astrium) and the German government and launched in 2007. Whilst it is operated by DLR, which is also responsible for scientific exploration, the commercial rights are exclusively hold by Airbus Defense and Space. The technical details of the satellites can be found in (Pitz & Miller, 2010).

Figure 5: TerraSAR-X and TanDEM-X flying in close formation (© DLR, Microwaves and Radar Institute)

The TanDEM-X (TerraSAR-X add-on for Digital Elevation Measurement) mission was initiated jointly by the DLR's Microwaves and Radar Institute and EADS Astrium GmbH in 2003 and placed in orbit in 2010. It opened a new era in spaceborne radar remote sensing, being the first single-pass SAR interferometer in space, with adjustable baselines in across- and in along-track directions. It is formed by adding a second (TDX), almost identical spacecraft to TerraSAR-X (TSX), the latter being in orbit since 2007. The two satellites fly in a closely controlled Helix formation. With typical across-track baselines of 200-400m a global Digital Elevation Model (DEM) with 2m relative height accuracy at a 12 m spatial sampling is presently close to being completed. Beyond this primary mission objective, TanDEM-X is used as a configurable SAR interferometry test bed for demonstrating new SAR techniques and applications (Krieger, et al., 2007).

5.1.3 Other EO Radar Missions

Similar to TerraSAR-X in Germany there are a couple of other national SAR missions. The Italian Space Agency (ASI) presently operates the dual-use (Civilian and Military) COSMO-SkyMed constellation composed of four satellites equipped with SAR sensors operating at X-band, whereas the Canadian Space Agency (CSA) presently develops the satellites of the Radarsat constellation mission at C-band (launch in 2018 as successor of Radarsat-2). One of their primary mission objectives is maritime control in the Mediterranean and Arctic Sea, respectively. Japan launched the ALOS-2 satellite in 2014 carrying an L-band SAR, India the Risat-1 satellite with C-band and China the HJ-1C with S-band radars on board, both in 2012. The UK presently builds the NovaSAR satellite, whereas Argentina is awaiting the launch of its first of two SAOCOM satellites to operate in L-band in 2017, similar to Spain having the PAZ satellite (a rebuild of TerraSAR-X) ready for launch as well.

All these satellites do not include sophisticated multi-channel features on-board, as will be discussed in section 5.3

5.1.4 Near Future Planetary Mission VERITAS

Due to the limited throughput of the available downlink, planetary missions appear as particularly predestined for the processing of the data on-board. It is interesting to discuss at this point the NASA-JPL mission proposal VERITAS (Venus Emissivity, Radio Science, InSAR, Topography, and Spectroscopy), presently considered for a Phase A study with contributions from ASI and DLR. One of the two sensors on board is the VISAR (Venus Interferometric Synthetic Aperture Radar), which will deliver a long awaited DEM (digital elevation model) at 250 m horizontal postings and with 5 m height accuracy. For this purpose, the SAR operates at X-band with two antennas separated by 3.1 m.

On-board processing of the data is foreseen using a space-qualified processor based on Xilinx V5 FPGA family, to reduce the data volume to levels roughly that of other NASA planetary orbiters. VERITAS onboard processing shall provide an approximate 100-fold reduction in data volume compared to the raw radar data. Multi-looked reflectivity images with different resolutions (15, 30, and 250 m) and the interferometric phase at the final DEM resolution will be directly downlinked to Earth, where further bundling and on-ground calibration algorithms occur (Seu, Smrekar, Hensley , & Lombardo, 2016).

The concept is extremely interesting, especially considering that on-board processing in state-of-the-art EO radar missions roughly stops at block adaptive quantization (BAQ) of the data. The VISAR on-board processor, on the contrary, effects a complete interferometric processing, including SAR image formation, interferogram generation, look averaging (wherein spatial resolution and spatial sampling are reduced), preliminary calibration, and further compression of the generated level-1 products. Because of its innovative character, we believe it worthwhile to consider the approach within S3NET as a paradigmatic single-pass interferometric mission and a first assessment of benefits will be presented in sections 5.4.1 and 5.3.2.2.

5.2 Earth Observation Using Signals of Opportunity

During the last decade several research activities were conducted towards evaluating the potential of using signals of opportunity (SoO) for addressing/measuring some of the geo-physical parameters of the Earth. SoO can be microwave signals emitted by geostationary communication and TV transmitters or – more promising for global analyses – those from Global Navigation Satellite Systems (GNSS). The concept is similar to a bistatic radar with non-cooperative transmitters, however it is commonly referred to as GNSS reflectometry (GNSS-R). An extensive tutorial on the topic has been compiled by (Zavorotny, Gleason, Cardellach, & Camps, 2014). Presently, the GNSS-R has evolved from ground-based and airborne experiments towards operating receivers in space, serving as technology demonstrators or addressing the monitoring of particular geo-physical parameters. Present day spaceborne GNSS-R missions will be summarized in section 5.2.2.

5.2.1 General concept of GNSS-R

GNNS-R basically consists in recording the direct and reflected signals of individual GNSS transmitters (GPS, GLONASS, Galileo, etc), then it performs their cross-correlation and displays the result in so-called Doppler-delay maps (DDM), which can later be geo-referenced. Usually, the reflected signals are very weak, such that only direct reflections / specular echoes from the glistening zone exhibit sufficient SNR, depending on surface roughness. All other samples of the DDMs are usually ambiguous due to the symmetry in observation geometry. Opposite to mono- and cooperative bistatic radar systems, the resolution is not primarily determined by the bandwidth of the transmitted signals, but given by the size of the specular (or glistening) zone, which is usually several (tens) of square kilometers large (Clarizia & Ruf, On the Spatial Resolution of GNSS Reflectometry, 2016).

Early GNSS-R receivers were ground or aircraft based and were able to record only single source GNSS signals. However, as the technique matured, we see nowadays spaceborne instruments capable of recording several GNSS signal sources simultaneously and also performing on-board processing of the received data to obtain DDMs with much reduced data amount for downlink.

Applications of GNSS-R demonstrated so far include roughness sensing, wind speed retrieval, soil moisture estimation, sea surface height measurements, tsunami detection and parameter estimation, and snow depth estimation.

5.2.2 Present day spaceborne GNSS-R systems

5.2.2.1 TechDemoSat-1

The TechDemoSat-1 satellite was launched in July 2014 by Surrey Satellite Technology Ltd. (UK) and serves as a technology demonstrator mission. Also known Sea State Payload (SSP) the GPS receiver was initially supposed to operate as a coarse altimeter receiving the reflected signals to determine ocean roughness. The information gathered can then be applied to meteorology, oceanography, climate science and ice monitoring. It already performs computations of DDMs onboard and is able to track both L1 & L2 GPS codes.

The system was recently shown to be useful also for sea target detection (e.g. ice-sheets, ships, oil platform) (di Simone, Park, Riccio, & Camps, 2017). TechDemoSat-1 is considered the precursor to the NASA CYGNSS constellation mission.

5.2.2.2 CyGNNS Observatory

NASA's Cyclone GNSS observatory, proposed and designed by the University of Michigan, consists of a constellation of 8 microsatellites (each <25kg, <20Watt power consumption). It operates in equatorial LEO (orbit height of approx. 500 km and inclination of 35 deg) and is dedicated to weather forecast improvement, in particular hurricane prediction.

All satellites were jointly air launched with Pegasus rocket from a L-1011 aircraft out of Cape Canaveral, Florida on December 15, 2016. The observatory performs measurements at approximately five hour intervals in the Earth's equatorial regions. The prime mission goals are the measurement of ocean surface wind speed in all precipitating conditions, including those experienced in the tropical cyclone (TC) eyewall, including the measurement of the ocean surface wind speed in the TC inner core with sufficient frequency to resolve genesis and rapid intensification. Each satellite carries a delay-Doppler Mapping Instrument (DDMI) capable of receiving & processing four DDMs simultaneously (CyGNSS - Cyclone Global Navigation Satellite System, 2017).

5.2.2.3 SMAP GNSS-R observations

NASA's Soil Moisture Active Passive Mission (SMAP) was supposed to measure soil moisture by means of combined radiometer and radar sensing in L-band. Unfortunately, the radar transmitter failed at the very beginning of mission lifetime. This opened the opportunity to tune the radar receiver to GPS L2 frequency, thus becoming a highly sensitive GNSS-R instrument. Due to its large reflector array the SNR of the recorded GNSS reflections is considerably improved and polarimetric measurements are possible as well, because of the H and V receive channels. Because of the improved SNR, evaluation of leading and trailing edges of the specular point reflections become possible.

Opposite to CyGNSS, the mission is operated along a polar orbit, offering observations also for high latitudes. Recent studies demonstrate the performance to discriminate different regimes of above-ground-biomass in tropical and boreal forest areas, soil moisture sensitivity as well as the potential to discriminate different ice regimes in polar latitudes (Carreno-Luengo, Lowe, Zuffada, Esterhuizen, & Oveisgharan, 2017).

5.2.3 Ongoing and future developments of GNSS-R

GNSS-R sensors are also foreseen for the 3Cat-3/MOTS mission to be flown on a 6U CubeSat platform (Castellvi Esturi, Camps, Carbera, & Alamús, 2017) and the GEROS-ISS mission, which stands for GNSS REflectometry, radio occultation, and scatterometry onboard the International Space Station (ISS) (Wickert, Cardellach, Martín-Neira, & et al, 2016). While GEROS-ISS targets primarily altimetric sea surface height at the mesoscale (10–100 km or longer scale) under all-weather conditions, 3Cat-3/MOTS intends to make use of synergy with optical data. Both missions must be considered as technology demonstrators being restricted to single platforms. For operational purposes revisit time and coverage are insufficient. In future it is expected that constellations of GNSS-R instrumentation will be deployed, similar to the CyGNNS mission, but extending to larger areas/higher latitudes and with increased performance with respect to recording additional GNSS signals at both polarisations and with improved SNR.

Within this S3NET project no further analysis of GNSS-R mission concepts is performed, as their requirements concerning formation flying, on-board processing and communication are considered modest in comparison with optical and SAR payload needs. However, the technology developments of S3NET might be valuable to support future GNSS-R missions as well.

5.3 Requirements and Prospective Plans for Future Radar Based EO Missions

5.3.1 High Resolution Wide Swath SAR Imaging

While several applications require uninterrupted time series of SAR images with short time intervals between consecutive acquisitions, all current high-resolution SAR systems are rather limited with regard to their acquisition capability. An example is TerraSAR-X, which provides multiple imaging modes for different trade-offs between resolution and coverage: In stripmap mode (spatial resolution of 3 m), only 2% of the Earth's landmass can be mapped during its 11 days repeat cycle (Werninghaus & Buckreuss, 2010).

Future SAR missions may require a mapping capability one or even two orders of magnitude better than that of TerraSAR-X. If a single satellite is available, however, frequent and seamless coverage can only be achieved if a wide swath is imaged. In conventional stripmap SAR, the swath width constrains the pulse repetition interval (PRI): to control range ambiguities, the PRI must be larger than the time it takes to collect returns from the entire illuminated swath. On the other hand, to avoid significant azimuth ambiguity levels, a large PRI, or equivalently a low pulse repetition frequency (PRF), implies the adoption of a small Doppler bandwidth and limits the achievable azimuth resolution. A wide swath can be also mapped using ScanSAR or TOPS, but the azimuth resolution is still impaired.

To overcome these limitations, new radar techniques have been developed, which allow for the acquisition of spaceborne high-resolution SAR images without the classical swath limitation imposed by range and azimuth ambiguities. These techniques are mainly based on **digital beamforming (DBF)** and **multiple azimuth displaced phase centre signal (MAPS)** recording.

A prominent example is the (X-band) TerraSAR-X follow-on high-resolution wide-swath (HRWS) SAR, currently under development at Airbus DS with support from DLR (Suess, Grafmueller, & Zahn, 2001). This system uses DBF on receive to steer in real-time a narrow beam towards the direction of arrival of the radar echo from the ground, exploiting the one-to-one relationship between the radar pulse

travel time and its direction of arrival (this is also referred to as scan-on-receive (SCORE) or Sweep-SAR). A large receiving antenna can hence be used to improve the sensitivity without narrowing the swath width. As the unambiguous swath width is no longer limited by the antenna length, a long antenna is deployed to map a wide swath. Moreover, to improve the azimuth resolution, the receive antenna is divided into multiple sub-apertures, mutually displaced in the along-track direction and connected to individual receive channels. By this, multiple samples of the synthetic aperture can be acquired for each transmitted pulse. The coherent combination of all signals in a dedicated multichannel processor enables the generation of a high-resolution wide-swath SAR image. This system allows mapping a swath in the order of 80 km with an azimuth resolution in the order of 1 m, but is not suited to map a wider swath (e.g., 350 km), as a very long antenna (in the order of 40 m) would be required for that.

In order to keep the antenna length down, several new instrument architectures and modes have been proposed (Krieger G. , Gebert, Younis, Bordoni, Patyuchenko, & Moreira, 2008). One example is the combination of displaced phase centres in azimuth with ScanSAR or TOPS mode. As in classical ScanSAR, azimuth bursts are used to map several swaths. The associated resolution loss from sharing the synthetic aperture among different swaths is compensated by collecting radar echoes with multiple displaced azimuth apertures. This concept will be adopted for the next generation of (C-band) Sentinel satellites (Sentinel-NG).

Besides multichannel ScanSAR, of great interest are concepts based on simultaneous recording of echoes of different pulses, transmitted by a wide beam illuminator and coming from different directions. This enables an increase of the coverage area without the necessity to either lengthen the antenna or to employ burst modes. A sufficiently large antenna in elevation is needed to separate the echoes from the different swaths by digital beamforming on receive, while a wide beam can either be accomplished by a separate small transmit antenna or a combined transmit-receive antenna together with tapering. An interesting alternative to a planar antenna is a reflector, fed by a multichannel array. A parabolic reflector focuses an arriving plane wave on one or a small subset of feed elements. As the swath echoes arrive as plane waves from increasing look angles, one needs hence to only read out one feed element after the other to steer a high-gain beam in concert with the arriving echoes. A drawback of the multi-beam mode is the presence of blind ranges across the swath, as the radar cannot receive while it is transmitting, which can be however overcome by the **staggered SAR concept**. A prominent example of future mission adopting this concept is Tandem-L, whose goal is the investigation of dynamic processes on the Earth's surface.

5.3.2 Companion Satellite Missions

A further concept expected to play a paramount role in SAR remote sensing in the near future is that of companion missions. A companion satellite is added to an existing mission for cooperative (e.g. bistatic) operation. The costs of the companion satellite can be significantly reduced with respect to the original one due to the reduced development effort caused by economies of scale or simplicity of hardware. In addition to the data provided by the reference mission (e.g., reflectivity, repeat-pass interferometry), companion SAR missions offer an efficient way to provide the single-pass interferometry information which is typically required for operational applications like (dynamic) DEM generation, tomography, or MTI.

As an example of the interest companion missions raise in the community, ESA is presently investigating the feasibility and performance of a receive-only L-band companion SAR satellite (CS) to

be launched and operated together with CONAE's SAOCOM (Satellites for Observation and Communications), scheduled to be launched in 2017. Further, a mission based on a pair of receive-only companions for future Sentinel-1 (SESAME, SEntinel-1 SAR Companion Multistatic Explorer) has been proposed to respond to the 9th Earth Explorer call for the dynamic monitoring of the Earth's surface. Both missions will be commented in further detail in the following below.

In this context, following TanDEM-X, a further German satellite formation mission is presently under study, Tandem-L (Moreira, et al., 2015). It foresees two fully polarimetric L-band SAR satellites flying in a similar close formation as TanDEM-X to acquire a new generation of information products from space. Tandem-L employs a revolutionary radar instrument, together with novel SAR imaging techniques, like digital beamforming (DBF), combined with the staggered SAR concept (see section 5.3.1). Since this mission concept is very similar to TanDEM-X it will not further be discussed here. Instead the focus here is on the new trend employing receive-only companion satellites.

5.3.2.1 SAOCOM-CS

The SAOCOM-CS mission is a single-pass interferometric mission consisting of a companion satellite to fly and operate together with CONAE's L-band SAOCOM. The mission is divided into four phases, with distinct geometries and objectives:

- A tomographic phase, with both spacecraft in close formation with along-track and across-track baselines smaller than 10 km will be used to acquire a stack of single-pass interferometric acquisitions to map the equatorial and boreal forests the using coherence-based tomography.
- An along-track bistatic phase (called bistatic 1) with the companion separated roughly 250 km from SAOCOM, with the main objective of providing a second line of sight for the estimation of 2D motion components using repeat-pass interferometry.
- A (companion) backward-looking phase (called bistatic 2) with the companion separated 250 km in both along-track and across-track looking backward to the imaged scene, as an intermediate step to reach the specular configuration. The objective of the phase is bistatic radiometry and interferometry for the estimation of surface roughness 2D motion components.
- A specular phase on the way towards de-orbiting with both spacecraft flying with an across-track baseline of about 500 km to investigate forward scattering and possible applications like soil moisture and surface roughness estimation.

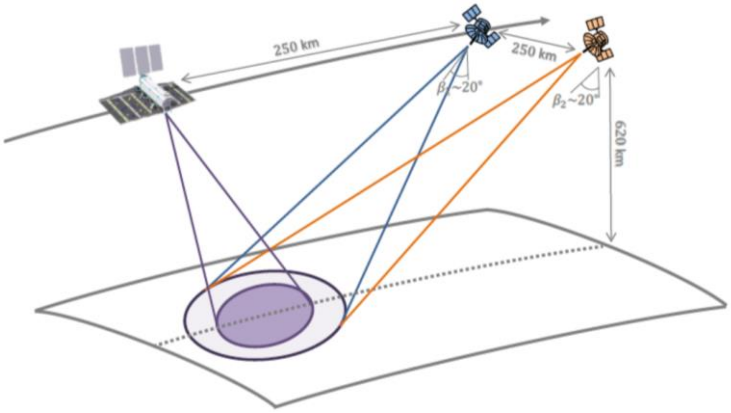

Figure 6: Schematic description of the SAOCOM-CS in the bistatic 1 and bistatic 2 configurations.

From the technological point of view, the SAOCOM-CS payload is a weakly-synchronised bistatic single-pass interferometer (Rodriguez-Cassola, Prats-Iraola, Nannini, Lopez-Dekker, Moreira, &

Carnicero-Dominguez, 2016). Unlike TanDEM-X, neither the SAOCOM payload nor the CS payload possesses a direct link to support clock synchronisation. The calibration of the time and phase references of the instrument are foreseen to be effected on ground with the help of an autonomous synchronisation approach (i.e., AutoSync) (Rodriguez-Cassola, Bistatic synthetic aperture radar data processing, 2013). The autonomous synchronisation on-board the receiver of a bistatic or multistatic constellation for very high resolution bistatic SAR imaging can be identified as one application of interest for the present study.

5.3.2.2 SESAME

The second companion satellite mission to be presented here is SESAME (SEntinel-1 SAR Companion Multistatic Explorer), which has been recently submitted in response to ESA's Call for Proposals for Earth Explorer Mission EE-9 (ESA's Call for Earth Explorer EE-9). It is dedicated to the observation of land surface topography, topographic change and bio-geophysical parameters in order to advance the scientific understanding and modelling of dynamic processes of the geosphere and biosphere. The observations focus at processes that are associated with distinct temporal changes of shape and elevation of land surfaces and ice bodies, as well as forest height and biomass.

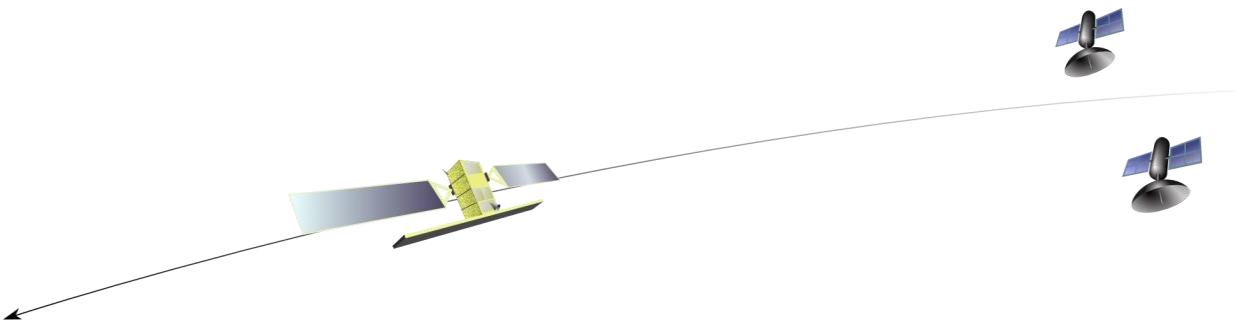

Figure 7: Cartoon illustrating SESAME's configuration, with the two SESAME spacecraft flying in close formation relative to each other, and in a loose formation with respect to a Sentinel-1 satellite.

SESAME´s system concept is to build a single-pass cross-track SAR interferometer using two receive-only C-band radar satellites flying in close formation relative to each other, and at an along-track distance of roughly 200 km with respect to Sentinel-1C or D, which will be used as a transmitter of opportunity. The dual spacecraft solution is seen as the most efficient and technically feasible solution to build an interferometric companion to Sentinel-1. Formation flying provides the opportunity to dynamically reconfigure the measuring apparatus according to specific observational requirements. The present mission concept foresees a synchronization link (between companions) for mutual synchronization (similar to TanDEM-X) and individual downlink capabilities for each of the companion satellites, competing with the available downlink resources of the Sentinel-1 master satellite. As customary in state-of-the-art SAR missions, on-board processing is limited to BAQ-based data compression.

5.3.3 General multi-static constellations

As sufficiently discussed in the previous section, a bistatic SAR is a distributed system that has separate antennas for transmission and reception. In the case of spaceborne radars, this separation of the antennas usually becomes a separation of instruments and spacecraft. Multi-static SAR is a constellation of monostatic and bistatic SARs which can benefit from the availability of more

transmitters and receiver channels for boosting the performance of the system. In particular, multi-static constellations may have improved revisit times, access, image throughput, swath width, resolution, and imaging capabilities. Figure 8 shows an example of a multi-static constellation with a transmitter satellite (in yellow) and several companion satellites with generic baselines.

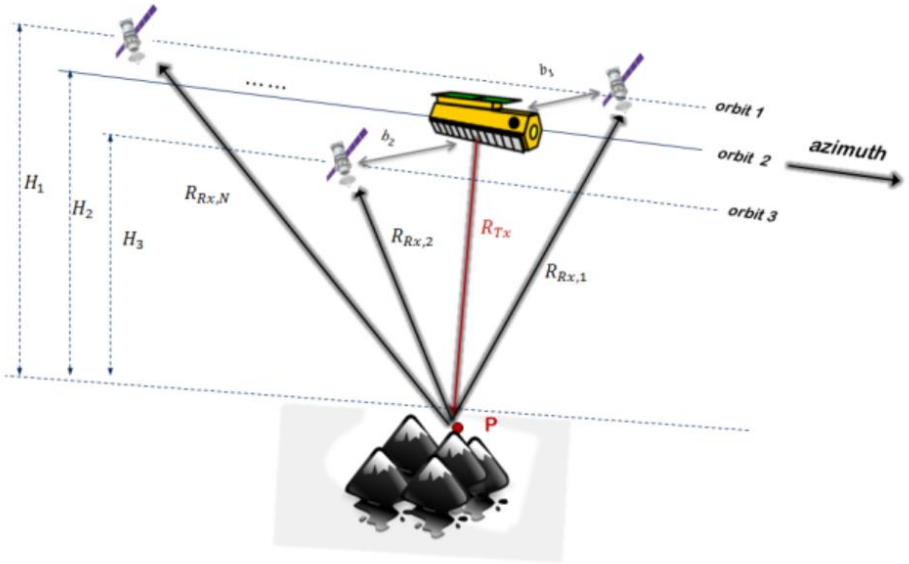

Figure 8: Schematic view of a general multi-static constellation with both along-track and across-track separation between satellites.

Depending on whether one or several transmitters are available, the multi-static constellation can be classified as a single-input multiple-output (SIMO) or multiple-input multiple-output (MIMO) system. The combination method discussed in the next section assumes an along-track geometry, whereas reconstruction approaches accommodating the across-track baselines are topography sensitive and need to account for the differential migration and spectral shift of the SAR data (Rodriguez-Cassola, et al., 2013).

The processing of multi-static SAR data depends on the intended applications of the mission. However, from a SAR processing point of view we can aim at separating these in two main groups:

- The data of the bistatic units of the multi-static constellation are sampled over Nyquist.

  Classical bistatic SAR image formation techniques can be applied on the data, and the combination of the focused data shall occur at image level. Resolution enhancement techniques (Prati & Rocca, 1992) (Massonet & Souyris, Imaging with Synthetic Aperture Radar, 2008) (Prats, et al., 2011) for general homogeneous scenes happen typically in a dense signal space. Other applications like layover solving and urban tomography are rather on a sparse signal space paradigm (Gini, Lombardini, & Montanari, Oct 2002) (Zhu & Bamler, 2010) (Fornaro & Serafino, 2006).

- The data of the bistatic units of the multi-static constellation are sampled under Nyquist

  There are numerous advantages of radar data acquisition under Nyquist, e.g., data-rate reduction, improved performance, or interrupted (more silent) operation. The improvement of the radar performance by sampling under Nyquist is based on the idea of twisting the

well-known time-frequency trade-off of SISO radars (Skolnik, 1980). In particular, as discussed in previous sections, the pulse repetition frequency (PRF) of the constellation can be reduced -hence increasing the available unambiguous swath while keeping the effective PRF (after reconstruction) over Nyquist for higher azimuth resolution.

5.3.3.1 The distributed SAR missions scenario

This concept is based on a cluster of satellites separated by an along-track baseline. As discussed in section 5.3.1, there is always the quest to realize high geometric resolutions combined with large cross-track coverage. Distributed SAR configurations reduce the PRF by substituting virtual antenna phase centre positions with physical ones. The pulse repetition frequency of the configuration PRF_{conf} is reduced in comparison to a single satellite SAR system and this allows for a swath width increase, see e.g. (Krieger & Moreira, Spaceborne bi- and multistatic SAR: potential and challenges, 2006).

The dispersed SAR concept discussed here is based on an along-track configuration of n SAR satellites, each capable of transmitting and receiving. The pulse transmission is alternating between the individual satellites, whilst all satellites receive the echoes of all transmitted pulses. In (Mittermayer, Lopez-Dekker, Kraus, & Krieger, 2016), it was shown how it is possible to distribute a large synthetic aperture onto several small satellites with realistic inter-satellite along-track separations larger than 150 m while maintaining a gap-free azimuth sampling. The so-called *Dispersed SAR* is based on a deterministic description of the azimuth positions of the small satellites at the time instants of transmission and reception. Figure 9 shows a possible transmit scheme with a small number of satellites, i.e. 5. The sequence of pulse transmitting satellites is from left to right, continuing from the rightmost satellite back to the leftmost. The satellite velocity direction is from left to right. The phase centre positions resulting from the transmit positions in green and the receive positions in red are indicated by a blue cross. The numbers above the phase centre positons describe the along-track orbital distance in multiples of a reference distance.

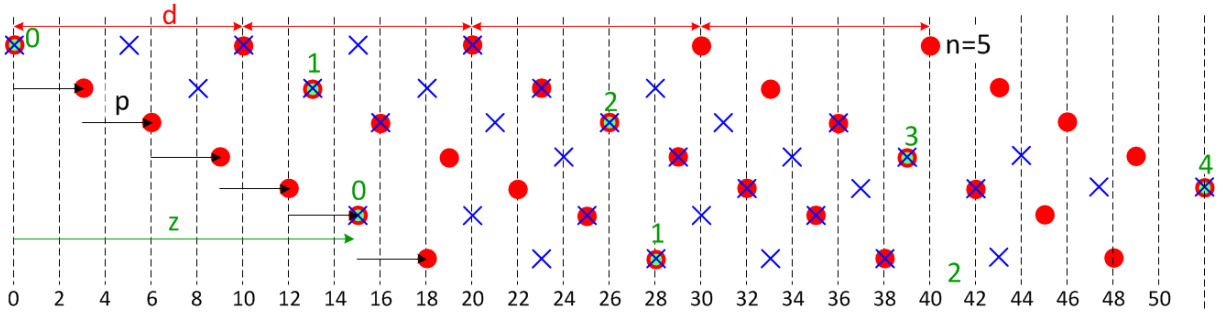

Figure 9: Example Dispersed SAR Configuration Pulse Transmission and Reception

As indicated by the black arrows, the whole constellation moves in-between two consecutive tx-pulses by the configuration repetition interval p, the inter-satellite separation is d and after a cycle z, the first satellite in the constellation repeats to transmit.

5.4 Qualitative Description of Radar Based EO Application Demands

5.4.1 Benefits of On-board SAR Image Processing

With new technological developments, SAR image formation can be partly shifted from the ground segment to on-board computers, thus better supporting real-time and near real-time services.

Especially for SAR sensors with their weather independent day and night imaging capability, this appears as the logical next step.

Consider first the example of a single SAR data acquisition: for a TerraSAR-X standard stripmap mode product of 3m resolution covering an area of 30km by 100km the data amount for downlink is approx. 1.2 GByte (assuming 4-bit BAQ quantisation). Within the ground segment this is processed within few minutes into a basic Level-1 product (single-look-complex - SLC) having a size of 6GByte and requiring approximately 200 GFLOP (giga floating point operations). However, for most NRT (near real-time) application purposes multi-looked and speckle filtered data are being used. In this case the data amount can be easily reduced to less than 100 Mbyte (more than one order of magnitude less compared to the initial raw data volume). Thus, considering that data downlink is presently the main bottleneck for high resolution SAR missions (and will likely be in future) one may define the first two radar use cases within S3Net as "*Generation of focused, high resolution generic SAR images" and "Multi-looking of focused SAR images for efficient downlink in support of near-real time applications*".

Although this sounds very appealing, there are plenty applications requiring SLC data. In this case some application-specific Level-2 processing might also be shifted to the space segment, which will further reduce the amount of data for download. For example, the wave-mode of Sentinel-1, designed for oceanographic applications, produces the L2-OCN product (comprising wind, wave and current information) with data size for one vignette (20km x20 km) in the order < 0.1 Mbytes, whereas presently the raw data size of one vignette is > 100 Mbyte (a factor of 1000!). Also L2 processors for ship and oil spill detections might be implemented on board, such that only the detection results are downlinked to Earth. This would than cover most of the maritime/oceanographic applications. A third radar use case within S3Net would thus be "*Level-2 product generation for maritime/oceanographic applications*".

Considering the diversity of land applications, the situation is slightly different, especially when considering the interferometric case, which requires single-look complex data. In this case one can assume that only parts of a scene are of interest (regions of interest - ROI) and need to be mapped regularly, whereas other parts require no mapping or at much reduced intervals. In these cases only the SLC data of the ROIs are transmitted to ground, which might correspond to less than 10% of the whole scene. For the TerraSAR-X example above this would correspond to 600 Mbyte to be transmitted to ground instead of the 6GByte SLC data of the full scene or the 1.2GByte of the raw data. One could imagine for example the "permanent scatterer subsidence measurement scenario", where only a city area is of interest and all of the surrounding and even the inner-city parks and lakes can be neglected. A forth radar use case would then be entitled "*ROI defined full resolution mapping for land applications*".

5.4.2 Digital Beamforming in Elevation

An advanced SAR technique, which is proposed to overcome the azimuth resolution vs. swath width trade-off, uses multiple independent receive channels in elevation. First thoughts have been already published in patents by Blythe in (Blythe, 1979) and by Kare in (Kare, 1998). Both propose analogue beam-steering in elevation with a phased-array antenna to follow the echo, which arrives just from a small angular interval compared to the whole illuminated swath. This technique was named *sweep SAR*. The same concept was extended by DBF in a patent by Suess et al. in 2002 (Suess M. a., 2002). This proposal is known under the name SCan-On-REceive (SCORE) and receives high attention in the

DBF-SAR community. Numerous publications (Feng He, 2014) (S. Huber, 2012) and purposeful proposals for spaceborne missions using this technique, were published in recent years (e.g. Tandem-L (Moreira, et al., 2015), Sentinel-NG, TerraSAR-NG (Adamiuk, Schaefer, Fischer, & Heer, 2014)). The advantages of SCORE are as follows:

- Increased SNR due to spatial filtering of noise from directions without any echo
- Known relation between AoA and ToA leads to the ability of suppressing range ambiguities
- Separation of spatio-temporal transmit waveforms in MIMO-SAR becomes possible (see (Krieger G. , MIMO-SAR: Opportunities and Pitfalls, 2014), (Tobias Rommel, 2014))

In the proposed technique, on transmit a short antenna with a broad Half-Power Beam-Width (HPBW) is used to illuminate the whole swath. Whereas on receive, a Uniform Linear Antenna (ULA) array in elevation is used (cf. Figure 10). On receive, due to the side-looking geometry, each point on the ground is seen under a different look angle. For a known topography, the relation between Time of Arrival (ToA) and Angle of Arrival (AoA) can be derived and a directional beam, following the expected response on the ground, can be synthesized. In the receiver, all elements of the planar array antenna are activated forming a high gain narrow beam. Time-variant digital phase shifters steer the antenna beam to the wanted AoA.

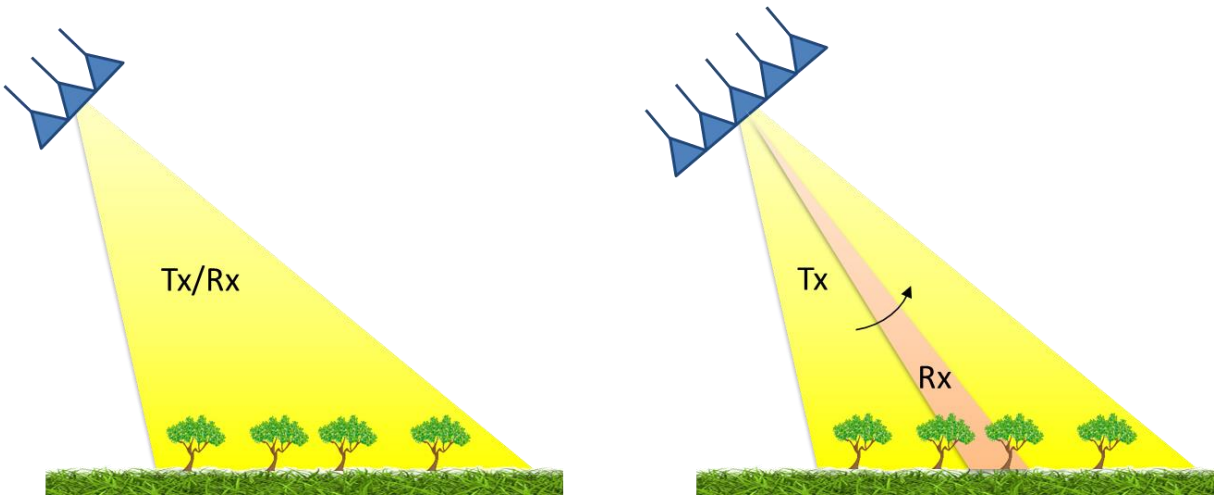

Figure 10: Left-hand side: Wide area illumination on transmit and receive with a small antenna aperture. Right-hand side: Wide area illumination on transmit and narrow receive antenna beam, which traces the echo signal on the ground.

The time-variant digital phase shifters need to work in real-time and realisation concepts/breadboard demonstrators presented so far make use of already space-qualified FPGA technology for the phase shifters, but convert the modified digitized signals of the individual receivers back to analogue ones for the subsequent addition (Adamiuk, Heer, & Ludwig, DBF Technology Development for Next Generation of ESA C, 2016). Without this on-board processing capability, the amounts of data of a SAR sensor with SCORE capability will be increased by the number of receive channels compared to a traditional sensor. This dedicated radar use case is entitled "*Beamforming for Scan-on-Receive*".

5.4.3 Processing of Multiple Azimuth Displaced Phase Centre Signals

The utilization of multiple phase centres in azimuth direction offers the ability to reduce ambiguities and therefore acquire wide swathes with high azimuth resolution. The usage of multiple azimuth channels for high-resolution wide-swath SAR imaging was proposed by (Currie & Brown, 1992) and called displaced phase centre (DPC) technique. SAR imaging modes employing a DPC antenna (DPCA)

are also said to offer multiple azimuth phase centre signal (MAPS) capabilities (Janoth, Gantert, Schrage, & Kaptein, 2013).

The SAR system transmits with a single, broadened (by tapering) azimuth antenna beam. In receive direction the aperture of the SAR antenna is divided in N (N≥2) sub-apertures. The corresponding receive antenna beams are assumed to coincide in the far-field region and to cover the same angular range as the transmit (Tx) antenna beams. A sketch of the scheme is shown in Figure 11 for a system with N= 3 receive (Rx) beams.

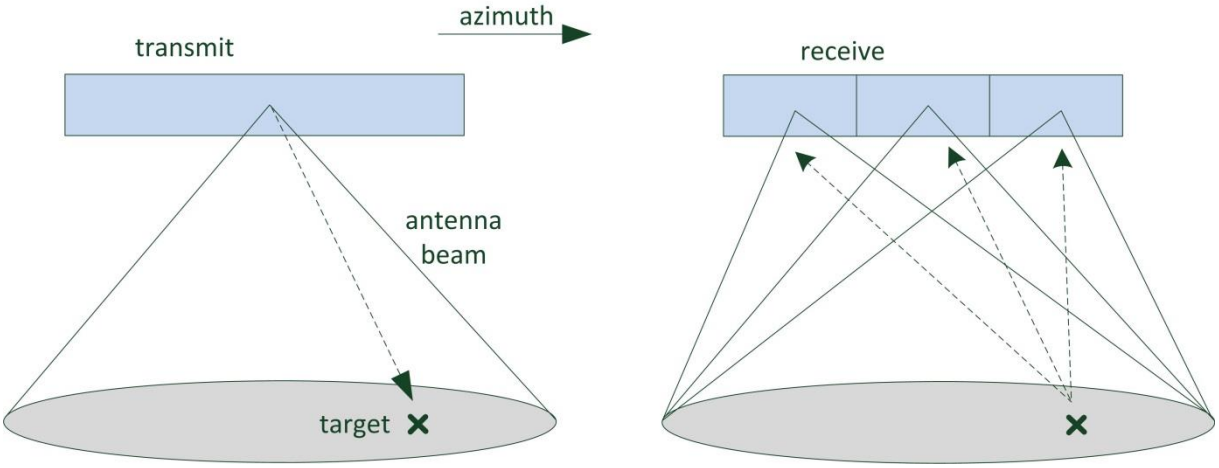

Figure 11 Displaced phase centre technique according to (Currie & Brown, 1992). Transmission with a single beam on the left and reception of the targets echo by several (here three) displaced azimuth beams on the right.

The signals of the sub-apertures are treated as separate channels. Each channel is down-converted, digitized and recorded. Consequently the system is gathering N echoes for each transmitted pulse, effectively increasing the sampling rate by a factor of N. This is true, if the pulse repetition frequency (PRF) is adjusted in a way that the sub-aperture spacing together with the satellite velocity leads to a regular sampling in the along-track direction. The spatial sampling for an example with five Rx-beams is depicted in Figure 12. The equivalent Tx/Rx positions are a result of the typically bistatic acquisition geometry. The Tx phase centre is in the centre of the whole antenna aperture. The Rx phase centres are in the centre of the sub-apertures, leading to equivalent sampling positions in the middle between the Tx and the Rx phase centres. If the whole SAR platform moves half of the antenna length between the transmissions of two consecutive pulses, the spatial sampling is regular. Then, a simple interleaving of the channels can be used to form a signal virtually sampled with the effective sampling rate $PRF_{eff} = N \cdot PRF$. The effectively increased sampling rate can be used to improve the azimuth resolution at a constant swath width. Another option is to decrease the PRF and therefore to enable a larger swath width without impairing the azimuth resolution while an acceptable amount of azimuth ambiguity-to-signal ratio (AASR) is maintained. Generally, the achievable resolution is defined by the size of the single sub-apertures whereas the whole azimuth antenna aperture size contributes to the attainable AASR.

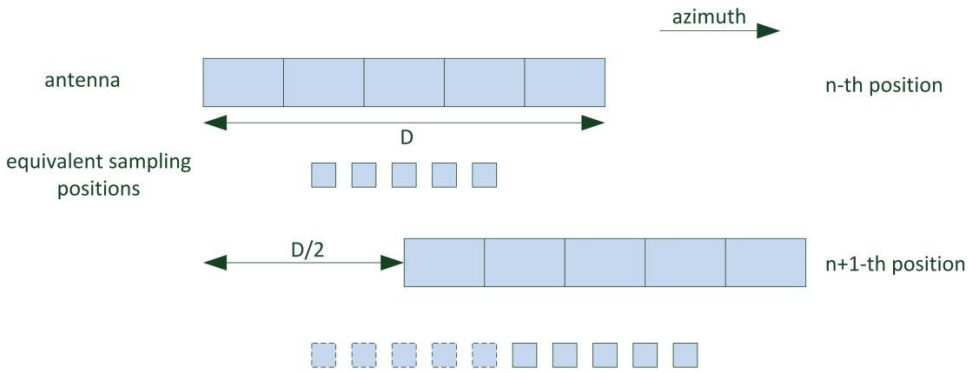

Figure 12 DPC sampling according to (Currie & Brown, 1992).

Any deviation of a regular sampling in azimuth direction leads to a degradation of the SAR performance. This causes stringent requirements on the selection of the PRF together with the sub-aperture spacing and the satellite velocity which might be in conflict with timing constraints of the system. However, a reconstruction algorithm for non-uniformly displaced phase centre sampling has been proposed (Krieger, Gebert, & Moreira, Unambiguous SAR Signal Reconstruction From Nonuniform Displaced Phase Center Sampling, 2004), (Gebert, Krieger, & Moreira, 2009). The algorithm is based on work of (Brown, 1981) and can be regarded as a time-variant beamforming on receive. Since it contains a matrix inversion step, this algorithm is called the matrix inversion method in (Cerutti-Maori, Sikaneta, Klare, & Gierull, 2014). Prior to the reconstruction of a single data stream out of multiple azimuth channels a channel balancing has to be applied in the frequency domain, i.e., after a Fourier transform (Gierull, 2003). This procedure removes phase and amplitude imbalances between the channels induced by the instruments hardware and can be regarded as a digital calibration (Younis, Laux, Al-Kahachi, Lopez-Dekker, Krieger, & Moreira, 2014). The high-level block diagram of the reconstruction approach is shown in Figure 13 for the case of N=3 displaced channels. Each channel is sampled by the PRF followed by a FFT in azimuth. For each Doppler bin the data are combined by using N different weights, which need to be computed through matrix inversion from parameters of the transfer functions of the different receive channels. The size of these square matrices corresponds to the number of receive channels (i.e. 3x3 in the Figure example), i.e. it is rather small. The filtered signals are later recombined to generate the full resolution azimuth signal. A calculation of the filter weights might be advisable at least once per acquisition (depending on the acquisition length). The usable PRF and the satellite velocity which determine the special sampling are varying over the orbit and therefore require updated weights. An update over the range direction is not necessary.

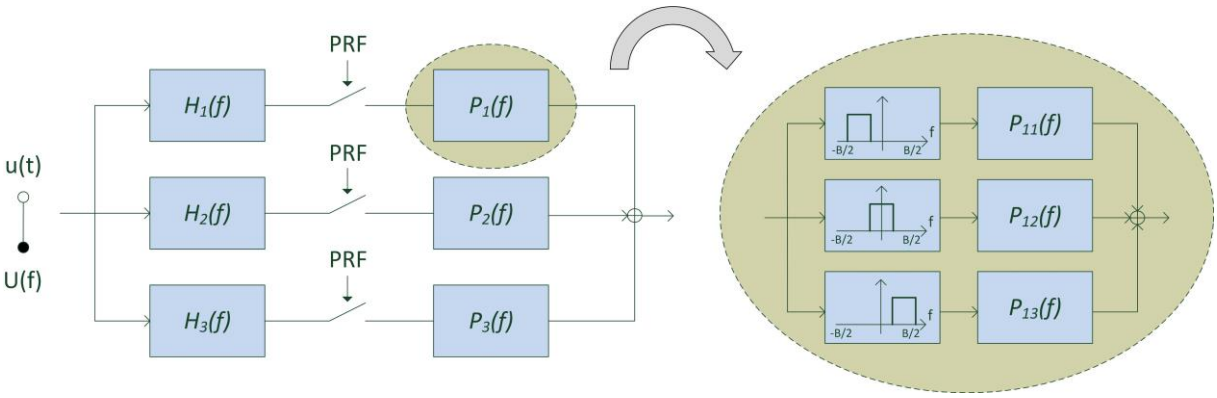

Figure 13: Reconstruction algorithm for non-uniformly displaced multiple azimuth phase center signals.

The applicability of the multi-channel reconstruction algorithm to actual space-borne SAR data has already been demonstrated with the TerraSAR-X (Kim, Younis, Prats-Iraola, Gabele, & Krieger, 2013) and cross-platform TanDEM-X systems (Kraus, Bräutigam, Bachmann, & Krieger, 2016). However, so far all processing has been performed on-ground, after the downlink of the complete multi-channel dataset. In the context of multi-channel SAR, on-board processing could offer the unique capability to reduce the amount of data for applications which demand an azimuth resolution coarser then the nominal one, e.g., ship monitoring. In this case the reconstruction algorithm for non-uniformly displaced phase centre sampling has to be implemented on-board and executed prior to image formation according to section 5.4.1. Only with this combination there is a potential for data volume reduction, as the reconstruction algorithm itself does not reduce noticeably the amount of samples. This dedicated radar use case is entitled "*Azimuth resampling for non-uniformly sampled DPC signals*".

5.4.4 Staggered SAR Data Resampling and Decimation

Staggered SAR is an innovative concept, based on multiple elevation beams and continuous variation of the pulse repetition interval (PRI) (Villano, Krieger, & Moreira, Staggered SAR: High-Resolution Wide-Swath Imaging by Continuous PRI Variation, 2014.) If the PRI is continuously varied, even in a cyclical manner, i.e., repeating a sequence of PRIs, there will still be ranges, from which the echoes are not received, because the radar is transmitting, but in general those ranges will be different for each transmitted pulse (Figure 14). If the PRIs of the sequence are selected such that two consecutive samples in the azimuth direction are never missed and the signal is averagely oversampled in azimuth, it is possible to accurately interpolate the data on a uniform grid and obtain a high resolution SAR image over a wide continuous swath.

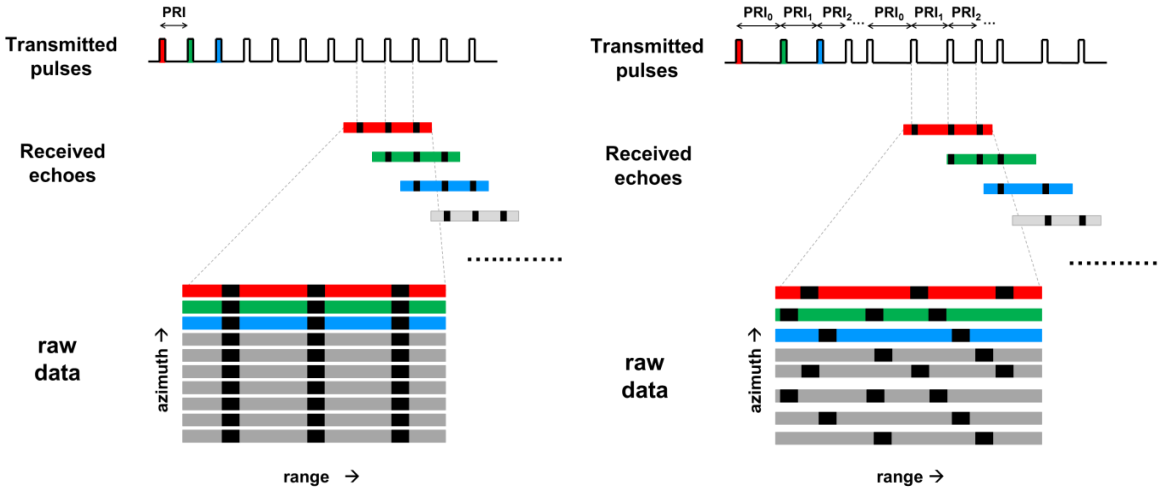

Figure 14: Location of blind ranges. (a) Constant PRI SAR. (b) Staggered SAR.

In particular, the sequence of PRIs has to be designed such that two consecutive azimuth samples are never missed within the imaged swath. Moreover, data have to be averagely oversampled in azimuth. The maximum distance between consecutive available azimuth samples is therefore bounded such that best linear unbiased (BLU) interpolation, can be used to recover uniformly sampled data, which, after SAR focusing, are still characterized by an acceptable level of azimuth ambiguities. Another essential point is that data have to be resampled before range compression, as discussed in (Villano, Krieger, & Moreira, A Novel Processing Strategy for Staggered SAR, 2014). As data are oversampled in azimuth, range ambiguous echoes come from directions closer to that of the desired signal in comparison to a SAR system with constant PRI, but their energy is incoherently integrated and partially filtered out during the SAR processing (Villano, Krieger, & Moreira, Ambiguities and Image Quality in Staggered SAR, 2015).

In order to meet typical azimuth ambiguity requirements, a staggered SAR system needs to employ a high mean PRF on transmit, i.e., data are to be oversampled in azimuth. This causes an increased data volume, which can be, however, reduced by on-board Doppler filtering and decimation (Villano, Krieger, & Moreira, Data Volume Reduction in High-Resolution Wide-Swath SAR Systems, 2015).

This data volume reduction strategy can be better understood considering first the case of a SAR system with constant PRI. If data were just decimated prior to downlink (e.g., by a factor of 2 if the PRF is larger than twice the processed Doppler bandwidth (PBW)), a considerable degradation of the AASR would occur. Figure 15 (a) shows the power spectral density (PSD) of the azimuth SAR signal at near range for a reflector antenna. The PSD is the joint transmit-receive antenna pattern displayed as a function of Doppler frequency. The unambiguous energy, the ambiguous energy, and the additional ambiguous energy due to the decimation are highlighted in green, red, and blue, respectively. As is apparent, the additional ambiguous energy due to decimation is significant, i.e., the total ambiguous energy is the same obtained for half the PRF. However, if Doppler filtering is performed before decimation, the additional ambiguous energy due to decimation can be substantially reduced, as shown in Figure 15 (b).

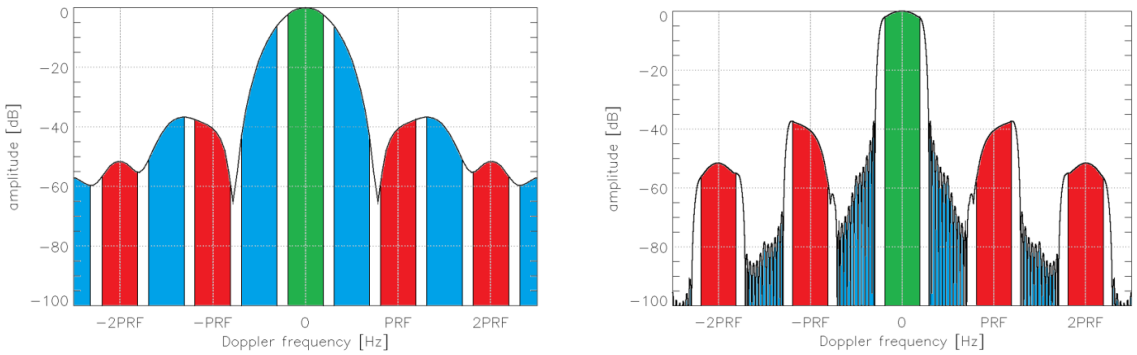

Figure 15: PSD of the azimuth SAR signal at near range for a reflector antenna. The energy of the unambiguous component, the ambiguous components, and the additional ambiguous components due to decimation are highlighted in green, red and blue, respectively. (a) Only decimation (no Doppler filtering). (b) Doppler filtering and decimation.

Due to the large amount of data, acquired by typical HRWS systems, the number of on-board operations per sample has to be minimized, while avoiding a degradation of the impulse response. The Doppler filtering can be therefore performed in time domain using a finite impulse response (FIR) filter with a relatively small number of taps. The filter will introduce a distortion of the Doppler spectrum of the signal, which can be compensated for in the SAR processing (on ground). The case of decimation by an integer factor is usually considered, as this is associated with a straightforward implementation and a much lower computational cost, but the proposed strategy can be also used in case of a rational decimation factor.

In a staggered SAR system, the Doppler filter has to be applied to raw data resampled to a uniform PRI, but, in practice, resampling, Doppler filtering, and decimation can be also jointly performed, as explained in the following. Figure 16 (a) shows how in the staggered SAR case the filtering has to be applied on resampled data, which are obtained from the raw staggered SAR (non-uniformly sampled) data through BLU interpolation. Each sample of the resampled data is obtained as a linear combination of some of the samples of the raw staggered SAR data, while each sample of the filtered data is obtained as a linear combination of some of the resampled data. This means that each sample of the filtered data can be obtained directly as a linear combination of some of the staggered SAR data (Figure 16 (b)). Moreover, there is no need to compute the samples, which would anyway be discarded by the decimation operation.

The radar use case associated to the staggered SAR processing is entitled "*Resampling and decimation for Staggered SAR*".

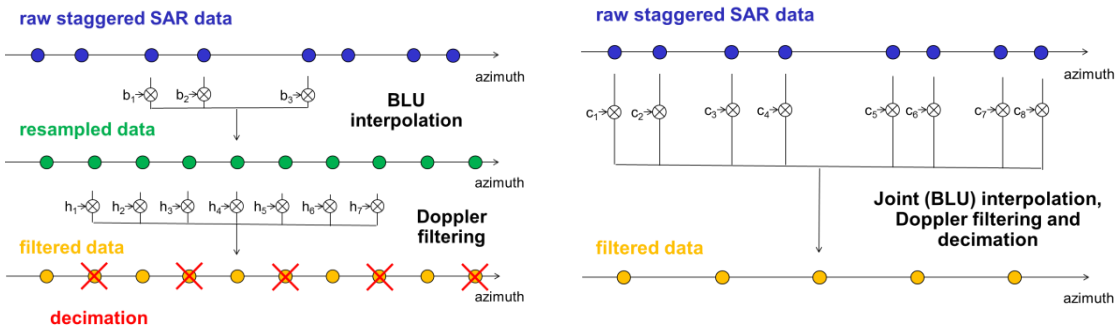

(a) (b)

Figure 16: (a) Interpolation, Doppler filtering, and decimation in the staggered SAR case. (b) Equivalent scheme, where interpolation, Doppler filtering, and decimation are jointly performed.

5.4.5 On-board synchronisation of companion satellite missions for high-resolution bistatic SAR imaging

As already discussed in previous sections, bistatic geometries offer many advantages with respect to the monostatic counterparts, e.g. , flexible observation geometries, silent operation, and the single-pass interferometric information. The latter two have already been identified as particularly benefitting from on-board processing capabilities. However, the use of two separate clocks in transmitter and receiver cause uncompensated time and phase errors in the bistatic radar data which pose a fundamental challenge in real time bistatic SAR imaging applications. As a rule of thumb, the typical accuracies in the estimate of the time and phase errors of a bistatic channel can be scaled to a few degrees.

Real-time on-board synchronisation of bistatic SAR data can be effected in three different ways:

- Using an external time reference (e.g., GNSS system) which is compared to the exact timing scheme of the instrument. GNSS-based synchronisation is computationally cheap and typically requires a low-order regression of the timing values of the radar pulses. Typical accuracies of this approach allow for a coarse estimate of the carrier offset between the instrument and the GNSS source.
- Using the signal transmitted through a direct link (Braubach & Völker, 2007), where the time and phase errors between the different clocks are estimated by means of a range-Doppler processing. The computational cost is at worst that of a range compression and interpolation.
- Using a data-based approach such as AutoSync (Rodriguez-Cassola, Bistatic synthetic aperture radar data processing, 2013), where the distortion of the bistatic image is locally estimated and used for the inversion of the time and phase errors of the clock.

The real-time synchronisation on-board the receiver of a bistatic or multistatic constellation is mandatory for on-board SAR image formation and is identified as a radar use case for S3NET: "*Real-time synchronisation of time and phase*".

5.4.6 Data volume reduction for single-pass interferometric satellite missions

The SESAME mission proposal foresees transmission to ground of 2 additional SAR raw data sets, one for each companion satellite, which would add almost a factor of 2 to the already considerable amount of data of Sentinel-1. Instead it could be advantageous to exploit the redundancy of the two

channels by means of a proper data volume reduction. Similar to the VERITAS-VISAR concept the two raw data sets could be focused on-board and interferometrically combined. Only the residual filtered interferogram, the coherence maps and the multi-look images need to be transmitted to ground. For this purpose the bistatic SAR focusing algorithms, the synchronisation processing and the complete interferometric processing (incl. co-registration, back-geocoding, phase flattening, and interferogram generation) would need to be made in space. The effort in on-board processing is only second to the savings in downlink resources; e.g. instead of 2 raw data streams of 1 GByte each, only 3 data sets of approx. 50-100 Mbyte would need to be downlinked. Performing the processing in space also requires that very precise (relative) orbit information is available, to allow synchronisation and co-registration without any performance loss in coherence. The associated radar use case is entitled "*On-board interferogram computation*".

5.4.7 Parametric interpolation of SAR data acquired in interrupted operation

Interrupted operation of SAR systems can be a consequence of power savings, partially silent operation, exchange of calibration information, or burst-mode operation scanning through different areas of the imaged scene. A parametric interpolation of the interrupted data may allow (Salzmann et al, TAES 2003) for a resolution enhancement in urban areas. The approach is based on the estimation of a parametric model fitting the spectral content of the data. The computational cost is that of a range-dependent solution of a linear system of order 5 to 10 specific for the acquired data.

5.4.8 Demands of distributed SAR systems

Opposite to the computational requirements of HRWS systems, the distributed SAR concepts primarily pose communication and formation flying demands.

In order to estimate some order of magnitudes for key parameters of the concept described in section 5.3.3.1, Figure 17 introduces the dispersed system example geometry with an orbit height of 1500 km. It shows a SAR configuration in stripmap mode. The individual satellites of the configuration fly in a SAR-train configuration along exactly the same orbit, with an equidistant separation d in along-track but without cross-track separation or cross-track baseline (Aguttes, 2003).

For example, in X-band with more than 10 satellites carrying antennas in the order of 1 m^2, an azimuth resolution of about 1 m can be achieved together with a ground range swath width in the order of 100 km. In the geometry of Figure 17 with incidence angles from 17° to 59° the accessible area on the ground is about 1300 km in ground range. A reasonable transmit peak power per satellite is in the order of 1 kW which appears high but on the other hand, the mean transmit power per satellite is only in the order of 10 W due to the configuration, in which transmit pulses alternate between the satellites and the radar echoes are received from all satellites.

The along-track inter-satellite separation can be more than 150 m and the required *relative* along track position accuracy of each individual satellite should be in the order of few decimetres (Mittermayer, Lopez-Dekker, Kraus, & Krieger, 2016). There are good techniques, e.g. (Krieger, Gebert, & Moreira, Unambiguous SAR Signal Reconstruction From Nonuniform Displaced Phase Center Sampling, 2004), to deal with the remaining small irregular phase centre sampling at the formation of the synthetic aperture in the SAR processing.

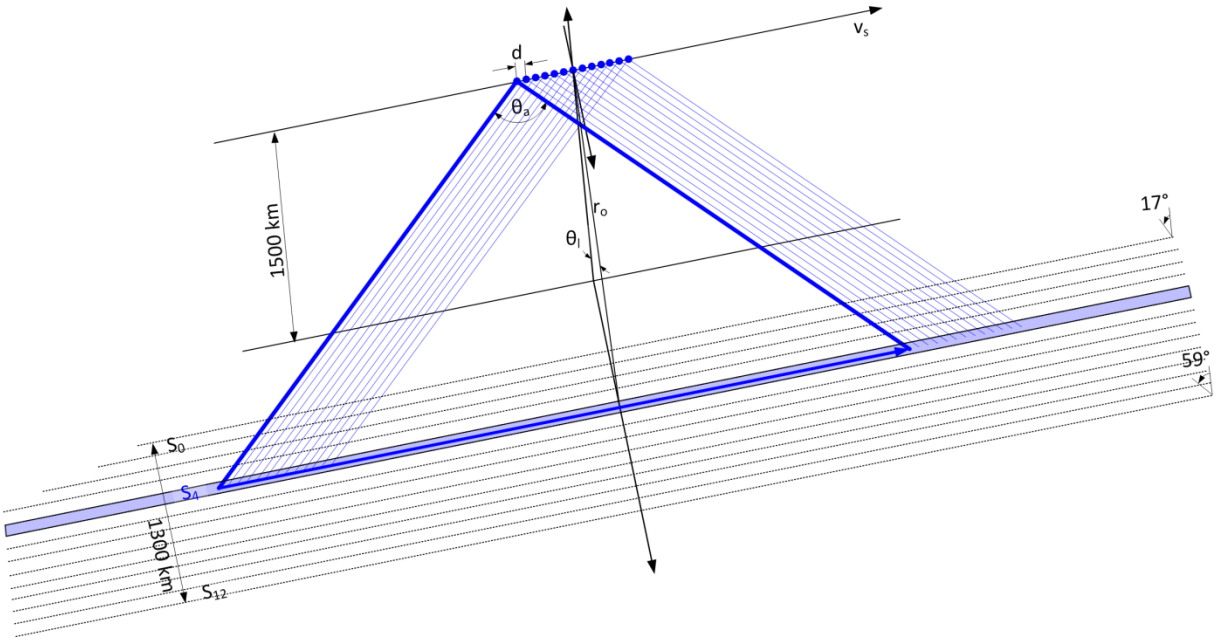

Figure 17: Example Dispersed SAR Configuration

For the example under discussion, and a ground range resolution in the order of 1m, the raw data rate that each satellite receives is in the order of 400 Mbit. This data rate has to be sent by each satellite either to ground, to a relay satellite or to a central on-board processing & downlink satellite that has to be added to the configuration. A decentralized on-board processing capability hosted by one of the satellites might be of advantage. For SAR image formation the algorithm described in section 5.4.3 must be adapted to the multi-platform environment and amended with synchronization operations to take into account the differentially drifting clocks of the individual receivers.

5.5 Summary of radar use cases and selection of applications for S3NET

5.5.1 Summary of radar use cases and selection of applications for S3NET

The following table summarizes the investigated radar use cases and identifies high level requirements for on-board processing, communication and formation control.

Use case	Radar Use Case	Requirements			Depen-dency
		computational / algorithmic	Commu-nication	Formation Flying	
1	*Generation of focused, high resolution (bistatic/generic) SAR images*	FFT, complex data interpolations	-	-	- (4 for SCORE systems; 5 for MAPS systems)
2	*Multi-looking of focused SAR images for efficient downlink in support of near-real time applications*	Detection (floating point additions and multiplications) & averaging			1
3	*Level-2 product generation for maritime/oceanographic*	FFT, statistical analysis	-	-	1

Use case	Radar Use Case	Requirements			Depen-dency
		computational / algorithmic	Commu-nication	Formation Flying	
	applications				
4	*ROI defined full resolution mapping for land applications*	geometry (sqrt, sin, cos), interpolations	-	-	1
5	*Beamforming for Scan-on-Receive*	Complex multiplications (real-time)	-	-	-
6	*Azimuth resampling for non-uniformly sampled DPC signals*	FFT, matrix inversion	-	-	-
7	*Resampling and decimation for Staggered SAR*	FIR filter with changing coefficients	-	-	-
8	*Real-time synchronisation of time and phase*	Linear regression Pulse compression SAR imaging and coregistration	availability of sync information from the other companion satellite	knowledge of baselines (rel. orbit positions)	-
9	*On-board interferogram computation*	Interpolations for resampling, geometry (sqrt, sin, cos), complex multiplications, floating point operations	Transfer of data to common compute node	Precise knowledge of (relative) orbits; req. accuracy depends on chosen baseline	1,8
10	*Dispersed SAR formation control*	-	low data rate position exchange	Along-track separation of 150m or more; relative along-track position knowledge in the order of 20cm; no cross-track baseline	
11	*Dispersed SAR image formation*	FFT, complex data interpolations, matrix inversion	400 Mbit/sec inter-satellite data link; low data rate command coordination link at 1Mbit/sec	Precise orbit position knowledge	6,1,8

Table 5: Summary of identified radar use cases

5.5.2 Selection of radar use cases for further investigation within S3NET

From the table above the following two primary radar use cases are selected for further evaluation:

- *Resampling and decimation for Staggered SAR (7):* This use case requires few operations per data sample and is considered of low implementation complexity. It may become of urgent need in case the Tandem-L formation flying mission concept is selected for implementation.
- *Generation of focused, high resolution (bistatic/generic) SAR images (1):* This use case is selected as it represents the basis for all other high performance formation flying use cases. It is considered of relatively high implementation complexity as it requires one order of magnitude larger computational effort.

Further, in order to better serve the purposes of S3NET, the following additional use cases shall be considered for a more detailed evaluation and quantification:

- *Real-time synchronisation of time and phase (8):* This use case is mandatory for the bistatic SAR image formation (e.g. in case of Rx-only companion satellites) and is of relatively low computational complexity.
- *Multi-looking of focused SAR images for efficient downlink in support of near-real time applications (2):* This use case is essential for data rate reduction for downlink. It requires only few operations per data sample.
- *Dispersed SAR formation control (10):* One of the critical issues in cross-platform SAR imaging is the ability to precisely control the formation. A suitable orbit choice is mandatory to keep the amount of manoeuvres at a minimum. The requirements for cross-platform SAR imaging shall be quantified.

5.5.2.1 Resampling and decimation for Staggered SAR

A publication on algorithms details is (Villano, Krieger, & Moreira, Data Volume Reduction in High-Resolution Wide-Swath SAR Systems, 2015).

The Doppler filter for staggered SAR requires saving the coefficients to weight the input data and performing multiplications and summations to produce the output data. The coefficients are different for each range and azimuth sample, but they repeat in azimuth after a number of samples equal to the number of PRIs of the sequence (in the order of 300). It has been estimated that a memory in the order of few Gbit is required for the Tandem-L staggered SAR system.

5.5.2.2 Generation of focused, high resolution generic SAR images

A good summary on SAR image focusing algorithms can be found in (Cumming & Wong, 2005). For near future SAR systems one single data acquisition corresponds to complex valued data matrices of several tens of thousands (range) by several tens of thousands (azimuth) samples (i.e. 1-100 GByte, depending on the sensor's frequency band and imaging mode). The on-board processing involves FFTs, complex data multiplications and interpolations. Usually good parallelization is possible; however, depending on hardware properties corner turns might be required.

6 REQUIREMENTS COLLECTION AND ANALYSIS

Definition and Comparison of Application attributes. Partners need to make sure that as many as possible potential constellations are covered by the collection of applications.

SAR	Optical
Attributes: - Few satellites. - Large payload/throughput. - Planned to process data jointly. - Different master slave configuration. - For now mainly science driven apps. - Challenge: consecutive downlink for close formations (up to 100km).	Attributes - Several satellites (max.10). - Medium payload/ throughput per satellite. - Jointly large throughput. - No joint processing. - (maybe) compression on each satellite, transmission through master satellite to ground station. - Challenge: attitude control for directed antenna configuration. - Commercially/institutionally driven - Sun synchronized orbits (dependency on light fuel consumption limitation needed)

6.1 Requirements for Formation Flying

Single satellite missions are typically designed to occupy a particular orbit about which periodic station keeping manoeuvres are conducted. This same approach can be extended to formations in which each satellite in the formation is controlled to a particular predetermined desired orbit. This approach is attractive from the perspective of allowing little or no cooperation or coordination between the spacecraft; however, it is expected to require more fuel than methods that exploit the coupled nature of mission objectives.

In leader/follower coordination methods, one leader spacecraft is controlled to a reference orbit and the other follower spacecraft in the formation control their relative states to that leader. This approach allows traditional periodic manoeuvres to keep the leader in a desired orbit or ground-track while the remaining satellites in the formation control their relative state with respect to the leader. This approach has the advantage that it allows most satellites in the formation to follow the natural dynamics of the absolute orbit of the leader, while only performing regular automatic control on the relative states of the formation. A number of researchers have proposed simple heuristic control laws for arranging arbitrarily large number of vehicles into regular arrangements based on local information. These swarming methods have the advantage that they easily scale to large numbers of vehicles without incurring large communication or computation burdens. However, they are typically not fuel-optimal and rarely include provisions guaranteeing collision avoidance.

Minimizing fuel use is critical in any space mission, because fuel is expensive to launch into orbit and non-replenishable. Fuel use is a primary concern in the design of any spacecraft formation controller, because the task of keeping a formation from drifting apart and achieving science requirements is expected to require significantly more fuel than station keeping a single spacecraft.

Several types of formation flying missions have been proposed: Interferometry, passive-aperture radar, and repeat ground-track observations. Each of these missions requires varying degrees of control to achieve observation objectives. Proposed interferometry missions require control of the

spacecraft's relative position with fine precision and to specific geometric templates. When the required geometry of a formation dictates that natural orbital perturbations be cancelled, significant amounts of fuel can be required to achieve the mission objectives.

A significant source of fuel use is expected to be navigation uncertainty. In monolithic satellite systems, navigation would typically be handled by a series of ground-based observations from which a guidance manoeuvre would be designed. For a formation, control bandwidth is expected to be sufficiently high that on-orbit navigation will be required. Errors in navigation will lead to errors in state corrections, guaranteeing some level of drift will always be present in the system, even if initial conditions are chosen that should completely eliminate drift. Correcting the drift in the system will require fuel.

Formation flying spacecraft pose several control challenges beyond the problem of controlling a monolithic spacecraft or a constellation. In a typical single-spacecraft mission, the term control would refer to maintaining and altering the attitude of the spacecraft, whereas guidance would encompass the maintenance and manipulation of the trajectory on the scale of an orbit. After launch and initial correcting manoeuvres, adjusting a spacecraft's orbit would be an occasional activity planned from the ground. A constellation of spacecraft is operated much the same way, because the constituent spacecraft operate in widely-spaced orbits (or spaced phase angles while in the same orbit), with short-term decoupled performance objectives. A formation of spacecraft is defined by the need for inter-satellite control cooperation. The satellites in a formation are typically represented as sharing a common reference orbit, that is, being close enough in terms of their position and velocity in a central body frame that their long-term, large-scale motion can be modelled using the dynamics of a single orbit. This proximity, while typical for rendezvous missions, is uncommon for satellite missions where there is an expectation for long-term collision-free operation. Formation flying is expected to require a level of autonomous on-board guidance that in most applications would be classified as automatic control.

Over the past decade, numerous formation flying missions have been conceived. These missions were driven by scientific and programmatic objectives ranging from sparse-aperture imaging of extra-solar planets to lunar gravitometry. The advantage of such a system is that the loss of one or more satellites in the formation has only limited impact on the cluster's performance, as remaining satellites could ``absorb'' the lost satellite's responsibilities.

The increased scientific return and the potential adaptability of formation flying satellites to changing mission goals have created new opportunities for the scientific endeavour. However, the control, measurement and modelling challenges of spacecraft formation flying rendered some of the proposed missions too costly. Thus, recent years have seen many proposed formation flying missions cancelled or transformed into technology-demonstration missions.

The approach of S3NET is stemming from the context of spacecraft formation flying technologies; but instead of letting a few satellites fly in formation, it is proposed to let all components of the same fractionated sensor fly in formation. In fact, spacecraft formation flying is already a state-of-the-art technology, while disaggregating a satellite to form a plug-and-play network of autonomous or semi-autonomous entities – is beyond the current state of the art.

S3NET is a high-level concept in distributed space systems. S3NET calls for a separation of the traditional monolithic satellite. Separate satellites can be launched independently from different locations.

The objective of the cluster flight research within S3NET is to achieve a breakthrough progress in flight algorithms for fractionated sensors, their implementability, survivability and verification and validation via a gradual perusal of theoretical and applied challenges. The high-level objectives are as follows:

1. Develop methods for semi-autonomous long-duration maintenance of a cluster network, including addition and removal of spacecraft to/from the cluster network under collision avoidance constraints.
2. Find ways to share resources across the cluster network with real-time guarantees, including distributed data processing, optimal resource allocation and distributed optimal estimation under time delays.
3. Develop and standardize algorithms for autonomously reconfiguring the cluster to retain critical functionality in the face of network degradation, component failures, or space debris damage.
4. Determine how to carry out a semi-autonomous cluster scatter and gather manoeuvres to rapidly evade space debris threats.

In the S3NET system, wireless cluster maintenance poses several constraints on the relative orbit geometry and relative dynamics. It is thus essential for the entire system to achieve a relative translational and rotational state that optimises the performance.

A related issue is the centralization/decentralization level of the S3NET cluster. This term refers to how the multiple spacecraft are hierarchically configured for communicating with each other. Setting a hierarchy of the different satellites is essential for adaptability and responsiveness to dynamically-changing mission scenarios.

This research will provide the space community with a new realm of possibilities for performing space missions in a much more robust and cost-effective method than the current state-of-the-art.

7 CONCLUSION

Most significant mission and application related challenges for fractionated/distributed satellite sensor systems have been identified for optical instrument based EO as well as for radar based EO and have been qualitatively investigated in detail. Societal challenges and opportunities have been described and have been set in correlation with candidate applications that potentially will enable such opportunities. The fractionated missions/applications under investigation in S3Net are mainly derived from current commercial as well as institutional missions including some of the Copernicus Program in order to support future European development and support especially European mission planners with outcomes/results from S3Net. A first set of requirements has been derived from application as well as from formation flying point of view. S3Net deepens the requirements analysis in D1.2, D1.3 and D1.4 regarding processing algorithms, concept compute system and communication simulation respectively. S3Net will further select the most relevant applications and develop, implement and benchmark algorithms/applications on a concept compute system that can become a future high-performance space processing system in the EO domain for different types of missions.

8 BIBLIOGRAPHY

8.1 Optical Applications

Aduah, M. S. (2007). Multitemporal Remote Sensing for Mapping and Monitoring Floods. An Approach Towards Validation of the KAFRIBA Model, Kafue Flats, Zambia 2007

Aguirre-Gutiérrez, J., Seijmonsbergen, A. C., & Duivenvoorden, J. F. (2012). Optimizing land cover classification accuracy for change detection, a combined pixel-based and object-based approach in a mountainous area in Mexico. Applied Geography, 34, 29-37.

Alba-Flores, R. (2005). Evaluation of the use of high-resolution satellite imagery in transportation applications.

Albinet, M., Camarero, R., Isnard, M., Poulet, C., & Perret, J. (2013, September). Improving multispectral satellite image compression using onboard subpixel registration. In SPIE Optical Engineering+ Applications (pp. 887106-887106). International Society for Optics and Photonics.

Alonso-Canas I., Chuvieco, E. (2015). Global burned area mapping from ENVISAT-MERIS and MODIS active fire data. Remote Sensing of Environment, Volume 163, 15 June 2015, Pages 140-152, ISSN 0034-4257, http://dx.doi.org/10.1016/j.rse.2015.03.011.

Alsdorf, D., Lettenmaier, D., & Vörösmarty, C. (2003). The need for global, satellite-based observations of terrestrial surface waters. EOS Trans. AGU, vol. 84, no. 29, pp. 275–276, 2003.

Alsdorf, D., Rodríguez, E., & Lettenmaier, D. (2007). Measuring surface water from space. Rev. Geophys., vol. 45, no. 2, p. RG2 002, 2007.

Anderson L. O., Shimabukuro Y. E., Defries R. S., Morton D. (2005). Assessment of deforestation in near real time over the Brazilian Amazon using multi temporal fraction images derived from Terra MODIS. IEEE Geosci Remote Sens Lett 3:315–318

Anuta, P. E. (1970). Spatial registration of multispectral and multitemporal digital imagery using fast Fourier transform techniques. IEEE Transactions on Geoscience Electronics, 8(4), 353-368..

Aprile, A., Dell'Acqua, F., Pellizzeri, T. M., & Ricardi, N. (2011). Fusion of Airborne MTI on SAR and Ancillary Information for Vehicle Tracking.

Aranki, N., Bakhshi, A., Keymeulen, D., & Klimesh, M. (2009, March). Fast and adaptive lossless on-board hyperspectral data compression system for space applications. In 2009 IEEE Aerospace conference (pp. 1-8). IEEE.

Argyriou, V., & Vlachos, T. (2004, May). Using gradient correlation for sub-pixel motion estimation of video sequences. In Acoustics, Speech, and Signal Processing, 2004. Proceedings.(ICASSP'04). IEEE International Conference on (Vol. 3,pp. iii-329). IEEE.

Arino O., P. Bicheron, F. Achard, et al. (2008). GLOBCOVER the most detailed portrait of earth. ESA Bullet.-Eur. Space Agency, 136 (2008), pp. 24–31

Auge, E., Santalo, J., Blanes, I., Serra-Sagrista, J., & Kiely, A. (2011, June). Review and implementation of the emerging CCSDS recommended standard for multispectral and hyperspectral lossless image coding. In Data Compression, Communications and Processing (CCP), 2011 First International Conference on (pp. 222-228). IEEE.

Baillarin, S., Bouillon, A., Bernard, M., & Chikhi, M. (2005). Using a three dimensional spatial database to orthorectify automatically remote sensing images. In ISPRS Workshop on Service and Application of Spatial Data Infracstructure (pp. 89-93).

Ballard, D. H. (1981). Generalizing the Hough transform to detect arbitrary shapes. Pattern recognition, 13(2), 111-122.

Ban, Y., Gong, P., Giri, C. (2015). Global land cover mapping using Earth observation satellite data: Recent progresses and challenges, ISPRS Journal of Photogrammetry and Remote Sensing, Volume 103, May 2015, Pages 1-6, ISSN 0924-2716, http://dx.doi.org/10.1016/j.isprsjprs.2015.01.001. (http://www.sciencedirect.com/science/article/pii/S0924271615000131)

Baohua, D., Wenchao, L., & Fuming, W. (1999). Analysis of Fractal Image and Design of Fractal Dimension Calculation Program [J]. Journal of University of Science and Technology, Beijing, 3,024.

Barat, C., & Ducottet, C. (2003, September). Pattern matching using morphological probing. In Image Processing, 2003. ICIP 2003. Proceedings. 2003 International Conference on (Vol. 1, pp. I-369). IEEE.

Bartholomé E. , Belward, A.S. (2005). GLC2000: a new approach to global land cover mapping from Earth observation data. Int. J. Remote Sens., 26 (2005), pp. 1959–1977

Barton, I. J., & Bathols J. M. (1989). Monitoring floods with AVHRR. Remote Sens. Environ., vol. 30, no. 1, pp. 89–94, Oct. 1989.

Bastarrika A. , Chuvieco, E., Martin, M.P. (2011). Mapping burned areas from Landsat TM/ETM + data with a two-phase algorithm: Balancing omission and commission errors. Remote Sensing of Environment, 115 (2011), pp. 1003–1012

Belward, A. S., & Skøien, J. O. (2015). Who launched what, when and why; trends in global land-cover observation capacity from civilian earth observation satellites. ISPRS Journal of Photogrammetry and Remote Sensing, 103, 115-128.

Bengio, Y. (2009). Learning deep architectures for AI. Foundations and trends® in Machine Learning, 2(1), 1-127.

Bennington, A. L. (2008). Application of multi-spectral remote sensing for crop discrimination in Afghanistan. PhD thesis. Cranfield University. url: https : / / dspace.lib.cranfield.ac.uk/handle/1826/8075.

Bentz, C., & Pellon de Miranda, F. (2001). Application of remote sensing data for oil spill monitoring in the Guanabara Bay, Rio de Janeiro, Brazil. International Geoscience and Remote Sensing Symposium, 2001. IGARSS '01(pp. 333–335). Sydney, Australia: IEEE.

Benz, U. H., & Heynen, M. (2004). Multi-resolution, object-oriented fuzzy analysis of remote sensing data for GIS ready information. ISPRS Journal of Photogrammetry & Remote Sensing, 239–258.

Bi, F., Zhu, B., Gao, L., & Bian, M. (2012). A visual search inspired computational model for ship detection in optical satellite images. IEEE Geoscience and Remote Sensing Letters, 9(4), 749-753.

Birkett, C. M., Mertes, L. A. K., Dunne, T., Costa, M. H., & Jasinski, M. J. (2002). Surface water dynamics in the Amazon Basin: Application of satellite radar altimetry. J. Geophys. Res.—Atmos., vol. 107, no. D20, p. 8059, 2002.

Blackburn, G. A. (1998). Quantifying chlorophylls and carotenoids at leaf and canopy scales: an evaluation of some hyperspectral approaches. Remote Sensing Environ., 1998, 66, 273–285.

Blackburn, G. A. (2007). Hyperspectral remote sensing of plant pigments. Journal of Experimental Botany, 58, 844–867.

Blaschke, T. (2010). Object based image analysis for remote sensing. ISPRS journal of photogrammetry and remote sensing, 65(1), 2-16.

Blasco, F., Bellan, M. F., & Chaudhury, M. U. (1992). Estimating the extent of floods in Bangladesh using SPOT data. Remote Sens. Environ., vol. 39, no. 3, pp. 167–178, Mar. 1992.

Bock, M., Xofis, P., Mitchley, J., Rossner, G., & Wissen, M. (2005). Object-oriented methods for habitat mapping at multiple scales–Case studies from Northern Germany and Wye Downs, UK. Journal for Nature Conservation, 13(2), 75-89.

Bontemps S. , Herold, M., Kooistra, L., et al. (2012). Revisiting land cover observation to address the needs of the climate modeling community. Biogeosciences, 9 (2012), pp. 2145–2157

Brakenridge, G. R., Nghiem, S. V., Anderson, E., & Mic, R. (2007). Orbital microwave measurement of river discharge and ice status. Water Resour. Res., vol. 43, no. 4, p. W04 405, 2007.

Brakenridge, G., & Anderson, E. (2003). Satellite gaging reaches: A strategy for MODIS-based river monitoring. In Proc. 9th Int. Symp. Remote Sens., Crete, Greece, 2003, vol. 4886, pp. 479–485.

Brakenridge, G., Anderson, E., Nghiem, S., Caquard, S., & Shabaneh, T. B. (2003). Flood warnings, flood disaster assessments, and flood hazard reduction: The roles of orbital remote sensing. In Proc. 30th Int. RSE, Honolulu, HI, Nov. 10–14, 2003.

Brakenridge, R. (2006). MODIS-based flood detection, mapping and measurement: The potential for operational hydrological applications. In Transboundary Floods: Reducing Risks Through Flood Management. New York: Springer-Verlag, 2006, pp.1–12.

Breidenbach, J., Astrup, R. (2012). Small area estimation of forest attributes in the Norwegian National Forest Inventory. Eur. J. For. Res., 131 (2012), pp. 1255–1267 http://dx.doi.org/10.1007/s10342-012-0596-7

Brekke C., Solberg A. (2005). Oil spill detection by satellite remote sensing. Remote Sensing of Environment. 2005; 95:1–13.

Brett, P.T. (2011). DigitalGlobe Systems and Products Overview, 10th Annual JACIE (Joint Agency Commercial Imagery Evaluation) Workshop, March 29-31, 2011, Boulder CO, USA.

Brousseau, B., & Rose, J. (2012, December). An energy-efficient, fast FPGA hardware architecture for OpenCV-compatible object detection. In Field-Programmable Technology (FPT), 2012 International Conference on (pp. 166-173). IEEE.

Brown C., Fingas M. (1997). Review of Oil Spill Remote Sensing. Spill Science & Technology Bulletin. 4.4:199–208.

Brown C., Fingas M. (2005) A review of current global oil spill surveillance, monitoring and remote sensing capabilities. Proc. 28th Arctic and Marine Oil Spill Program (AMOP) Tech. Seminar; Calgary, Canada. Jun. 7–9, pp. 789–798.

Brown C., Fingas M., Hawkins R. (2003). Synthetic Aperture Radar Sensors: Viable for Marine Oil Spill Response?. Proc. 26th Arctic and Marine Oil Spill Program (AMOP) Technology Seminar; Victoria, Canada. June 10–12, pp. 299–310.

Buchanan G.M., Nelson, A., Mayaux, P., et al. (2009). Delivering a global, terrestrial, biodiversity observation system through remote sensing. Conserv. Biol., 23 (2) (2009), pp. 499–502

Burgess, D. W. (1993). Automatic ship detection in satellite multispectral imagery. Photogrammetric engineering and remote sensing, 59(2), 229-237.

Burlina, P., Parameswaran, V., & R. Chellappa. (1997). Sensitivity analysis and learning strategies for context-based vehicle detection algorithms. Proc. DARPA Image Understanding Workshop.

Cai, G., Huang, X., Du, M., & Liu, Y. (2011). Detection of natural oil seeps signature from SST and ATI in South Yellow Sea combining ASTER and MODIS data. International Journal of Remote Sensing, 31, 4869–4885.

Camarero, R., Thiebaut, C., Dejean, P., & Speciel, A. (2010, August). CNES studies for on-board implementation via HLS tools of a cloud-detection module for selective compression. In SPIE Optical Engineering+ Applications (pp. 781004-781004).International Society for Optics and Photonics.

Carter, G. A., & Knapp, A. K. (2001). Leaf optical properties in higher plants: linking spectral characteristics to stress and chlorophyll concentration. American Journal of Botany, 88, 677–684.

Castano, R., Mazzoni, D., Tang, N., Greeley, R., Doggett, T., Cichy, B., ... & Davies, A. (2006, August). Onboard classifiers for science event detection on a remote sensing spacecraft. In Proceedings of the 12th ACM SIGKDD internationalconference on Knowledge discovery and data mining (pp. 845-851). ACM.

Castilla, G., & Hay, G. J. (2008). Image objects and geographic objects. In Object-based image analysis (pp. 91-110). Springer Berlin Heidelberg.

Champagne, C. M., Staenz, K., Bannari, A., Mcnairn, H. and Deguise, J. C. (2003). Validation of a hyperspectral curve-fitting model for the estimation of plant water content of agricultural canopies Remote Sensing Environ., 2003, 87, 148–160.

Chan, T. F., & Vese, L. A. (2001). Active contours without edges. IEEE Transactions on image processing, 10(2), 266-277.

Chang D., Song, Y. (2009). Comparison of L3JRC and MODIS global burned area products from 2000 to 2007. Journal of Geophysical Research, 114 (2009) http://dx.doi.org/10.1029/2008JD11361

Chen X., Liu L., Huang W. (2016). The detection and prediction for oil spill on the sea based on the infrared images. Infrared Physics & Technology 77; 391–404

Chen, C. -F., & Chang, L. -Y. (2010). Extraction of oil slicks on the sea surface from optical satellite images by using an anomaly detection technique. Journal of Applied Remote Sensing, 4, 043565.

Chien, S., Sherwood, R., Tran, D., Cichy, B., Rabideau, G., Castano, R., ... & Boyer, D. (2005). Using autonomy flight software to improve science return on Earth Observing One. Journal of Aerospace Computing, Information, and Communication, 2(4), 196-216.

Chien, S., Tran, D., Schaffer, S., Rabideau, G., Davies, A. G., Doggett, T., ... & Castano, R. (2009, August). Onboard classification of hyperspectral data on the Earth Observing One mission. In 2009 First Workshop on Hyperspectral Imageand Signal Processing: Evolution in Remote Sensing (pp. 1-4). IEEE.

Chirici, G., Barbati, A., Corona, P., Marchetti, M., Travaglini, D., Maselli, F., Bertini, R. (2008). Non-parametric and parametric methods using satellite images for estimating growing stock volume in alpine and Mediterranean forest ecosystems. Remote Sens. Environ., 112 (2008), pp. 2686–2700 http://dx.doi.org/10.1016/j.rse.2008.01.002

Christou P, Twyman R (2004): The potential of genetically enhanced plants to address food insecurity. Nutr Res Rev 17:23–42

Chuinsiri, S., Blasco, F., Bellan, M. F., & Kergoat, L. (1997). A poppy survey using high resolution remote sensing data. International Journal of Remote Sensing 18.2, pp. 393–407. url: http://dx.doi.org/10.1080/014311697219132.

Chuvieco E., Opazo, S., Sione, W., Del Valle, H., Anaya, J., Di Bella, C. et al. (2008). Global burned land estimation in Latin America using MODIS composite data. Ecological Applications, 18 (2008), pp. 64–79

Cihlar J. (2000). Land cover mapping of large areas from satellites: status and research priorities. Int. J. Remote Sens., 21 (2000), pp. 1093–1114

Clark, R. N. (1999). Spectroscopy of rocks and minerals, and principles of spectroscopy. In A. N. Rencz (Ed.),Manual of Remote Sensing, Remote Sensing for the Earth Sciences (pp. 3–58). New York: John Wiley and Sons.

Clark, R. N., Swayze, G. A., Leifer, I., et al. (2010). A method for quantitative mapping of thick oil spills using imaging spectroscopy. U.S. Geological Survey Open-File Report Number 2010-1167(pp. 51).

Clevers, J. G. P. W., & Kooistra, L. (2012). Using hyperspectral remote sensing data for retrieving canopy chlorophyll and nitrogen content. IEEE J. Sel. Top. Appl. Earth Observ. Remote Sens., vol. 5, no. 2, pp. 574–583, Apr. 2012.

Cochran, W. G. (1977). Sampling Techniques. 3rd. New York: John Wiley & Sons

Colombo, R., Bellingeri, D., Fasolini, D. & Marino, C. M. (2003). Retrieval of leaf area index in different vegetation types using high resolution satellite data. Remote Sensing of Environment, 86, 120–131.

Consulative Committee for Space Data Systems (CCSDS), Image Data Compression CCSDS 122.0-B-1, ser. Blue Book. CCSDS, Nov. 2005.

Consultative Committee for Space Data Systems (CCSDS). [Online]. Available: http://www.ccsds.org

Copernicus service, [Online]. Available: http://copernicus.eu/main/security. [Accessed on 2 August 2016].

Coppin, P., Jonckheere, I., Nackaerts, K., Muys, B., & Lambin, E. (2004). Review ArticleDigital change detection methods in ecosystem monitoring: a review. International journal of remote sensing, 25(9), 1565-1596.

Corbane, C., Najman, L., Pecoul, E., Demagistri, L., & Petit, M. (2010). A complete processing chain for ship detection using optical satellite imagery. International Journal of Remote Sensing, 31(22), 5837-5854.

Corbane, C., Pecoul, E., Demagistri, L., & Petit, M. (2008, December). Fully automated procedure for ship detection using optical satellite imagery. In Asia-Pacific Remote Sensing (pp. 71500R-71500R). International Society for Optics andPhotonics.

Corbari, C., & Mancini, M. (2014). Calibration and validation of a distributed energy water balance model using satellite data of land surface temperature and ground discharge measurements Journal of hydrometeorology, 15, 376-392

Corbari, C., Mancini, M., Li, J. & Su, Z. (2015). Can satellite land surface temperature data be used similarly to ground discharge measurements for distributed hydrological model calibration? Hydrological Sciences Journal, 60(2), 202-217. doi:10.1080/02626667.2013.866709

Corbari, C., Mancini, M., Su, Z., & Li, J. (2014). Evapotranspiration 1 estimate from water balance closure using satellite data for the Upper Yangtze river basin. Hydrology Research, 45, 603–614.

Crisp, D.J. (2004). The State-of-the-Art in Ship Detection in Synthetic Aperture Radar Imagery. Technical Report. Australian Government, Department of Defense Press, Austria

Culjak, I., Abram, D., Pribanic, T., Dzapo, H., & Cifrek, M. (2012, May). A brief introduction to OpenCV. In MIPRO, 2012 Proceedings of the 35th International Convention (pp. 1725-1730). IEEE.

Dalal, N., & Triggs, B. (2005, June). Histograms of oriented gradients for human detection. In 2005 IEEE Computer Society Conference on Computer Vision and Pattern Recognition (CVPR'05) (Vol. 1, pp. 886-893). IEEE.

Davies, A. G., Chien, S., Baker, V., Doggett, T., Dohm, J., Greeley, R., ... & Tran, D. (2006). Monitoring active volcanism with the autonomous sciencecraft experiment on EO-1. Remote Sensing of Environment, 101(4), 427-446.

Dawelbait M., Morari F. (2012). Monitoring desertification in a Savannah region in Sudan using Landsat images and spectral mixture analysis Journal of Arid Environments 80:45–55 doi:10.1016/j.jaridenv.2011.12.011

De Roeck T., Van de Voorde, T., Canters, F. (2009). Full hierarchical versus non-hierarchical classification approaches for mapping sealed surfaces at the rural–urban fringe using high-resolution satellite data. Sensors, 9 (2009), pp. 22–45 http://dx.doi.org/10.3390/s90100022

Deer, P. (1995). Digital change detection techniques in remote sensing.

DeFries R., Townshend, J.R. (1994). NDVI-derived land-cover classifications at a global-scale Int. J. Remote Sens., 15 (17) (1994), pp. 3567–3586

Delalieux, S., van Aardt, J., Keulemans, W., & Coppin, P. (2007). Detection of biotic stress (Venturia inaequalis) in apple trees using hyperspectral data: non-parametric statistical approaches and physiological implications. European Journalof Agronomy, 27, 130–143.

Delegido J. et al. (2013). A red-edge spectral index for remote sensing estimation of green LAI over agroecosystems. Eur. J. Agron., vol. 46, pp. 42–52, Apr. 2013.

Dell'Acqua, F. & Gamba, P. (2003). Texture-Based Characterization of Urban Environments on Satellite SAR Images. IEEE TRANSACTIONS ON GEOSCIENCE AND REMOTE SENSING, 153-159.

Dell'Acqua, F. & Gamba, P.? (2006). Discriminating urban environments using multiscale texture and multiple SAR images. International Journal of Remote Sensing, 3797–3812.

DMSG (2003). The Use of Earth Observing Satellites for Hazard Support: Assessments and Scenarios—Final Report of the CEOS Disaster Management Support Group, 2003

Dobson A. (2005). Monitoring global rates of biodiversity change: challenges that arise in meeting the Convention on Biological Diversity (CBD) 2010 goals. Phil. Trans. Roy. Soc. B, 360 (2005), pp. 229–241

Doggett, T., Greeley, R., Chien, S., Castano, R., Cichy, B., Davies, A. G., ... & Dohm, J. (2006). Autonomous detection of cryospheric change with hyperion on-board Earth Observing-1. Remote Sensing of Environment, 101(4), 447-462.

Durden, S. L., Fischman, M. A., Johnson, R. A., Chu, A. J., Jourdan, M. N., & Tanelli, S. (2007). An FPGA-Based Doppler Processor for a Spaceborne Precipitation Radar. Journal of Atmospheric and Oceanic Technology, 24(10), 1811-1815.

Eastman, R. D., Le Moigne, J., & Netanyahu, N. S. (2007, June). Research issues in image registration for remote sensing. In 2007 IEEE Conference on Computer Vision and Pattern Recognition (pp. 1-8). IEEE.

Eikvil, L., Aurdal, L., & Koren, H. (2009). Classification-based vehicle detection in high-resolution satellite images. ISPRS Journal of Photogrammetry and Remote Sensing, 64(1), 65-72.

El-Araby, E., Taher, M., El-Ghazawi, T., & Le Moigne, J. (2005, December). Prototyping automatic cloud cover assessment (ACCA) algorithm for remote sensing on-board processing on a reconfigurable computer. In

Proceedings. 2005 IEEE International Conference on Field-Programmable Technology, 2005. (pp. 207-214). IEEE.

Falkowski, M.J., Wulder, M.A., White, J.C., Gillis, M.D. (2009). Supporting large-area, sample-based forest inventories with very high spatial resolution satellite imagery. Prog. Phys. Geogr., 33 (2009), pp. 403–423 http://dx.doi.org/10.1177/03,09133E+14

Fazio, M., Villari, M., & Puliafito, A. (2011, November). Sensing technologies for homeland security in cloud environments. In Sensing Technology (ICST), 2011 Fifth International Conference on (pp. 165-170). IEEE.

Fingas, M., & Brown, C. E. (2011). Oil spill remote sensing: A review. Oil spill science and technology(pp. 111–169). Boston: Gulf Professional Publishing.

Finocchio, P., Prasad, R., & Ruggieri, M. (Eds.). (2008). Aerospace Technologies and Applications for Dual Use. River Publishers.

Flatley, T. (2010, June). Advanced hybrid on-board science data processor-SpaceCube 2.0. In Earth Science Technology Forum.

Foody G.M. and Mathur A. (2004). A relative evaluation of multiclass image classification by support vector machines. IEEE Transactions on Geoscience and Remote Sensing, 1336–1343.

Foroosh, H., Zerubia, J. B., & Berthod, M. (2002). Extension of phase correlation to subpixel registration. IEEE transactions on image processing, 11(3), 188-200.

Fourie, C., & Schoepfer, E. (2014). Data transformation functions for expanded search spaces in geographic sample supervised segment generation. Remote Sensing, 6(5), 3791-3821.

France, M. & Hedges, P. (1986). A hydrological comparison of Landsat TM, Landsat MSS, and black and white aerial photography. In Proc. 7th Int. Symp. ISPRS, Enschede, The Netherlands, Aug. 1986, pp. 717–720.

Freixenet, J., Muñoz, X., Raba, D., Martí, J., & Cufí, X. (2002, May). Yet another survey on image segmentation: Region and boundary information integration. In European Conference on Computer Vision (pp. 408-422). Springer Berlin Heidelberg.

Freund, Y., & Schapire, R. E. (1996, January). Game theory, on-line prediction and boosting. In Proceedings of the ninth annual conference on Computational learning theory (pp. 325-332). ACM.

Fritz S., See, L., You, L.Z., et al. (2013). The need for improved maps for global croplands. EOS Trans. AGU, 91 (3) (2013), pp. 31–32

Fröhlich, Björn, et al. (2013). Land cover classification of satellite images using contextual information. ISPRS Annals of the Photogrammetry, Remote Sensing and Spatial Information Sciences 3 (2013): W1

Gale, S. J., & Bainbridge, S. (1990). The floods in eastern Australia. Nature, vol. 345, no. 6278, p. 767, 1990.

Gallager, R., & Van Voorhis, D. (1975). Optimal source codes for geometrically distributed integer alphabets (Corresp.). IEEE Transactions on Information theory, 21(2), 228-230.

Gallaun, H., Zanchi, G., Nabuurs, G.J., Hengeveld, Schardt, M., Verkerk, P.J. (2010). EU-wide maps of growing stock and above-ground biomass in forests based on remote sensing and field measurements. For. Ecol. Manage., 260 (2010), pp. 252–261http://dx.doi.org/10.1016/j.foreco.2009.10.011

Gallego, F. J. (2004). Remote sensing and land cover area estimation. International Journal of Remote Sensing 25.15, pp. 3019–3047. url: http://www.informaworld. com/10.1080/01431160310001619607.

Garcia-Vilchez, F., & Serra-Sagrista, J. (2009). Extending the CCSDS recommendation for image data compression for remote sensing scenarios. IEEE Transactions on Geoscience and Remote Sensing, 47(10), 3431-3445.

Garnier, B., & Andritsos, F. (2010, November). A port waterside security systemic analysis. In 2010 International WaterSide Security Conference (pp. 1-6). IEEE.

Gebbers, R., & Adamchuk, V. I. (2010). Precision agriculture and food security. Science, vol. 327, no. 5967, pp. 828–31, Feb. 2010.

Gersho, A. (1984). Adaptive filtering with binary reinforcement. IEEE Transactions on Information Theory, 30(2), 191-199.

Gevaert, C. M., Suomalainen, J., Tang J., & Kooistra, L. (2015). Generation of Spectral–Temporal Response Surfaces by Combining Multispectral Satellite and Hyperspectral UAV Imagery for Precision Agriculture Applications. in IEEE Journalof Selected Topics in Applied Earth Observations and Remote Sensing, vol. 8, no. 6, pp. 3140-3146, June 2015. doi: 10.1109/JSTARS.2015.2406339

Giglio L. , Randerson, J.T., Werf, G.R., Kasibhatla, P.S., Collatz, G.J., Morton, D.C., et al. (2010). Assessing variability and long-term trends in burned area by merging multiple satellite fire products. Biogeosciences Discuss, 7 (2010), pp.1171–1186 (1110.5194/bg-1177-1171-2010)

Giri C., Pengra, B., Long, J., Loveland, T.R. (2013). Next generation of global land cover characterization, mapping and monitoring. Int. J. Appl. Earth Obs. Geoinf., 25 (2013), pp. 30–37

Giri C., Zhu, Z., Reed, B. (2005). A comparative analysis of the Global Land Cover 2000 and MODIS land cover data sets. Remote Sens. Environ., 94 (2005), pp. 123–132

Goodman R. (1994) Overview and Future Trends in Oil Spill Remote Sensing. Spill Science & Technology Bulletin. 1.1:11–21.

Greidanus, H., & Kourti, N. (2003). State of the art–Vessel Detection in SAR imagery. In 2nd workshop Marine SAR, EC/JRC DECLIMS-Detection and Classification of Marine Traffic from Space. http://fish. jrc. cec. eu. int/declims.

Greidanus, H., Clayton, P. J., Indregard, M., Staples, G., Suzuki, N., Vachon, P. W., ... & Ringrose, R. (2004, September). Benchmarking operational SAR ship detection. In IGARSS (pp. 4215-4218).

Grodecki, J., Dial, G. (2003). Block adjustment of high-resolution satellite images described by rational polynomials. Photogrammetric Engineering and Remote Sensing 69; 1 (2003): 59-68.

Grüner K., Reuter R., Smid H. (1991). A New Sensor System for Airborne Measurements of Maritime Pollution and of Hydrographic Parameters. Geojournal. 24.1:103–117.

Guindon, B., Zhang, Y., & Dillabaugh, C. (2004). Landsat urban mapping based on a combined spectral-spatial methodlogy. Remote Sensing of Environment, 218-232.

Guizar-Sicairos, M., Thurman, S. T., & Fienup, J. R. (2008). Efficient subpixel image registration algorithms. Optics letters, 33(2), 156-158.

Guo, C., Ma, Q., & Zhang, L. (2008, June). Spatio-temporal saliency detection using phase spectrum of quaternion fourier transform. In Computer vision and pattern recognition, 2008. cvpr 2008. ieee conference on (pp. 1-8). IEEE.

Haboudane, D., Miller, J. R., Tremblay, N., Zarco-Tejada, P. J., & Dextraze, L. (2002). Integrated narrow-band vegetation indices for prediction of crop chlorophyll content for application to precision agriculture. Remote Sens. Environ.,vol.81, no. 2–3, pp. 416–426, Aug. 2002.

Haboudane, D., Miller, J. R., Trembley, N., Zarco-Tejada, P. J. and Dextraze, L. (2002). Integrated narrow-band vegetation indices for prediction of crop chlorophyll content for application to precision agriculture. Remote Sensing Environ., 2002, 81, 416–426.

Hamlin, L., Green, R. O., Mouroulis, P., Eastwood, M., Wilson, D., Dudik, M., & Paine, C. (2011, March). Imaging spectrometer science measurements for terrestrial ecology: AVIRIS and new developments. In Aerospace Conference, 2011 IEEE (pp. 1-7). IEEE.

Hansen M.C. , DeFries, R.S., Townshend, J.R.G., et al. (2000). Global land cover classification at 1 km spatial resolution using a classification tree approach. Int. J. Remote Sens., 21 (2000), pp. 1331–1364

Haralick, R. M. (1979). Statistical and structural approaches to texture. Proceedings of the IEEE, 67(5), 786-804.

Harb, M., Gamba, P., & Dell'Acqua, F. (2016). Automatic Delineation of Clouds and Their Shadows in Landsat and CBERS (HRCC) Data. IEEE Journal of Selected Topics in Applied Earth Observations and Remote Sensing, 9(4), 1532-1542.

Hardin, P. (1994). Parametric and nearest-neighbor methods for hybrid classification: a comparison of pixel assignment accuracy. Photogrammetric Engineering and Remote Sensing, 1439–1448.

Hartzell, C. M., & Cheng, S. R. (2010, March). A feasibility study of on-board cloud detection and compression. In Aerospace Conference, 2010 IEEE (pp. 1-11). IEEE.

Harvey, N. R., Porter, R., & Theiler, J. (2010, April). Ship detection in satellite imagery using rank-order grayscale hit-or-miss transforms. In SPIE Defense, Security, and Sensing (pp. 770102-770102). International Society for Optics and Photonics.

Hashemi S., Fallah C. M. (2013). Investigation of NDVI in relation to the growth phases of beech leaves in forest. Arab J Geosci 6:3341–3347

Herold M., Mayaux, P., Woodcock, C.E., et al. (2008). Some challenges in global land cover mapping: an assessment of agreement and accuracy in existing 1 km datasets. Remote Sens. Environ., 112 (2008), pp. 2538–2556

Herold, M., & Liu, X. A. (2003). Spatial metrics and image texture for mapping urban land use. Photogrammetric Engineering and Remote Sensing, 991–1001.

Hinz, S. (2004). Detection of vehicles and vehicle queues for road monitoring using high resolution aerial images. Photogrammetrie Fernerkundung Geoinformation, pp. 201–213

Hu, J. H., Xu, S. S., Chen, H. L., & Zhang, Z. (2009). Detection of ships in harbor in remote sensing image based on local self-similarity. Journal of Image and Graphics, 14(4), 591-597.

Hu, M. K. (1962). Visual pattern recognition by moment invariants. IRE transactions on information theory, 8(2), 179-187.

Hu, X., Weng, Q. (2011). Impervious surface area extraction from IKONOS imagery using an object-based fuzzy method. Geocarto International, 26 (1) (2011), pp. 3–20 10.1080/10106049.2010.535616

Huang, B. (Ed.). (2011). Satellite data compression. Springer Science & Business Media.

Huang, G. B., Liang, N. Y., Rong, H. J., Saratchandran, P., & Sundararajan, N. (2005). On-Line Sequential Extreme Learning Machine. Computational Intelligence, 2005, 232-237.

Huang, G. B., Zhou, H., Ding, X., & Zhang, R. (2012). Extreme learning machine for regression and multiclass classification. IEEE Transactions on Systems, Man, and Cybernetics, Part B (Cybernetics), 42(2), 513-529.

Huang, G. B., Zhu, Q. Y., & Siew, C. K. (2006). Extreme learning machine: theory and applications. Neurocomputing, 70(1), 489-501.

Hung, M., & Ridd, M. (2002). A subpixel classifier for urban land-cover mapping based on a maximum-likelihood approach and expert system rules. Photogrammetric Engineering and Remote Sensing, 1173–1180.

Hunt, J., Ramond, E. and Rock, B. N. (1989). Detection in changes in leaf water content using near and mid-infrared reflectance. Remote Sensing Environ., 1989, 30, 45–54.

Hussain, M., Chen, D., Cheng, A., Wei, H., & Stanley, D. (2013). Change detection from remotely sensed images: From pixel-based to object-based approaches. ISPRS Journal of Photogrammetry and Remote Sensing, 80, 91-106.

Iannelli G. C., Dell'Acqua, F. & Gamba, P?. (2013). Comparing different textural approaches to extract human settlement from CBERS-2B data. Anais XVI Simpósio Brasileiro de Sensoriamento Remoto - SBSR. Foz do Iguaçu,PR, Brasil: INPE.

Image Data Compression, Recommendation for Space Data System Standards, CCSDS 122.0-B-1, November 2005.

Immitzer, M., Stepper, C., Böck, S., Straub, C., Atzberger, C. (2016). Use of WorldView-2 stereo imagery and National Forest Inventory data for wall-to-wall mapping of growing stock, Forest Ecology and Management, Volume 359, 1 January 2016, Pages 232-246, ISSN 0378-1127, http://dx.doi.org/10.1016/j.foreco.2015.10.018.

Ip, F., Dohm, J. M., Baker, V. R., Doggett, T., Davies, A. G., Castano, R., ... & Sherwood, R. (2006). Development and testing of the Autonomous Spacecraft Experiment (ASE) floodwater classifiers: real-time smart reconnaissance of transient flooding. Rem. Sens. Environ, 101.

Irish, R. R. (2000, August). Landsat 7 automatic cloud cover assessment. In AeroSense 2000 (pp. 348-355). International Society for Optics and Photonics.

Iwasaki, A., & Fujisada, H. (2005). ASTER geometric performance. IEEE Transactions on Geoscience and Remote Sensing, 43(12), 2700-2706.

Jacquemoud, S. et al. (2009). PROSPECT + SAIL models: a review of use for vegetation characterization. Remote Sensing Environ., 2009, 113, S56–S66.

Jafari-Khouzani, K., & Soltanian-Zadeh, H. (2005). Radon transform orientation estimation for rotation invariant texture analysis. IEEE Transactions on Pattern Analysis and Machine Intelligence, 27(6), 1004-1008.

Jayant, N. S., & Noll, P. (1984). Digital Coding of Waveforms--Principles and Applications to Speech and Video Englewood Cliffs.

Jensen, J. R., Hodgson, M. E., Christensen, E., Mackey, H. E., Tinney, L. R., & Sharitz, R. R. (1986). Remote-sensing inland wetlands—A multispectral approach. Photogramm. Eng. Remote Sens., vol. 52, no. 1, pp. 87–100, 1986.

Jia, K., Wu, B., Tian, Y., Li, Q., & Du., X. (2011). Spectral Discrimination of Opium Poppy Using Field Spectrometry. Geoscience and Remote Sensing, IEEE Transactions on 49.9, pp. 3414–3422.

Jin, X., & Davis, C. H. (2007). Vehicle detection from high-resolution satellite imagery using morphological shared-weight neural networks. Image and Vision Computing, 25(9), 1422-1431.

Jolliffe, I. (2002). Principal component analysis. John Wiley & Sons, Ltd.

Jovanovic, V. M., Bull, M. A., Smyth, M. M., & Zong, J. (2002). MISR in-flight camera geometric model calibration and georectification performance. IEEE Transactions on Geoscience and Remote Sensing, 40(7), 1512-1519.

Kachmar M. , Sanchez-Azofeifa, G.A. (2006). Detection of post-fire residuals using high- and medium-resolution satellite imagery. Forestry Chronicle, 82 (2006), pp. 177–186

Karimi, N., Golian, S. & Karimi, D. Arab J Geosci (2016) 9: 214. doi:10.1007/s12517-015-2250-4

Kawato, S., & Tetsutani, N. (2001). Circle-Frequency Filter and its Application (3rd International Workshop on Advanced Image Technology (IWAIT2000)). Technical Report IEICE. IE, Image engineering, 100(616), 49-54.

Kelarestaghi A., Jafarian J. Z. (2011). Land use/cover change and driving force analyses in parts of northern Iran using RS and GIS techniques. Arab J Geosci 4:401–411. doi:10.1007/s12517-009-0078-5

Kemper, T., Jenerowicz, M., Pesaresi, M., & Soille, P. (2011). Enumeration of dwellings in Darfur Camps from GeoEye-1 satellite images using mathematical morphology. IEEE Journal of Selected Topics in Applied Earth Observations and RemoteSensing, 4(1), 8-15.

Keymeulen, D., Aranki, N., Hopson, B., Kiely, A., Klimesh, M., & Benkrid, K. (2012, March). GPU lossless hyperspectral data compression system for space applications. In Aerospace Conference, 2012 IEEE (pp. 1-9). IEEE.

Klimesh, M. (2005). Low-complexity lossless compression of hyperspectral imagery via adaptive filtering.

Koukal, T., Suppan, F., Schneider, W., (2007). The impact of relative radiometric calibration on the accuracy of kNN-predictions of forest attributes. Remote Sens. Environ., 110 (2007), pp. 431–437 http://dx.doi.org/10.1016/j.rse.2006.08.016 (ForestSAT Special Issue ForestSAT 2005 Conference “Operational tools in forestry using remote sensing techniques”)

Krajník, T., Šváb, J., Pedre, S., ?ížek, P., & P?eu?il, L. (2014). FPGA-based module for SURF extraction. Machine vision and applications, 25(3), 787-800.

Laben, C.A., Brower, B. V., (2000). Process for Enhancing the Spatial Resolution of Multispectral Imagery Using Pan-sharpening. U.S. Patent No. 6,011,875, Eastman Kodak Company; 2000.

Labutina, I. (2004). Interpretation of aerospace images. Moscow.: Aspect-Press, 2004,p.184.

Lacava, T., Pergola, N., Sannazzaro, F. & Tramutoli, V. (2010). Improving flood monitoring by the Robust AVHRR Technique (RAT) approach: The case of the April 2000 Hungary flood. Int. J. Remote Sens., vol. 31, no. 8, pp. 2043-2062, 2010

Lambert-Nebout, C., Lebedeff, D., Latry, C., rome Fraleu, J., & Moury, G. A. (2002, November). Fixed data rate wavelet compressor for multispectral satellite systems. In International Symposium on Optical Science and Technology (pp. 346-357).International Society for Optics and Photonics.

Lammoglia, T., & Filho, C. R. d. S. (2011). Spectroscopic characterization of oils yielded from Brazilian offshore basins: Potential applications of remote sensing. Remote Sensing of Environment, 115, 2525–2535.

Latry, C., Panem, C., & Dejean, P. (2007, July). Cloud detection with SVM technique. In 2007 IEEE International Geoscience and Remote Sensing Symposium (pp. 448-451). IEEE.

Lawrence R., Bunn A., PowellL S. and Zmabon M. (2004). Classification of remotely sensed imagery using stochastic gradient boosting as a refinement of classification tree analysis. Remote Sensing of Environment, 331–336.

Lee, D. S., Storey, J. C., Choate, M. J., & Hayes, R. W. (2004). Four years of Landsat-7 on-orbit geometric calibration and performance. IEEE Transactions on Geoscience and Remote Sensing, 42(12), 2786-2795.

Leifer, I., Luyendyk, B., & Broderick, K. (2006). Tracking an oil slick from multiple natural sources, Coal Oil Point, California.Marine and Petroleum Geology, 23, 621–630

Liang, N. Y., Huang, G. B., Saratchandran, P., & Sundararajan, N. (2006). A fast and accurate online sequential learning algorithm for feedforward networks. IEEE Transactions on Neural networks, 17(6), 1411-1423.

Liang, Y. L., Wang, J., et al. (2014). Knowledge discovery by mapping remote sensing-based land cover classification efforts in the world. Int. J. Remote Sens., 35 (13) (2014), pp. 4573–4588

Lin, J., Yang, X., Xiao, S., Yu, Y., & Jia, C. (2012). A line segment based inshore ship detection method. In Future Control and Automation (pp. 261-269). Springer Berlin Heidelberg.

Lin, R., Cao, X., Xu, Y., Wei, C., & Qiao, H. (2008, October). Airborne moving vehicle detection for urban traffic surveillance. In 2008 11th International IEEE Conference on Intelligent Transportation Systems (pp. 163-167). IEEE.

Lin, R., Cao, X., Xu, Y., Wu, C., & Qiao, H. (2009, June). Airborne moving vehicle detection for video surveillance of urban traffic. In Intelligent Vehicles Symposium, 2009 IEEE (pp. 203-208). IEEE.

Lisini, G., Gamba, P., Dell'Acqua, F., & Holecz, F. (2011). First results on road network extraction and fusion on optical and SAR images using a multi-scale adaptive approach. International Journal of Image and Data Fusion, 2(4), 363-375.

Liu, C., Vachon, P. W., & Geling, G. W. (2005). Improved ship detection with airborne polarimetric SAR data. Canadian Journal of Remote Sensing, 31(1), 122-131.

Liu, G., Zhang, Y., Zheng, X., Sun, X., Fu, K., & Wang, H. (2014). A new method on inshore ship detection in high-resolution satellite images using shape and context information. IEEE Geoscience and Remote Sensing Letters, 11(3), 617-621.

Liu, W. G., & Woodcock, C. (2004). Uncertainty and confidence in land cover classification using a hybrid classifier approach. Photogrammetric Engineering and Remote Sensing, 963–972.

Lossless Data Compression, Recommendation for Space Data System Standards, CCSDS 121.0-B-1, May 1997.

Loveland T.R., Reed, B.C., Brown, J.F., et al. (2000). Development of a global land cover characteristics database and IGBP DISCover from 1 km AVHRR data. Int. J. Remote Sens., 21 (2000), pp. 1303–1330

Lu, D., Weng, Q. (2009). Extraction of urban impervious surfaces from IKONOS imagery. International Journal of Remote Sensing, 30 (5) (2009), pp. 1297–1311

Lu, D.S., Weng, V. (2007). A survey of image classification methods and techniques for improving classification performance. Int. J. Remote Sens., 28 (5) (2007), pp. 823–870

M. Sonka, V. Hlavac, and R. Boyle, Image Processing, Analysis, and Machine Vision., 2nd ed. Pacific Grove, CA: Brooks/Cole, 2002.

Madani, H., Carr, J. L., & Schoeser, C. (2004, September). Image registration using autolandmark. In Geoscience and Remote Sensing Symposium, 2004. IGARSS'04. Proceedings. 2004 IEEE International (Vol. 6, pp. 3778-3781). IEEE.

Mahajan, G. R., Sahoo, R. N., Pandey, R. N., Gupta, V. K. and Kumar, D. (2014). Using hyperspectral remote sensing techniques to monitor nitrogen, phosphorus, sulphur and potassium in wheat (Triticum aestivum L.). Precision Agric., 2014,15(2), 227–240.

Mahlein, A. K., Steiner, U., Dehne, H. W., & Oerke, E.-C. (2010). Spectral signatures of sugar beet leaves for the detection and differentiation of diseases. Precision Agriculture, 11, 413–431.

Mahlein, A., Oerke, E., Steiner, U. et al. (2012) Recent advances in sensing plant diseases for precision crop protection. Eur J Plant Pathol (2012) 133: 197. doi:10.1007/s10658-011-9878-z

Main, R., et al., (2011). An investigation into robust spectral indices for leaf chlorophyll estimation. ISPRS J. Photogramm. Remote Sens., vol. 66, no. 6, pp. 751–761, Nov. 2011

Malnes, E., Solb, S., Lauknes, I., Evertsen, G. J., Tollefsen T. A., Solheim, I. & Indregard, M. (2005). FloodMan-Global near real-time flood monitoring for hydrological users. Proc. ACTIF Workshop, pp. 1-9, 2005

Mandrake, L., Wagstaff, K. L., Gleeson, D., Rebbapragada, U., Tran, D., Castaño, R., ... & Pappalardo, R. T. (2009, March). Onboard detection of natural sulfur on a glacier via a SVM and Hyperion data. In 2009 IEEE Aerospace conference (pp. 1-15). IEEE.

Manjunath, K. R. et al. (2014). Developing spectral library of major plant species of Western Himalayas using ground observations. J. Indian Soc. Remote Sensing, 2014, 42(1), 201–216.

Marcus, W. & Fonstad, M. (2008). Optical remote mapping of rivers at submeter resolutions and watershed extents. Earth Surf. Process. Landforms, vol. 33, no. 1, pp. 4–24, Jan. 2008.

Masek, J.G., Hayes, D.J., Hughes, M.J., Healey, S.P., Turner, D.P. (2015). The role of remote sensing in process-scaling studies of managed forest ecosystems. For. Ecol. Manage., 355 (2015), pp. 109–123

Mattar, C., Franch, B., Sobrino, J.A., Corbari, C., Jiménez-Muñoz, J.C. , Olivera-Guerra, L., Skokovic, V., Sória, G., Oltra-Carriò, R., Julien, Y., & Mancini, M. (2014). Impacts of the broad-band albedo on actual evapotranspiration estimatedby S-SEBI model over an agricultural area. Remote Sensing of the Environment, 147, 23–42.

McDonnell, M. J., & Lewis, A. J. (1978). Ship detection from LANDSAT imagery. Photogrammetric Engineering and Remote Sensing, 44(3).

McRoberts, R.E., Andersen, H.E., Næsset, E. (2014). Using airborne laser scanning data to support forest sample surveys in M. Maltamo, E. Næsset, J. Vauhkonen (Eds.), Forestry Applications of Airborne Laser Scanning, Managing Forest Ecosystems, Springer, Netherlands (2014), pp. 269–292

McRoberts, R.E., Liknes, G.C., Domke, G.M. (2014). Using a remote sensing-based, percent tree cover map to enhance forest inventory estimation. For. Ecol. Manage., 331 (2014), pp. 12–18 http://dx.doi.org/10.1016/j.foreco.2014.07.025

McRoberts, R.E., Nelson, M.D., Wendt, D.G. (2002). Stratified estimation of forest area using satellite imagery, inventory data, and the k-Nearest Neighbors technique. Remote Sens. Environ., 82 (2002), pp. 457–468 http://dx.doi.org/10.1016/S0034-4257(02)00064-0

McRoberts, R.E., Tomppo, E.O. (2007). Remote sensing support for national forest inventories. Remote Sens. Environ., 110 (2007), pp. 412–419 http://dx.doi.org/10.1016/j.rse.2006.09.034

Merchant, C. J., Harris, A. R., Maturi, E., & MacCallum, S. (2005). Probabilistic physically based cloud screening of satellite infrared imagery for operational sea surface temperature retrieval. Quarterly Journal of the Royal Meteorological Society, 131(611), 2735-2755.

Middleton, E. M., Ungar, S. G., Mandl, D. J., Ong, L., Frye, S. W., Campbell, P. E., ... & Pollack, N. H. (2013). The earth observing one (EO-1) satellite mission: Over a decade in space. IEEE Journal of Selected Topics in Applied Earth Observations and Remote Sensing, 6(2), 243-256.

Moshou, D., Bravo, C., West, J., Wahlen, S., McCartney, A., & Ramon, H. (2004). Automatic detection of 'yellow rust' in wheat using reflectance measurements and neural networks. Computers and Electronics in Agriculture, 44, 173–188.

Mouat, D. A., Mahin, G. G., & Lancaster, J. (1993). Remote sensing techniques in the analysis of change detection. Geocarto International, 8(2), 39-50.

Mulla, D.J. (2013). Twenty five years of remote sensing in precision agriculture: Key advances and remaining knowledge gaps. Biosyst. Eng., vol. 114, no. 4, pp. 358–371, Apr. 2013.

Næsset, E. (2014). Area-based inventory in Norway from innovation to an operational reality. M. Maltamo, E. Næsset, J. Vauhkonen (Eds.), Forestry Applications of Airborne Laser Scanning, Managing Forest Ecosystems, Springer, Netherlands (2014), pp. 215–240

Nandy, P., Post, B. N., Smith, J. L., & Decker, M. L. (2004, August). Edge-based correlation image registration algorithm for the multispectral thermal imager (MTI). In Defense and Security (pp. 197-207). International Society for Opticsand Photonics.

Nelson, J., Ames, A., Williams, J., Patschke, R., Mott, C., Joseph, J., ... & Mah, G. (2012, March). Landsat Data Continuity Mission (LDCM) space to ground mission data architecture. In Aerospace Conference, 2012 IEEE (pp. 1-13). IEEE.

Nian, Y., Xu, K., Wan, J., Wang, L., & He, M. (2016). Block-based KLT compression for multispectral images. International Journal of Wavelets, Multiresolution and Information Processing, 14(04), 1650029.

NRC (2003). Oil in the sea III: Inputs, fates, and effects(pp. 265). Washington, D.C.: National Academy of Sciences.

Oerke, E. C., & Steiner, U. (2010). Potential of digital thermography for disease control. In E. C. Oerke, R. Gerhards, G. Menz, & R. A. Sikora (Eds.), Precision crop protection—the challenge and use of heterogeneity (pp. 167–182). Dordrecht,Netherlands: Springer.

Oerke, E. C., Fröhling, P., & Steiner, U. (2011). Thermographic assessment of scab disease on apple leaves. Precision Agriculture, doi:10.1007/s11119-010-9212-3

Oerke, E. C., Steiner, U., Dehne, H. W., & Lindenthal, M. (2006). Thermal imaging of cucumber leaves affected by downy mildew and environmental conditions. Journal of Experimental Botany, 57, 2121–2132.

Osawa, Y. (2004). OPTICAL AND MICROWAVE SENSORS ON JAPANESE MAPPING SATELLITE – ALOS. Photogrammetric Engineering and Remote Sensing, Volume XXXV, Part B1, 2004; pp.309-312.

Otremba, Z., & Piskozub, J. (2004). Modelling the bidirectional reflectance distribution function (BRDF) of seawater polluted by an oilfilm.Optics Express, 12, 1671–1676.

Pereira, H.M., Ferrier, S., Walters, M., et al. (2013). Essential biodiversity variables. Science, 399 (2013), pp. 277–278

Phinn, S., Stanford, M., Scarth, P. M., & Shyy, P. (2002). Monitoring the composition of urban environments based on the vegetation-impervious surface-soil (VIS) model by subpixel analysis techniques. International Journal of Remote Sensing, 4131–4153.

Pietrzykowski, E., Stone, C., Pinkard, E., & Mohammed, C. (2006). Effects of Mycosphaerella leaf disease on the spectral reflectance properties of juvenile Eucalyptus globules foliage. Forest Pathology, 36, 334–348.

Pingree, P. J. (2010). Advancing NASA's On-Board Processing Capabilities with Reconfigurable FPGA Technologies. INTECH Open Access Publisher.

Plaza, A., Benediktsson, J. A., Boardman, J. W., Brazile, J., Bruzzone, L., Camps-Valls, G., et al. (2009). Recent advances in techniques for hyperspectral image processing. Remote Sensing of Environment, 113, 110–122.

Prabhakar, M., Prasad, Y. G., Thirupathi, M., Sreedevi, G., Dharajothi, B. and Venkateswarlu, B. (2011). Use of ground based hyperspectral remote sensing for detection of stress in cotton caused by leafhopper (Hemiptera: Cicadellidae). Comput.Electron. Agric., 2011, 79, 189–198.

Pradhan, S., Bandyopadhyay, K. K., Sahoo, R. N., Sehgal, V. K., Singh, R., Gupta, V. K. & Joshi, D. K. (2014). Predicting wheat grain and biomass yield using canopy reflectance of booting stage. J. Indian Soc. Remote Sensing, 2014; doi: 10.1007/s12524-014-0372-x.

Prasannakumar, N. R., Chander, S. and Sahoo, R. N. (2014). Characterization of brown plant hopper damage on rice crops through hyperspectral remote sensing under field conditions. Phytoparasitica, 2014, 42, 387–395.

Proia, N., & Pagé, V. (2010). Characterization of a bayesian ship detection method in optical satellite images. IEEE Geoscience and Remote Sensing Letters, 7(2), 226-230.

Pu R., Gong, P. (2004). Determination of burnt scars using logistic regression and neural network techniques from a single post-fire Landsat-7 ETM + image. Photogrammetric Engineering and Remote Sensing, 70 (2004), pp. 841–850

Puech, C. & Raclot, D. (2002). Using geographical information systems and aerial photographs to determine water levels during floods. Hydrol. Process., vol. 16, no. 8, pp. 1593–1602, Jun. 2002.

Qi, S., Ma, J., Lin, J., Li, Y., & Tian, J. (2015). Unsupervised Ship Detection Based on Saliency and S-HOG Descriptor From Optical Satellite Images. IEEE Geoscience and Remote Sensing Letters, 12(7), 1451-1455.

Qian, S. E. (2013). Optical Satellite Data Compression and Implementation. SPIE – The International Society for Optical Engineering.

Quin, J., Burks, T. F., Ritenour, M. A., & Bonn, W. G. (2009). Detection of citrus canker using hyperspectral reflectance imaging with spectral information divergence. Journal of Food Engineering, 93, 183–191.

R. C. Gonzalez and R. E. Woods, Digital Image Processing, 2nd ed. Upper Saddle River, NJ: Prentice-Hall, 2002.

Raikes C., L. L. Burpee (1998): Use of Multispectral Radiometry for Assessment of Rhizoctonia Blight in Creeping Bentgrass. Phytopathology 1998 88:5, 446-449

Ramirez-Marquez, J. E., & Sauser, B. J. (2009). System development planning via system maturity optimization.IEEE Transactions on Engineering Management, 56, 533–548

Ranjan, R., Chopra, U. K., Sahoo, R. N., Singh, A. K. and Pradhan, S. (2012). Assessment of plant nitrogen stress through hyperspectral indices. Int. J. Remote Sensing, 2012, 22(20), 6342–6360.

Rashed, T., Weeks, J., & Gadalla, M. a. (2001). Revealing the anatomy of cities through spectral mixture analysis of multispectral satellite imagery: a case study of the Greater Cairo region, Egypt. . Geocarto International, 5–15.

Rasid, H. & Pramanik, M. (1993). Areal extent of the 1988 flood in Bangladesh: How much did the satellite imagery show?. Nat. Hazards, vol. 8, no. 2, pp. 189–200, Sep. 1993.

Ravela, S. S. (2003). On multi-scale differential features and their representations for image retrieval and recognition (Doctoral dissertation, University of Massachusetts Amherst).

Reed, I. S., & Yu, X. (1990). Adaptive multiple-band CFAR detection of an optical pattern with unknown spectral distribution. IEEE Transactions on Acoustics, Speech, and Signal Processing, 38(10), 1760-1770.

Reese, H., Nilsson, M., Sandström, P., Olsson, H. (2002). Applications using estimates of forest parameters derived from satellite and forest inventory data. Comput. Electron. Agric., 37 (2002), pp. 37–55 http://dx.doi.org/10.1016/S0168-1699(02)00118-7

Roy D.P., Boschetti, L., Justice, C.O. (2008). The collection 5 MODIS burned area product — Global evaluation by comparison with the MODIS active fire product. Remote Sensing of Environment, 112 (2008), pp. 3690–3707

Rumpf, T., Mahlein, A. K., Steiner, U., Oerke, E. C., Dehne, H. W., & Plümer, L. (2010). Early detection and classification of plant diseases with Support Vector Machines based on hyperspectral reflectance. Computers and Electronics in Agriculture, 74, 91–99.

Sader, S. A. (1990). Remote sensing of narcotic crops with special reference to techniques for detection and monitoring of poppy production in Afghanistan. Prepared for the Narcotics Awareness Control Project, USAID. Technical report, Development Alternatives, 104 REFERENCES Inc. 624 Ninth Street, N.W. Washington, D.C. 20001. url: http://pdf.usaid. gov/pdf_docs/PNABT431.pdf.

Saghri, J. A., Tescher, A. G., & Reagan, J. T. (1995). Practical transform coding of multispectral imagery. IEEE Signal Processing Magazine, 12(1), 32-43.

Sahoo, R. N., Ray, S. S., & Manjunath, K. R. (2015). Hyperspectral remote sensing of agriculture. Curr. Sci 108.5 (2015): 848-859.

Salisbury J., D'aria D., Sabins F. (1993). Thermal Infrared Remote Sensing of Crude Oil Slicks. Remote Sensing of Environment. 45:225–231.

Samberg A. (2005) Advanced oil pollution detection using an airborne hyperspectral lidar technology. Proceedings of SPIE, the International Society for Optical Engineering. 5791:308–317.

Sandholt, I., Nyborg, L., Fog, B., Lô, M., Boucum, O., & Rasmussen, K. (2003). Remote sensing techniques for flood monitoring in the Senegal River Valley. Geogr. Tidsskr., vol. 103, no. 1, pp. 71–81, 2003.

Santos, L., Berrojo, L., Moreno, J., López, J. F., & Sarmiento, R. (2016). Multispectral and Hyperspectral Lossless Compressor for Space Applications (HyLoC): A Low-Complexity FPGA Implementation of the CCSDS 123 Standard. IEEE Journal ofSelected Topics in Applied Earth Observations and Remote Sensing, 9(2), 757-770.

Schöpfer, E., Lang, S., & Strobl, J. (2010). Segmentation and object-based image analysis. In Remote Sensing of Urban and Suburban Areas (pp. 181-192). Springer Netherlands.

Schumann, G. J. P., Domeneghetti, A. (2016). Exploiting the proliferation of current and future satellite observations of rivers. Hydrological Processes, Volume 30, Issue 16, pages 2891–2896, 30 July 2016

Schumann, G., Bates, P., Horritt, M., Matgen, P., & Pappenberger, F. (2009). Progress in integration of remote sensing-derived flood extent and stage data and hydraulic models. Rev. Geophys., vol. 47, no. 4, p. RG4 001, 2009.

Schwenk, K., Goetz, K., von Schoenermark, M., & Huber, F. (2011, September). Real-time evaluation of remote sensing data on board of satellites. In 2011 21st International Conference on Field Programmable Logic and Applications (pp. 399-400).IEEE.

Shan, N., Wang, X. S., & Wang, Z. S. (2010, September). Efficient FPGA implementation of cloud detection for real-time remote sensing image processing. In 2010 Asia Pacific Conference on Postgraduate Research in Microelectronics and Electronics (PrimeAsia) (pp. 190-193). IEEE.

Shan, N., Zheng, T. Y., & Wang, Z. S. (2009, August). Onboard real-time cloud detection using reconfigurable FPGAs for remote sensing. In 2009 17th International Conference on Geoinformatics (pp. 1-5). IEEE.

Shi, Z., Yu, X., Jiang, Z., & Li, B. (2014). Ship detection in high-resolution optical imagery based on anomaly detector and local shape feature. IEEE Transactions on Geoscience and Remote Sensing, 52(8), 4511-4523.

Sims, D. A., & Gamon, J. A., (2002). Relationships between leaf pigment content and spectral reflectance across a wide range of species, leaf structures and developmental stages. Remote Sens. Environ., vol. 81, no. 2–3, pp. 337–354, Aug.2002.

Singh, A. (1989). Review article digital change detection techniques using remotely-sensed data. International journal of remote sensing, 10(6), 989-1003.

Smith, L. C. (1997). Satellite remote sensing of river inundation area, stage, and discharge: A review. Hydrol. Process., vol. 11, no. 10, pp. 1427–1439, 1997.

Song, P. & Liu, Y. (2010). Temporal influences on thresholding for satellite retrieval of water surface areas: A case in the Poyang Lake, China. Proc. 6th Int. Conf. WiCOM Netw. Mob. Comput., pp. 1-4, 2010

Song, S., Xu, B., Li, Z., & Yang, J. (2016). Ship Detection in SAR Imagery via Variational Bayesian Inference. IEEE Geoscience and Remote Sensing Letters, 13(3), 319-323.

Stancalie, G., Craciunescu, V., Zlatanova, P. & Fendel, E. M. (2005). Geo-Information for Disater Management pp. 1315-1332, 2005, Springer-Verlag

Stancalie, G., Diamandi, A., Corbus, C., & Catana, S. (2004). Application of EO data in flood fore-casting for the Crisuri Basin, Romania. In Flood Risk Management: Hazards, Vulnerability and Mitigation Measures. New York: Springer-Verlag, 2004, p. 101.

Stasolla, M., Santamaria, C., Mallorqui, J. J., Margarit, G., & Walker, N. (2015, July). Automatic ship detection in SAR satellite images: Performance assessment. In 2015 IEEE International Geoscience and Remote Sensing Symposium (IGARSS)(pp.2473-2476). IEEE.

Steddom, K., Bredehoeft, M. W., Khan, M., & Rush, C. M. (2005). Comparison of visual and multispectral radiometric disease evaluations of Cercospora leaf spot of sugar beet. Plant Disease, 89, 153–158.

Stein, D. W., Beaven, S. G., Hoff, L. E., Winter, E. M., Schaum, A. P., & Stocker, A. D. (2002). Anomaly detection from hyperspectral imagery. IEEE signal processing magazine, 19(1), 58-69.

Steinmann, K., Mandallaz, D., Ginzler, C., Lanz, A. (2013). Small area estimations of proportion of forest and timber volume combining Lidar data and stereo aerial images with terrestrial data. Scand. J. For. Res., 28 (2013), pp. 373–385http://dx.doi.org/10.1080/02827581.2012.754936

Stepper, C., Straub, C., Pretzsch, H. (2015). Using semi-global matching point clouds to estimate growing stock at the plot and stand levels: application for a broadleaf-dominated forest in central Europe. Can. J. For. Res., 45 (2015), pp. 111–123 http://dx.doi.org/10.1139/cjfr-2014-0297

Stilla, U., Michaelsen, E., Soergel, U., Hinz, S., & Ender, H. J. (2004). Airborne monitoring of vehicle activity in urban areas. International Archives of Photogrammetry and Remote Sensing, 35(B3), 973-979.

Stoffels, J., Hill, J., Sachtleber, T., Mader, S., Buddenbaum, H., Stern, O., Langshausen, J., Dietz, J., Ontrup, G. (2015). Satellite-based derivation of high-resolution forest information layers for operational forest management. Forests, 6(2015), pp. 1982–2013 http://dx.doi.org/10.3390/f6061982

Strachan, I. B., Pattey, E. and Boisvert, J. B. (2002). Impact of nitrogen and environmental conditions on corn as detected by hyperspectral reflectance. Remote Sensing Environ., 2002, 80, 213–224.

Strange R. N., Scott P. R. (2005) Plant disease: a threat to global food security Annu. Rev. Phytopathol. 43, 83–116. (doi:10.1146/annurev.phyto.43.113004.133839)

Sylvander, S., Henry, P., Bastien-Thiry, C., Meunier, F., & Fuster, D. (2000). VEGETATION geometrical image quality. Bulletin de la Société Française de Photogrammétrie et de Télédétection, 159, 59-65.

Takayasu, H. (1990). Fractals in the physical sciences. Manchester University Press.

Tang, J., Deng, C., Huang, G. B., & Zhao, B. (2015). Compressed-domain ship detection on spaceborne optical image using deep neural network and extreme learning machine. IEEE Transactions on Geoscience and Remote Sensing, 53(3), 1174-1185.

Tang, J., Deng, C., Huang, G. B., & Zhao, B. (2015). Compressed-domain ship detection on spaceborne optical image using deep neural network and extreme learning machine. IEEE Transactions on Geoscience and Remote Sensing,53(3), 1174-1185.

Tansey, K., Grégoire, J.M., Defourny, P., Leigh, R., Peckel, J.F., Bogaert, E.V., et al. (2008). A new, global, multi-annual (2000–2007) burnt area product at 1 km resolution. Geophysical Research Letters, 35 (2008), p. L01401 http://dx.doi.org/10.1029/2007GL03156

Tateishi, R., Uriyangqai, B., Al-Bilbisi, H. et al. (2011). Production of global land cover, GLCNMO Int. J. Digital Earth, 4 (2011), pp. 22–49

Taubman, D. (2000). High performance scalable image compression with EBCOT. IEEE Transactions on image processing, 9(7), 1158-1170.

Thenkabail, P. S., Smith, R. B. and Pauw, E. D. (2000). Hyperspectral vegetation indices and their relationships with agricultural crop characteristics. Remote Sensing Environ., 2000, 71, 158–182.

Thenkabail, P. S., Smith, R. B., & De Pauw, E. (2000). Hyperspectral vegetation indices and their relationship with agricultural crop characteristics. Remote Sensing of Environment, 71, 158–182.

Thompson, D. R., Green, R. O., Keymeulen, D., Lundeen, S. K., Mouradi, Y., Nunes, D. C., ... & Chien, S. A. (2014). Rapid spectral cloud screening onboard aircraft and spacecraft. IEEE Transactions on Geoscience and Remote Sensing, 52(11), 6779-6792.

Tian, Y., Wu, B., Zhang, L., Li, Q., Jia, K. & Wen., M. (2011). Opium poppy monitoring with remote sensing in North Myanmar. International Journal of Drug Policy 22.4, pp. 278–284. url: http://dx.doi.org/10.1016/j.drugpo.2011.02.001.

Tomppo, E., Olsson, H., Ståhl, G., Nilsson, M., Hagner, O., Katila, M. (2008). Combining national forest inventory field plots and remote sensing data for forest databases. Remote Sens. Environ., 112 (2008), pp. 1982–1999 http://dx.doi.org/10.1016/j.rse.2007.03.032

Topputo, F., Massari, M., Lombardi, R., Gianinetto, M., Marchesi, A., Aiello, M., ... & Banda, F. (2015, July). Space shepherd: Search and rescue of illegal immigrants in the mediterranean sea through satellite imagery. In 2015 IEEE International Geoscience and Remote Sensing Symposium (IGARSS) (pp. 4852-4855). IEEE.

Tramutoli, V. & Zilioli, E. (1998). Robust AVHRR Techniques (RAT) for Environmental Monitoring: Theory and applications. Proc. SPIE Earth Surface Remote Sensi. II, vol. 3496, pp. 101-113, 1998

Tramutoli, V. (2007). Robust Satellite Techniques (RST) for natural and environmental hazards monitoring and mitigation: Theory and applications. Proc. 4th Int. Workshop Anal. MultiTemp. Remote Sens. Images, pp. 1-6, 2007

Tramutoli, V., Liang, S., Liu, J., Li, X. N., Liu, R. & Schaepman, M. (2005). Robust Satellite Techniques (RST) for natural and environmental hazards monitoring and mitigation: Ten years of successful applications. Proc. 9th ISPRS Phys. Meas.Sign. Remote Sens., vol. 37, pp. 792-795, 2005

Tseng, W. Y., & Chiu, L. S. (1994). AVHRR observations of Persian Gulf oil spills. Geoscience and remote sensing symposium. IGARSS '94. Surface and atmospheric remote sensing: Technologies, data analysis and interpretation(pp. 779–782)

Tucker C. J. (1979) Red and photographic infrared linear combinations for monitoring vegetation Remote Sensing of Environment 8:127–150 doi:10.1016/0034-4257(79)90013-0

Tyc, G., Tulip, J., Schulten, D., Krischke, M., Oxfort, M. (2005). The RapidEye mission design. Acta Astronautica Volume 56, Issues 1-2, January 2005; pp.213-219.

Ud Din, S., Al Dousari, A., & Literathy, P. (2008). Evidence of hydrocarbon contamination from the Burgan oilfield, Kuwait—Interpretations from thermal remote sensing data. Journal of Environmental Management, 86, 605–615.

Van de Voorde T., B. Verbeiren, Y. Cornet, M. Binard, J. Van der Kwast, G. Engelen, F. Canters and O. Batelaan. (2013). Mapping and modelling urban growth and its impact on the hydrology of urban watersheds with satellite imagery. earthzine.org (July 2013).

Van de Voorde T., De Genst, W., Canters, F., Stephenne, N., Wolf, E., Binard, M. (2004). Extraction of land use/land cover—related information from very high resolution data in urban and suburban areas. R. Goossens (Ed.), Remote sensing in transition: Proceedings of the 23rd symposium of the European Association of Remote Sensing Laboratories, June 2–5, 2003, Ghent, Belgium (2004), pp. 237–244

Van de Voorde, T., De Roeck, T., Canters, F. (2009). A comparison of two spectral mixture modelling approaches for impervious surface mapping in urban areas. International Journal of Remote Sensing, 30 (18) (2009), pp. 4785–4806 http://dx.doi.org/10.1080/01431160802665918

Vanderhaegen S., De Munter, K., Canters, F. (2015). High resolution modelling and forecasting of soil sealing density at the regional scale, Landscape and Urban Planning, Volume 133, January 2015, Pages 133-142, ISSN 0169-2046, http://dx.doi.org/10.1016/j.landurbplan.2014.09.016.

Verbeke L.P.C., Vabcoillie F.M.B. and De Wulf R.R. (2004). Reusing back-propagating artificial neural network for land cover classification in tropical savannahs. International Journal of Remote Sensing, 2747–2771.

Verburg, P.H., Neumann, K., Nol, L. (2011). Challenges in using land use and land cover data for global change studies. Glob. Change Biol., 17 (2011), pp. 974–989

Vespe, M., & Greidanus, H. (2012). SAR image quality assessment and indicators for vessel and oil spill detection. IEEE Transactions on Geoscience and Remote Sensing, 50(11), 4726-4734.

Vincent, P., Larochelle, H., Bengio, Y., & Manzagol, P. A. (2008, July). Extracting and composing robust features with denoising autoencoders. In Proceedings of the 25th international conference on Machine learning (pp. 1096-1103). ACM.

Vladimirova, T., & Steffens, A. (2005, June). Compression of multispectral images on-board observation satellites. In Proceedings of the International Conference on Space, Ecology, Safety (SES'05) (Vol. 1, pp. 10-13).

Voigt, S., Schoepfer, E., Fourie, C., & Mager, A. (2014, October). Towards semi-automated satellite mapping for humanitarian situational awareness. In Global Humanitarian Technology Conference (GHTC), 2014 IEEE (pp. 412-416). IEEE.

Wadsworth A., Looyen W. J., Reuter R., Petit M. (1992). Aircraft experiments with visible and infrared sensors. International Journal of Remote Sensing.13.6:1175–1199.

Walter V. (2004). Object-based classification of remote sensing data for change detection. ISPRS Journal of Photogrammetry & Remote Sensing, 225–238.

Wang, F. M., Huang, J. F. and Wang, X. Z. (2008). Identification of optimal hyperspectral bands for estimation of rice biophysical parameters. J. Integr. Plant Biol., 2008, 50(3), 291–299.

Wang, J. J., Zhang, Y., & Bussink., C. (2014). Unsupervised multiple endmember spectral mixture analysis-based detection of opium poppy fields from an EO- 1 Hyperion image in Helmand, Afghanistan. The Science of the total environment 476-477pp. 1–6. url: http://www.sciencedirect.com/science/article/ pii/S0048969714000151.

Wang, Y. (2004). Using Landsat 7 TM data acquired days after a flood event to delineate the maximum flood extent on a coastal floodplain. Int. J. Remote Sens., vol. 25, no. 5, pp. 959–974, Mar. 2004.

Wang, Y., Colby, J. D., & Mulcahy, K. A. (2002). An efficient method for mapping flood extent in a coastal floodplain using Landsat TM and DEM data. Int. J. Remote Sens., vol. 23, no. 18, pp. 3681–3696, Sep. 2002.

Wang, Z., Xiong, X., & Li, Y. (2015). Update of VIIRS on-orbit spatial parameters characterized with the Moon. IEEE Transactions on Geoscience and Remote Sensing, 53(10), 5486-5494.

Wang, Z., Zhang, T., Yan, L., & Gong, C. (2010, October). A high performance fully pipelined architecture for lossless compression of satellite image. In Multimedia Technology (ICMT), 2010 International Conference on (pp. 1-4). IEEE.

Watson, J. P. (1991). A visual interpretation of a LANDSAT mosaic of the Okavango-delta and surrounding area. Remote Sens. Environ., vol. 35, no. 1, pp. 1–9, Jan. 1991.

Weinberger, M. J., Seroussi, G., & Sapiro, G. (2000). The LOCO-I lossless image compression algorithm: principles and standardization into JPEG-LS. IEEE Transactions on Image processing, 9(8), 1309-1324.

Weiss, S. (2010). VIIRS geolocation algorithm theoretical basis document ATBD. Northrop Grumman, Falls Church, VA, Doc. No.: D43776, 2010.

Wettle, M., Daniel, P. J., Logan, G. A., & Thankappan, M. (2009). Assessing the effect of hydrocarbon oil type and thickness on a remote sensing signal: A sensitivity study based on the optical properties of two different oil types and the HYMAP and Quickbird sensors. Remote Sensing of Environment, 113, 2000–2010.

Wieland, M., Pittore, M., Parolai, S., Zschau, J., Moldobekov, B., Begaliev, U. (2012). Estimating building inventory for rapid seismic vulnerability assessment: Towards an integrated approach based on multi-source imaging. Soil Dynamicsand Earthquake Engineering, Volume 36, May 2012, Pages 70-83, ISSN 0267-7261, http://dx.doi.org/10.1016/j.soildyn.2012.01.003

Willhauck, G., Caliz, J. J., Hoffmann, C., Lingenfelder, I., & Heynen, M. (2005). Object-oriented ship detection from VHR satellite images. Semana Geomática.

Williams, J. A., Dawood, A. S., & Visser, S. J. (2002, December). FPGA-based cloud detection for real-time onboard remote sensing. In Field-Programmable Technology, 2002.(FPT). Proceedings. 2002 IEEE International Conference on (pp. 110-116).IEEE.

Wolfe, R. E., Nishihama, M., Fleig, A. J., Kuyper, J. A., Roy, D. P., Storey, J. C., & Patt, F. S. (2002). Achieving sub-pixel geolocation accuracy in support of MODIS land science. Remote Sensing of Environment, 83(1), 31-49.

Wu, G., de Leeuw, J., Skidmore, A. K., Liu, Y., & Prins, H. H. (2009). Performance of Landsat TM in ship detection in turbid waters. International Journal of Applied Earth Observation and Geoinformation, 11(1), 54-61.

Wu, X., & Memon, N. (1997). Context-based, adaptive, lossless image coding. IEEE transactions on Communications, 45(4), 437-444.

Wulder, M.A., Franklin, S.E. (2003). Remote Sensing of Forest Environments: Concepts and Case Studies (first ed.), Kluwer Academic Publishers, Boston, Dordrecht, London (2003)

Wulder, M.A., Hall, R.J., Coops, N.C., Franklin, S.E. (2004). High spatial resolution remotely sensed data for ecosystem characterization BioScience, 54 (2004), pp. 511–521

Xie, Y., & Xiong, X. (2011). On-orbit spatial characterization of MODIS with ASTER aboard the Terra spacecraft. IEEE Geoscience and Remote Sensing Letters, 8(5), 993-996.

Xiong, X., Che, N., & Barnes, W. (2005). Terra MODIS on-orbit spatial characterization and performance. IEEE Transactions on Geoscience and Remote Sensing, 43(2), 355-365.

Xiong, X., Che, N., & Barnes, W. (2005). Terra MODIS on-orbit spatial characterization and performance. IEEE Transactions on Geoscience and Remote Sensing, 43(2), 355-365.

Xiong, X., Sun, J., Angal, A., Xie, Y., Choi, T., & Wang, Z. (2011, September). Results of MODIS band-to-band registration characterization using on-orbit lunar observations. In SPIE Optical Engineering+ Applications (pp. 81531R-81531R).International Society for Optics and Photonics.

Xu H. (2007). Extraction of urban built-up land features from landsat imagery using a thematic oriented index combination technique. Photogrammetric Engineering and Remote Sensing, 1381-1391.

Xu, J., Fu, K., & Sun, X. (2011, August). An invariant Generalized Hough Transform based method of inshore ships detection. In Image and Data Fusion (ISIDF), 2011 International Symposium on (pp. 1-4). IEEE.

Xu, J., Sun, X., Zhang, D., & Fu, K. (2014). Automatic detection of inshore ships in high-resolution remote sensing images using robust invariant generalized Hough transform. IEEE Geoscience and Remote Sensing Letters, 11(12), 2070-2074.

Yang L., Huang, C., Homer, C., Wylie, B., Coan, M. (2003). An approach for mapping large-area 419 impervious surfaces: Synergistic use of Landsat-7 ETM+ and high spatial resolution imagery. Canadian Journal of Remote Sensing, 29 (2003), pp. 230–240 10.5589/m02-098

Yang X., Liu, Z. (2005). Use of satellite-derived landscape imperviousness index to characterize urban spatial growth. Computers, Environment and Urban Systems, 29 (2005), pp. 524–540 http://dx.doi.org/10.1016/j.compenvurbsys.2005.01.005

Yang, C., Everitt, J. H., Du, Q., Luo B., & Chanussot, J. (2013). Using High-Resolution Airborne and Satellite Imagery to Assess Crop Growth and Yield Variability for Precision Agriculture in Proceedings of the IEEE, vol. 101, no. 3, pp.582-592, March 2013. doi: 10.1109/JPROC.2012.2196249

Yang, G., Li, B., Ji, S., Gao, F., & Xu, Q. (2014). Ship detection from optical satellite images based on sea surface analysis. IEEE Geoscience and Remote Sensing Letters, 11(3), 641-645.

Yu, G., Vladimirova, T., & Sweeting, M. (2007, July). A new automatic on-board multispectral image compression system for Leo Earth observation satellites. In 2007 15th International Conference on Digital Signal Processing (pp. 395-398).IEEE.

Yu, G., Vladimirova, T., & Sweeting, M. (2007, July). A new automatic on-board multispectral image compression system for Leo Earth observation satellites. In 2007 15th International Conference on Digital Signal Processing (pp. 395-398).IEEE.

Yu, G., Vladimirova, T., & Sweeting, M. (2007, November). Autonomous band registration for on-board applications. In Signal Processing and Communications, 2007. ICSPC 2007. IEEE International Conference on (pp. 1327-1330). IEEE.

Yu, G., Vladimirova, T., Wu, X., & Sweeting, M. N. (2008, June). A new high-level reconfigurable lossless image compression system for space applications. In Adaptive Hardware and Systems, 2008. AHS'08. NASA/ESA Conference on (pp. 183-190). IEEE.

Yu, Y., Guan, H., & Ji, Z. (2015). Rotation-Invariant Object Detection in High-Resolution Satellite Imagery Using Superpixel-Based Deep Hough Forests. IEEE Geoscience and Remote Sensing Letters, 12(11), 2183-2187.

Yuhaniz, S., Vladimirova, T., & Gleason, S. (2007, August). An intelligent decision-making system for flood monitoring from space. In Bio-inspired, Learning, and Intelligent Systems for Security, 2007. BLISS 2007. ECSIS Symposium on (pp. 65-71). IEEE.

Zhang, F., Wu, B., Zhang, L., Huang, H., & Tian, Y. (2006, October). Illicit vessel identification in inland waters using SAR image. In Geoinformatics 2006: Remotely Sensed Data and Information (pp. 64190S-64190S). International Society for Optics and Photonics.

Zhao, T., & Nevatia, R., (2001). Car detection in low resolution aerial images. In: Proceedings of International Conference on Computer Vision, Vancouver, Canada July 9–12, 2001. pp. 710–717

Zhenwei, S., Jun, W., Shuo, Y., & Zhiguo, J. (2012). RX and its variants for anomaly detection in hyperspectral images [J]. Infrared and Laser Engineering, 3, 050.

Zhou Y.Y., Wang, Y.Q. (2008). Extraction of impervious, surface areas from high spatial resolution imagery by multiple agent segmentation and classification. Photogrammetric Engineering and Remote Sensing, 74 (7) (2008), pp. 857–868 10.14358/PERS.74.7.857

Zhu, C., & Wang, R. (2012). Local multiple patterns based multiresolution gray-scale and rotation invariant texture classification. Information Sciences, 187, 93-108.

Zhu, C., Zhou, H., Wang, R., & Guo, J. (2010). A novel hierarchical method of ship detection from spaceborne optical image based on shape and texture features. IEEE transactions on geoscience and remote sensing, 48(9), 3446-3456.

Zhu, Y., Li, Y., Feng, W., Tian, Y., Yao, X. and Cao, W. (2006). Monitoring leaf nitrogen in wheat using canopy reflectance spectra. Can. J. Plant Sci., 2006, 86, 1037–1046.

Zlinszky, A., Heilmeier, H., Balzter, H., Czúcz, B., Pfeifer, N. (2015). Remote sensing and GIS for habitat quality monitoring: new approaches and future research. Remote Sens., 7 (2015), pp. 7987–7994 http://dx.doi.org/10.3390/rs70607987

8.2 Radar Applications & GNSS-R

Adamiuk, G., Heer, C., & Ludwig, M. (2016). DBF Technology Development for Next Generation of ESA C. Proceedings EUSAR, (S. 825-828). Hamburg.

Adamiuk, G., Schaefer, C., Fischer, C., & Heer, C. (2014). SAR Architectures based on DBF for C- and X-band applications. Proceedings EUSAR. Hamburg.

Aguttes, J. (2003). The SAR train concept: Required antenna area distributed over N smaller satellites, increase of performance by N. IGARSS.

Auterman, J. (1984). Phase stability requirements for bistatic SAR. IEEE Radar Conference. Atlanta.

Blythe, J. H. (September 1979). Patentnr. 4253098. United States.

Braubach, H., & Völker, M. (2007). Patentnr. 7209072. United States.

Brown, J. L. (February 1981). Multi-Channel Sampling of Low-Pass Signals. IEEE Transactions on Circuits and Systems, S. 101-106.

Castellvi Esturi, J., Camps, A., Carbera, J., & Alamús, R. (2017). 3CAT-3/MOTS. An Experimental Nanosatellite for Multispectral and GNSS-R Observations: Mission Concept and Analysis. Proceedings IGARSS, S. 2752-2755.

Cerutti-Maori, D., Sikaneta, I., Klare, J., & Gierull, C. H. (August 2014). MIMO SAR Processing for Multichannel High-Resolution Wide-Swath Radars. IEEE Transactions on Geoscience and Remote Sensing, S. 5034-5055.

Clarizia, M. P., & Ruf, C. (August 2016). On the Spatial Resolution of GNSS Reflectometry. IEEE Geoscience and Remote Sensing Letters, 13(8), S. 1064-1068.

Clarizia, M. P., & Ruf, C. (August 2016). Wind Speed Retrieval Algorithm for the Cyclone Global Navigation Satellite System (CYGNSS) Mission. IEEE Transactions on Geoscience and Remote Sensing, 54(8), S. 4419 - 4432.

Cumming, I., & Wong, F. (2005). *Digital Processing of SAR Data.* Norwood, MA: Artech House.

Currie, A., & Brown, M. (1992, April). Wide-swath SAR. *IEE Proceedings-F*, pp. 122-135.

CyGNSS - Cyclone Global Navigation Satellite System. (2017). Retrieved 12 06, 2017, from http://clasp-research.engin.umich.edu/missions/cygnss/

di Simone, A., Park, H., Riccio, D., & Camps, A. (2017, September). Sea Target Detection Using Spaceborne GNSS-R Delay-Doppler Maps: Theory and Experimental Proof of Concept Using TDS-1 Data. IEEE Journal of Selected Topics in Applied Earth Observation and Remote Sensing, 10(9), pp. 4237-4255.

ESA's Call for Earth Explorer EE-9. (kein Datum). Von http://explorercall.esa.int/index.php/15-mission-ee9 abgerufen

Feng He, X. M. (December 2014). Digital Beamforming on Receive in Elevation for Multidimensional Waveform Encoding SAR Sensing. (IEEE, Hrsg.) IEEE Geoscience and Remote Sensing Letters, 12, S. 2173–2177.

Fornaro, G., & Serafino, F. (Dec 2006). Imaging of single and double scatterers in urban areas via SAR tomography. IEEE Transactions on Geoscience and Remote Sensing, 44(12), S. 3497–3505.

Gebert, N., Krieger, G., & Moreira, A. (April 2009). Digital Beamforming: Techniques and Optimization Strategies for High-Resolution Wide-Swath SAR Imaging. IEEE Transactions on Aerospace and Electronic Systems, S. 564-592.

Gierull, C. H. (2003). Digital cahnnel balancing of along-track interferometric SAR data. Canada-Ottawa: Defence R&D.

Gini, F., Lombardini, F., & Montanari, M. (Oct 2002). Layover solution in multibaseline sar interferometry. IEEE Transactions on Aerospace and Electronic Systems, 38(4), S. 1344–1356.

I. Hajnsek, M. S.-D. (June 2014). Tandem-L: Science Requirements and Mission Concept. 10th European Conference on Synthetic Aperture Radar, EUSAR, S. 1255–1258.

Janoth, J., Gantert, S., Schrage, T., & Kaptein, A. (2013). TerraSAR-X Next Generation - Mission Capabilities. Proceedings of the IGARSS , S. 2297-2300.

Kare, J. T. (June 1998). Patentnr. 6175326 B1. United States.

Kim, J.-H., Younis, M., Prats-Iraola, P., Gabele, M., & Krieger, G. (January 2013). First Spaceborn Demonstration of Digital Beamforming for Azimuth Ambiguity Suppression. IEEE Transactions on Geoscience and Remote Sensing, S. 579-590.

Kraus, T., Bräutigam, B., Bachmann, M., & Krieger, G. (Juni 2016). Multistatic SAR Imaging: First Results of a Four Phase Center Experiment with TerraSAR-X and TanDEM-X. Proceedings of the EUSAR.

Krieger, G. (May 2014). MIMO-SAR: Opportunities and Pitfalls. IEEE Transactions on Geoscience and Remote Sensing, 52, S. 2628–2645.

Krieger, G., & Moreira, A. (June 2006). Spaceborne bi- and multistatic SAR: potential and challenges. IEE Proc.-Radar Sonar Navig., 153(3).

Krieger, G., Gebert, N., & Moreira, A. (2004). Unambiguous SAR Signal Reconstruction From Nonuniform Displaced Phase Center Sampling. IEEE Geosince and Remote Sensing Letters, S. 260-264.

Krieger, G., Gebert, N., Younis, M., Bordoni, F., Patyuchenko, A., & Moreira, A. (2008). Advanced Concepts for Ultra-Wide-Swath SAR Imaging. Proceedings of the EUSAR. Friedrichshafen, Germany.

Krieger, G., Moreira, A., Fiedler, H., Hajnsek, I., Werner, M., Younis, M., et al. (11. 11 2007). TanDEM-x: A Satellite Formation for High Resolution SAR Interferometry. IEEE Transactions on Geoscience and Remote Sensing, S. 3317-3341.

Massonet, D. (2003). Capabilities and Limitations of the Interferometric Cartwhee. IEEE Transaction on Geoscience and Remote Sensing, 39(3), S. 506-520.

Massonet, D., & Souyris, J.-C. (2008). Imaging with Synthetic Aperture Radar. EPFL Press.

Mittermayer, J., Lopez-Dekker, F., Kraus, T., & Krieger, G. (2016). J. Mittermayer, P. López-Dekker, T. Kraus, G. Krieger, “Small Satellite Dispersed Synthetic Aperture Radar. Proc. of The 4S Symposium. Valetta, Malta.

Moreira, A., Krieger, G., Hajnsek, I., Papathanassiou, K., Younis, M., Lopez-Dekker, F., et al. (2015). Tandem-L: A Highly Innovative Bistatic SAR Mission for Global Observation of Dynamic Processes on the Earth's Surface. IEEE Geoscience and Remote Sensing Magazine (GRSM), 3(2), S. 8-23.

Pinheiro, M., Rodriguez-Cassola, M., Prats, P., Reigber, A., & Moreira, A. (2013). Reconstruction of missing data in interferometric SAR systems. IGARSS. Melbourne.

Pitz, W., & Miller, D. (February 2010). The TerraSAR-X Satellite. IEEE TRANSACTIONS ON GEOSCIENCE AND REMOTE SENSING, VOL. 48, NO. 2, FEBRUARY 2010, 48(2), S. 615-622.

Prati, C., & Rocca, F. (1992). Range resolution enhancement with multiple SAR surveys combination. IGARSS, (S. 1576–1578).

Prats, P., Lopez-Dekker, F., De Zan, F., Wollstadt, S., Bachmann, M., Steinbrecher, U., et al. (2011). Distributed imaging with TerraSAR-X and TanDEM-X. IGARSS, (S. 3963–3966).

Rodriguez-Cassola, M. (2013). Bistatic synthetic aperture radar data processing. DLR Research Report.

Rodriguez-Cassola, M., Prats, P., Steinbrecher, U., Schulze, D., Krieger, G., Reigber, A., et al. (2013). Cross-platform spaceborne SAR imaging: Demonstration using TanDEM-X. IGARSS. Melbourne.

Rodriguez-Cassola, M., Prats-Iraola, P., Nannini, M., Lopez-Dekker, F., Moreira, A., & Carnicero-Dominguez. (2016). Calibration Concept for Weakly-Synchronised SAR Companion Missions: ESA’s SAOCOM/CS case. EUSAR. Hamburg.

S. Huber, M. Y. (October 2012). Spaceborne Reflector SAR Systems with Digital Beamforming. (IEEE, Hrsg.) IEEE Transactions on Aerospace and Electronic Systems, 48, S. 3473–3493.

Salzman, J., & Kirk, J. (2002). Interrupted Synthetic Aperture Radar. IEEE AESS Systems Magazine.

Seu, R., Smrekar, S., Hensley , S., & Lombardo, P. (2016). A SAR Interferometer Experiment to Explore the Surface of Venus. Proceedings EUSAR, S. 1242-1244.

Skolnik, M. (1980). Introduction to Radar Systems. Singapore: McGraw-Hill.

Suess, M. a. (September 2002). Patentnr. EP 1 241 487. Europe.

Suess, M., Grafmueller, B., & Zahn, R. (2001). A novel high resolution, wide swath SAR system. Proceeding of the IGARSS. Sidney, Australia.

Tobias Rommel, S. H. (June 2014). An Orthogonal Waveform for MIMO-SAR Applications. Proceedings of EUSAR; 10th European Conference on Synthetic Aperture Radar.

Torres, R., Snoeij, P., Geudtner, D., Bibby, D., Davidson, M., Attema, E., et al. (15. May 2012). GMES Sentinel-1 mission. Remote Sensing of Environment, S. 9–24.

Villano, M., Krieger, G., & Moreira, A. (2014). A Novel Processing Strategy for Staggered SAR. IEEE Geoscience and Remote Sensing Letters, 11(11), 1891-1895.

Villano, M., Krieger, G., & Moreira, A. (2014.). Staggered SAR: High-Resolution Wide-Swath Imaging by Continuous PRI Variation. IEEE Transactions on Geoscience and Remote Sensing, 52(7), 4462-4479.

Villano, M., Krieger, G., & Moreira, A. (2015). Ambiguities and Image Quality in Staggered SAR. Proceeding of the APSAR. Marina Bay Sands, Singapore.

Villano, M., Krieger, G., & Moreira, A. (2015). Data Volume Reduction in High-Resolution Wide-Swath SAR Systems. Proceeding of the APSAR. Marina Bay Sands, Singapore.

Werninghaus, R., & Buckreuss, S. (2010). The TerraSAR-X Mission and System Design. IEEE Transactions on Geoscience and Remote Sensing, 48(2), 606-614.

Wickert, J., Cardellach, E., Martín-Neira, M., & et al. (October 2016). GEROS-ISS: GNSS Reflectometry, Radio Occultation, and Scatterometry Onboard the ISS. IEEE Journal of Selected Topics in Applied Earth Observations and Remote Sensing, 9(10), S. 4552-4581.

Younis, M., Laux, C., Al-Kahachi, N., Lopez-Dekker, P., Krieger, G., & Moreira, A. (2014). Calibration of Multi-Channel Spaceborn SAR - Challenges and Strategies. Proceedings of the EUSAR.

Zavorotny, V. U., Gleason, S., Cardellach, E., & Camps, A. (2014, December). Tutorial on Remote Sensing Using GNSS Bistatic Radar of Opportunity. IEEE Geoscience and Remote Sensing Magazine.

Zhu, X., & Bamler, R. (Dec 2010). Very high resolution spaceborne SAR tomography in urban environment. IEEE Transactions on Geoscience and Remote Sensing, 48(12), S. 4296–4308